Purdue University
Purdue e-Pubs

Open Access Dissertations | Theses and Dissertations

Spring 2015

Black-box printer models and their applications

Yanling Ju
Purdue University

Follow this and additional works at: https://docs.lib.purdue.edu/open_access_dissertations

Part of the Computer Engineering Commons

Recommended Citation
Ju, Yanling, "Black-box printer models and their applications" (2015). *Open Access Dissertations*. 481.
https://docs.lib.purdue.edu/open_access_dissertations/481

This document has been made available through Purdue e-Pubs, a service of the Purdue University Libraries. Please contact epubs@purdue.edu for additional information.

Graduate School Form 30
(Updated 11/20/2014)

PURDUE UNIVERSITY
GRADUATE SCHOOL
Thesis/Dissertation Acceptance

This is to certify that the thesis/dissertation prepared

By Yanling Ju

Entitled
Black-Box Printer Models and Their Applications

For the degree of Doctor of Philosophy

Is approved by the final examining committee:

JAN P. ALLEBACH

CHARLES A. BOUMAN

MARY L. COMER

MIREILLE BOUTIN

To the best of my knowledge and as understood by the student in the Thesis/Dissertation Agreement, Publication Delay, and Certification/Disclaimer (Graduate School Form 32), this thesis/dissertation adheres to the provisions of Purdue University's "Policy on Integrity in Research" and the use of copyrighted material.

Approved by Major Professor(s): JAN P. ALLEBACH

Approved by: Michael R. Melloch 03/02/2015

Head of the Department Graduate Program Date

BLACK-BOX PRINTER MODELS AND THEIR APPLICATIONS

A Dissertation

Submitted to the Faculty

of

Purdue University

by

Yanling Ju

In Partial Fulfillment of the

Requirements for the Degree

of

Doctor of Philosophy

May 2015

Purdue University

West Lafayette, Indiana

To my parents, my husband, and my lovely daughter.

ACKNOWLEDGMENTS

I wish to express my gratitude to my thesis advisor and commitee members; my labmates and other friends at Purdue; my research sponser - the Hewlett-Packard Company who made this thesis possible; and my family who have supported me all these years.

First of all, I deeply wish to express my sincere gratitude to my major advisor, Prof. Jan P. Allebach, for providing me the wonderful opportunty to work with him. I would like to thank him for his priceless instructions and experiences mentoring during each step of my research, for his energetic and organized work and life style that influence me forever, and for his support and help during my 5 years Ph.D. life. I know Professor Allebach through a senior undergraduate course ECE438. I was impressed by the way he taught that using real applications to make the hard problem interesting and easy to understand. His dedication to education and research inspired many students in that class including me. I appreciate my advisor not just as an expert mentor to show me how to do the research but also as a friend who supported me at all times.

I would also like to give sincere thanks to all other committee members: Prof.Charles A. Bouman, Prof. Mary Comer, and Prof. Mireille Boutin. They were extreme nice and encouraging to me. They were always approachable and gave me good advice and careful guidance for my research and thesis.

I will contribute my work to our research sponsors, the Hewlett-Packard Company, whose support and precious inputs make the research possible. I also would like to thank all the EISL members who have worked with me during these years.

Lastly, I would also like to thank my parents and my parents-in-law for all their support to my study and research. I sincerely appreciate my husband for his support

to my work and his great effort to create a better future. I heartfully thank my lovely daughter Anna for all the joy and happiness she bring to us.

TABLE OF CONTENTS

	Page
LIST OF TABLES	vii
LIST OF FIGURES	viii
SYMBOLS	xii
ABBREVIATIONS	xiii
ABSTRACT	xiv
1 INTRODUCTION	1
1.1 Digital Halftoning	1
1.2 Printer Model	3
1.3 Black Box Printer Models and Their Applications	6
2 REVIEW OF PRINTER MODEL	9
2.1 Notation	9
2.2 Equation Development for Printer Model	11
2.3 Review of Printer Model	12
3 BLACK BOX PRINTER MODEL	16
3.1 Print-to-Scan Analysis Procedure	16
3.2 Preliminary Experiments for Large Area Influence	21
3.2.1 Printed dot profile performance	21
3.2.2 Large area influence in digital halftone	23
3.3 Model-5×5	25
3.4 Black Box Model-45×45	28
3.4.1 Test page design for Model-45×45	29
3.4.2 Structure of black box Model-45×45	31
3.4.3 Standard definition black box Model-45×45	35
3.4.4 High definition black box Model-45×45	39

Page

3.5 Validation of Dot Area Measurement 46
3.5.1 Review of dot area coverage 47
3.5.2 Experiment and results 47
3.6 Conclusion 49
4 SAMPLE FUNCTION GENERATION BLACK BOX MODEL 51
4.1 Sample Function Generator 51
4.1.1 Equation development for sample function generator 52
4.2 Sample Function Generation Black Box Model 54
4.3 Test of SFG-BBM on BBM Training Page 56
4.4 Conclusion 57
5 TONER USAGE PREDICTION 58
5.1 Two-Stage Approach for Toner Usage Estimation 60
5.1.1 Absorptance predictor 60
5.1.2 Toner usage mapping 65
5.2 Implementation of Two-Stage Approach for Toner Usage Estimation 66
5.3 Conclusion 68
6 PRINTED IMAGE QUALITY EVALUTION 69
6.1 Visualization Tool for Image Graininess 69
6.2 Autonomously Detect the Text Fading in Prints 70
6.2.1 Training samples and psychophysical experiment 73
6.2.2 Text fade detection algorithm 75
6.2.3 Experimental results 80
6.3 Conclusion 82
7 SUMMARY 84
REFERENCES 86
VITA 90

LIST OF TABLES

Table Page

3.1 Computational structure of the black box models. 33

3.2 Summary of black box model statistics. 34

3.3 SD-BBM Model-fit and cross-validation prediction RMSE averaged over 31 gray levels*. 39

3.4 Model-fit and cross-validation prediction RMSE of SD and HD M45×45 C3b *. 44

5.1 Absorptance ranges and the corresponding toner usage weight. 66

5.2 Comparison between our new two-stage predictor and the pixel-counting algorithm. 68

LIST OF FIGURES

Figure Page

1.1 Example of aperiodic dispersed-dot halftone a), periodic clustered-dot halftone b), and irregular clustered-dot halftone c). 2

1.2 Digital halftone (a) and 4000 dpi scan of its print sample resulting from HP LaserJet 4M prints at (b) 300 dpi, and (c) 600 dpi (magnified by 2). 5

2.1 Example of human visual system filter. 11

2.2 Using Model-3×3 to generate the equivalent grayscale image. 14

3.1 Epson Expression 10000 XL scanner (a) and Personal Image Analysis System II (b). 17

3.2 Print-to-scan analysis procedure for the black box models. 18

3.3 Analysis of scanned printed test pages analysis for black box models. . 18

3.4 Sub-scanner-pixel estimation of the absorptance of each pixel/subpixel of interest for SD and HD BBM, to account for misregistration between the printer and scanner lattices and the non-integer ratio of their resolutions. 19

3.5 Contour of mean absorptance of the printed 3×3 printer addressable pixels black dot profile. a) scan using Epson scanner with 0° rotation, b) scan using Epson scanner with 90° rotation, c) PIAS with 0° rotation, d) PIAS with 90° rotation. 23

3.6 Large-area influence in digital halftoning: (a) portion of test page, (b) experiment result. 24

3.7 Test page for Model-5×5. 25

3.8 a) estimate the centroid of the fiducial mark, b) locate the center for all dot pattern. 26

3.9 Tone reproduction curve for HP Indigo Press 5000. a) tone reproduction curve for dispersed-dot halftones, b) tone reproduction curve for clustered-dot halftones. 30

Figure Page

3.10 (a) Test page for Model-45 × 45 for irregular, clustered-dot halftone texture, (b) Portion of test page. Each of the four halftone squares in (b) corresponds to one of the small squares in (a). The fiducial marks in (b) are used to register the pixels in the scanned image of the printed test page to the pixels in the digital image sent to the press. 31

3.11 Structure of Model-45×45 Class 3a that is used to predict both absorptance and standard deviation at a given printer-addressable pixel. The predicted value is the sum of five components. The first four components $w^k_{\chi_k}, k = 1, 2, 3, 4$, are weights obtained from lookups into four different tables indexed according to the binary halftone patterns in each of the four overlapping 3×3 neighborhoods shown. Here χ_k is the index corresponding to the 3×3 binary neighborhood. The last component c_g accounts for the contribution of the average gray value in the surrounding 45×45-5×5 neighborhood. It is computed by interpolation between 32 values stored in a LUT, as shown in the lower left. All the model parameters are trained using the test page shown in Fig. 3.10. 36

3.12 The model-fit and cross-validation predictor performance for 32 gray levels. (a)Root mean square prediction error. (b)Mean prediction error. 38

3.13 Cross-validation model prediction images and absolute value error images for mean absorptance. The example clustered-dot halftone has an average gray level 96/255. (a) Digital halftone, (b) Estimated measurement, (c) ULM5×5 prediction, (d) M45×45 Class 2a prediction, (e) M45×45 Class 3b prediction, (f) ULM5×5 prediction error image, (g) M45×45 Class 2a prediction error image, (h) M45×45 Class 3b prediction error image. The three error images are computed by forming the absolute value of the error at each pixel, and then identically scaling the images to map the maximum across all three images to black and the minimum across all three images to white. 40

3.14 Structure of HD M45×45 C3b that is used to predict both absorptance and standard deviation at a given sub-printer-addressable pixel. The predicted value is the sum of six components. The first five components $w^k_{\chi_k}, k = 1, 2, 3, 4, 5$, are weights obtained from lookups into five different tables indexed according to the binary halftone patterns in each of the five overlapping 3×3 neighborhoods shown. Here χ_k is the index corresponding to the 3×3 binary neighborhood. The last component c_g accounts for the contribution of the average gray value in the surrounding 45×45-5×5 neighborhood. It is computed by interpolation between 32 values stored in a LUT, as shown in the lower left. All the model parameters are trained using the test page shown in Fig. 3.10. 41

Figure Page

3.15 Example of using HD M45×45 C3b to predict the absorptance of one subpixel within the corresponding printer-addressable pixel. 43

3.16 Compare cross-validation model predicted images using SD and HD M45×45 C3b. The example clustered-dot halftone has an average gray level 96/255. 45

3.17 Compare cross-validation model predicted images using SD and HD M45×45 C3b. The example clustered-dot halftone has an average gray level 96/255. 45

3.18 Compare cross-validation model predicted images using SD and HD M45×45 C3b. We use the HD estimated image as ground truth to calculate the RMSE. 46

3.19 Test page for dot area validation. 48

3.20 Results of dot area validation. 49

4.1 Obtain the SFG-BBM prediction by adding the BBM mean absorptance prediction with the printing variation prediction. 51

4.2 Sample function generator (3-neighbor) for printing variation prediction. 52

4.3 The flowchart of SFG-BBM. We can obtain the SFG-BBM prediction by adding the BBM mean absorptance prediction with the printing variation prediction. 55

4.4 Original digital halftone and SFG-BBM prediction. 55

4.5 Test of SFG-BBM on BBM training page. 56

5.1 Toner usage prediction. 58

5.2 Overwiew of the two-stage toner usage predictor. 60

5.3 Procedure for developing the absorptance predictor. 61

5.4 Three different types of training pages: (a) the random text file; (b) the vertical and horizontal lines file; and (c) an 8-bits per pixel digital image. 62

5.5 A clipped portion of the text file. 62

5.6 Structure of absorptance predictor 63

5.7 Illustration of the absorptance predictor: (a) a 4-bit per pixel halftone example of the letter “k”; (b) the 5×5 predictor window with pixel index indicated (the pixel in blue is the one under estimation); (c) 5×5 absorptance predictor LUT; (d) predicted scanned image of letter “k”; and (e) scanned image of letter “k”. 64

5.8 Procedure for toner usage mapping. 65

Figure Page

5.9 Implementation of toner usage predictor. 67

6.1 Visualization tool for image graininess. 70

6.2 Visualization tool to show the scanned image graininess. 71

6.3 Scanned diagnostic page of the test suite for black cartridge. It contains text, fiducial marks, and a solid color block. 73

6.4 Text region of (a) Most unfaded sample (reference page) among the training samples; (b) Most faded sample among the training samples. 74

6.5 Entire flowchart for text fade detection algorithm. 77

6.6 The flow chart and all the technologies we used for common mask. . . . 78

6.7 (a) Common mask alignment on the binary test page. We use cyan for the binary image, and magenta for the common mask. Thus blue means overlap of the binary image with the common mask. (b) Magnification of portion of (a) to better show the alignment result. 79

6.8 (a) Histogram of measured average ΔE of all connected components for reference page. (b) Histogram of measured average ΔE of all connected components for most faded page. (c) Histogram of measured standard deviation of ΔE of all connected components for reference page. (d) Histogram of measured standard deviation of ΔE of all connected components for most faded page. 81

6.9 (a) Mean value of the histogram of the measured average ΔE for all connected components for all training pages. Dash line means the mean value of the histogram of the measured average ΔE for all connected components for testing page. (b) Mean value of the histogram of the measured standard deviation of ΔE for all connected components for all training pages. Dash line means the mean value of the histogram of the measured standard deviation of ΔE for all connected components for testing page. 82

SYMBOLS

(x, y)	continuous spatial coordinates
$[m, n]$	discrete spatial coordinates at the printer resolution
$[M, N]$	discrete spatial coordinates at high definition model prediction
$[k, l]$	discrete spatial coordinates at the scanner resolution
$g(x, y)$	continuous-tone gray scale image
$\hat{g}(x, y)$	equivalent continuous-tone gray scale image
$g[m, n]$	discrete halftone image
$s[k, l]$	scanned printed halftone
$\hat{g}[M, N]$	high definition model prediction
$\hat{g}[m, n]$	standard definition model prediction
$\tilde{g}[M, N]$	estimated measurement for high definition model
$\tilde{g}[m, n]$	estimated measurement for standard definition model
$h(x, y)$	human visual system
$p(x, y)$	point spread function
λ^*	the overall prediction of the central pixel absorptance for each specific black box model
c_g^*	the constant weight term with gray level g
W	weights vector of the black box model

ABBREVIATIONS

BBM	Black Box Model
SD-BBM	Standard Definition Black Box Model
HD-BBM	High Definition Black Box Model
EM	Estimated Measurement
SFG-BBM	Sample Function Generation Black Box Model
DBS	Direct Binary Search
HVS	Human Visual System
HCD	Hard Circular Dot
EP	Electrophotographic
PSF	Point Spread Function
CSF	Contrast Sensitivity Function
CSFT	Continuous Space Fourier Transform
OPC	Organic Photo Conductor
LUT	Lookup Table

ABSTRACT

Yanling Ju Ph.D., Purdue University, May 2015. Black-Box Printer Models and their Applications. Major Professor: Jan P. Allebach.

In the electrophotographic printing process, the deposition of toner within the area of a given printer addressable pixel is strongly influenced by the values of its neighboring pixels. The interaction between neighboring pixels, which is commonly referred to as dot-gain, is complicated. The printer models which are developed according to a pre-designed test page can either be embedded in the halftoning algorithm, or used to predict the printed halftone image at the input to an algorithm being used to assess print quality.

In our research, we examine the potential influence of a larger neighborhood (45×45) of the digital halftone image on the measured value of a printed pixel at the center of that neighborhood by introducing a feasible strategy for the contribution. We developed a series of six models with different accuracy and computational complexity to account for local neighborhood effects and the influence of a 45×45 neighborhood of pixels on the central printer-addressable pixel tone development. All these models are referred to as Black Box Model (BBM) since they are based solely on measuring what is on the printed page, and do not incorporate any information about the marking process itself. We developed two different types of printer models Standard Definition (SD) BBM and High Definition (HD) BBM with capture device Epson Expression 10000XL (Epson America, Inc., Long Beach, CA, USA) flatbed scanner operated at 2400 dpi under different analysis resolutions. The experiment results show that the larger neighborhood models yield a significant improvement in the accuracy of the prediction of the pixel values of the printed halftone image.

The sample function generation black box model (SFG-BBM) is an extension of SD-BBM that adds the printing variation to the mean prediction to improve the prediction by more accurantly matching the characteristics of the actual printed image. We also followed a structure similar to that used to develop our series of BBMs to develop a two-stage toner usage predictor for electrophotographic printers. We first obtained on a pixel-by-pixel basis, the predicted absorptance of printed and scanned page with the digital input using BBM. We then form a weighted sum of these predicted pixel values to predict overall toner usage on the printed page. Our two-stage predictor significantly outperforms existing method that is based on a simple pixel counting strategy, in terms of both accuracy and robustness of the prediction.

1. INTRODUCTION

In this document, we look into the nonlinear printing behavior of the Electrophotographic (EP) Printers by examining the neighboring dots influence in the digital halftoning on the central pixel absorptance. And we introduce a feasible strategy to model the measured statistic data for each printer addressable pixel. This model can be applied to different situation: help to design the halftoning algorithm - models built from the dispersed-dot halftone can be applied in the model based direct binary search (DBS) algorithm, and models built from the irregular clustered-dot halftone can be used to design the irregular screen for Electrophotographic Printers; embed into other application for specific purpose. We introduce two applications for the printer model in this thesis: sample function generation black box model and toner usage prediction for Electrophotographic Printers.

1.1 Digital Halftoning

Digital halftoning is the process of representing a continuous-tone image with a limited number of tone levels. Digital halftoning is very important for reproducing continuous-tone image on the device, such as printer, that can only produce a limited number of states. The output image that produced by the digital halftoning process is called the digital halftone. One most common application of the digital halftone is used as the input to the printer, here the tone levels of the halftone represent as presence or absence of dots for binary case. The objective of halftoning is that the rendered halftone image should be visually the same as original continuous-tone image, although there will be microscopic differences between those two. The digital halftone can work since the human visual system (HVS) acts as a spatial low-pass filter, which can blur the rendered halftone image. The halftone image can

be perceived as a continuous-tone image if the differences between them are of high spatial frequency. However, human can still easily find the low frequency differences. Ulichney [1] demonstrates through many examples that halftones containing energy predominantly in the high frequency region appear pleasing because the low frequency noise is absent. That is why acceptable halftones have minimal energy content in low frequency region [2].

We can classify the halftones by the size and distribution of dots in the halftones. For example, the dispersed-dot halftone represents the gray level by modulating the density of dots, while keeping their size fixed. But the periodic clustered-dot halftone represents a gray level by modulating the size of dots, keeping their distances fixed on a regular lattice. There is another type of halftone which is studied widely in digital printing. That is irregular clustered-dot halftone which is generated using a irregular screening algorithm. Of these two types of clustered-dot halftones, periodic and irregular, periodic halftone is much smoother, but they also suffer from a serious drawback of periodic moiré artifact resulting from periodic interference between halftones of different color channels. Irregular clustered-dot halftones provide an alternative solution because there are many more irregular screens than regular ones and they provide a larger set of screen combinations to aviod the periodic interference [3, 4].

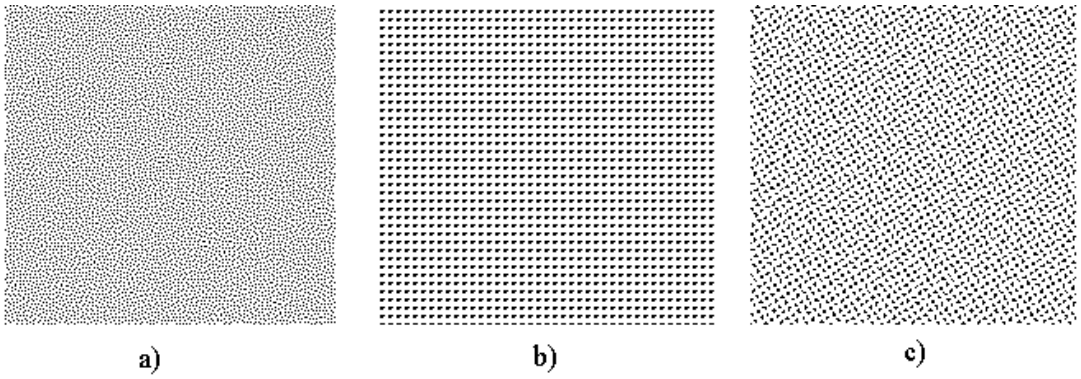

Fig. 1.1. Example of aperiodic dispersed-dot halftone a), periodic clustered-dot halftone b), and irregular clustered-dot halftone c).

Even though we can design the halftones for all the three mentioned types to have spectral energy outside the visible low frequency region, there exist the most appropriate type halftone for different type of printer. For example, printers using InkJet technology can print stable isolated dots, therefore, dispersed-dot halftones can be printed using InkJet printers well. Printers using LaserJet technology cannot render isolated dots stably, and lead to many artifacts such as banding in midtone and dot-withdrawal in highlight. Therefore, we will choose clustered-dot halftones as the preferable type for LaserJet printers [5, 6].

1.2 Printer Model

For Electrophotographic Printer, the deposition of toner within the area of a given printer addressable pixel is strongly influenced by the halftone values of the immediately neighboring pixels. To account for these effects, it is necessary to embed a printer model in the halftoning algorithm when applying the halftoning process. Traditional halftoning algorithms assume that there is no interaction or just additive ones between neighboring dots. This means that the absorptance of a printed binary pattern is linearly proportional to the number of black dots printed on the paper, and we can assume a logical OR at dot placement locations to resolve the multiple dot overlap. This is an ideal assumption that does not hold for most printers. The actual printed result may differ substantially from that which might be expected based on the bitmap generated by the halftoning algorithm. The nature and source of these differences will vary depending on the marking technology – be it electrophotography or inkjet, and the specific characteristics of the print mechanism. With electrophotography, the deposition of toner within the area of a given printer-addressable pixel is strongly influenced by not just the halftone value at that pixel, but also by the halftone values of the immediately neighboring pixels. This local influence can be attributed to the fact that the spot size of the laser write beam is larger than a single printer addressable pixel; the complex field interactions that are set up by the

charge distribution on the photoconductor and in the toner in the gap between the photoconductor and the developer, and how this influences development; the further spreading of toner during the transfer and fusing processes; and optical scattering of incident light within the media.

For Electrophotographic Printer, the printed image is often darker than expected. This phenomenon is called dot gain and it is nonlinear. Several approaches have been taken to account for this nonlinear behavior [7]. One approach is to use clustered-dot textures. Clustered-dot screens are very suitable for the printing processes that cannot render stable isolated dots, but they result in visible dot texture and loss of detail because the clustered-dot halftone textures have more energy at lower frequencies. The second approach is to use tone correction. This gives correct average tone but does not give good detail rendition. The third approach is to use a printer model within the halftoning algorithm [8].

Among the different derived printer models, the most commonly used is the hard circular dot (HCD) printer model. The HCD model assumes that the shape of the black dots produced by a printer is a circular spot with constant absorptance, and multiple dot overlap is resolved by a logical OR [7,9–14]. But Baqai suggested that at higher resolutions, the HCD model will not accurately predict the microstructure of the dots printed with the EP processl [8]. The stochastic printer model is another type of commonly used printer model [8, 15–17]. Lin and Wiseman [15] proposed the use of a stochastic printer model for an EP printer that is based on a probability density function to model the random placement of toner particles on a microlattice. Flohr and Allebach [17] used it to improve DBS textures. Unfortunately, incorporating these stochastic models within the DBS algorithm is computationally very expensive. Moreover, the efficacy of these methods is dependent on how well the probability density function models the actual printer behavior.

Our approach for modeling the nonlinear behavior between pixels is a tabular equivalent grayscale model. The tabular equivalent grayscale model based on empirically determined parameters was first proposed by Pappas and Dong [13] in 1993.

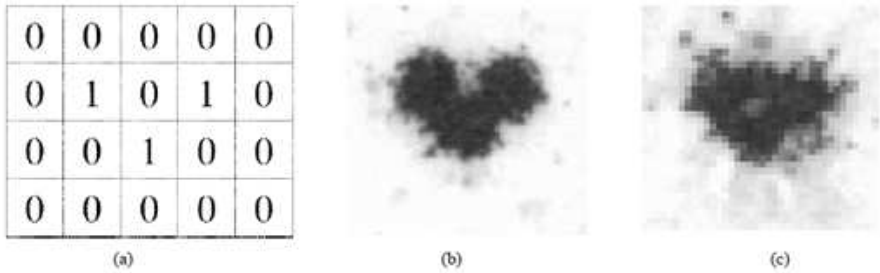

Fig. 1.2. Digital halftone (a) and 4000 dpi scan of its print sample resulting from HP LaserJet 4M prints at (b) 300 dpi, and (c) 600 dpi (magnified by 2).

Pappas and Dong determined the parameters of their model via a macroscale approach. They printed specially designed halftone patches and measured the large-area average absorptance of these patches. They then solved a set of linear equations to determine the parameter values. It has proven to be an effective means to deal with non-ideal printer behaviors. Baqai and Allebach [8] determined the parameters of their tabular equivalent grayscale model via a microscale approach. For their 3×3 model, they printed all 512 instances of the binary halftone pattern of this size, and used fiducial marks to estimate the value of the center printer-addressable pixel within this 3×3 region. They then incorporated this model within the search-based DBS algorithm. This type of model has also been successfully used to improve stochastic, dispersed-dot halftone image quality for inkjet printers [18].

The tabular equivalent grayscale model was extended to account for the influence of a larger 5×5 neighborhood on the printed absorptance of a given printer-addressable pixel with stochastic, dispersed-dot [19], and stochastic, clustered-dot [20] halftone textures. It was further extended [21–23] to account for the influence of an even larger 45×45 neighborhood that is intended to capture the effect of long-path scattering of light between the point where it is incident on the surface of the printed media and where it finally exits, known as the Yule-Nielsen effect [24]. More recently, a similar model was proposed to predict toner usage with dry toner laser EP print-

ers [25]. We refer to all these models as Black Box Model (BBM), since they are based solely on measuring what is on the printed page, and do not incorporate any information about the marking process itself.

1.3 Black Box Printer Models and Their Applications

In this work, we will first research on the potential influence of a larger neighborhood of the digital halftone image on the measured value of a printed pixel at the center of that neighborhood with HP Indigo Press. Although the redearch was done with HP Indigo Press, our results and ideas can be broadly applied to all electrophotographic printers.

Indigo is a series of digital offset printing presses developed by Benny Landa in Ness Ziona, Israel. The technology of HP Indigo Digital Presses is based on HP ElectroInk, which uses small colour particles suspended in imaging oil that can be attracted or repelled by means of a voltage differential. The liquid ink forms a very thin and smooth plastic layer on the paper surface. These particles are so small that the printed image does not mask the underlying surface roughness/gloss of the paper, bringing Indigo printing closer in appearance to conventional offset lithography. The hot transfer blanket of the press maintains high quality with substrate independence and minimal impact on the substrate with no fusers. HP Indigo Digital Presses can achieve a high image quality at a high printing speed. Studies present a general review of HP Indigo technology and presses [26–28]. An organic photoconductor foil is placed on a rotating drum. After passing a charging unit which is scorotron or charged roller, a latent image is created by a multi-beam laser scanning unit. The ink is developed onto the latent image by one of the colored ink development stations. After ink transfers to the blanket using an electric field, the carrier liquid is evaporated off onto the hot blanket, and the resultant hot melted ink is transferred to the substrate by means of pressure and tackiness. The latent image directly dictates the amount of toner that gets deposited on the exposed regions, and hence primarily determines

the resulting absorptance on the corresponding parts of the printed paper [19]. The developed toner mass at any point in the image is a nonlinear function of the halftone in the neighborhood of that point. This influence of large neighboring dots is believed to be due to the scattering of light within the media, rather than the other factors mentioned above.

As a conservative estimate of the size of this larger neighborhood, we take it to be a 45×45 region of 1/812.8 × 1/812.8 in^2 printer addressable pixels for the Indigo Press [21]. We developed a series of six models with different accuracy and computational complexity to account for local neighborhood effects and the influence of a 45 × 45 neighborhood of pixels on the central printer-addressable pixel tone development. We developed two different types of printer models Standard Definition (SD) BBM and High Definition (HD) BBM with capture device Epson Expression 10000XL (Epson America, Inc., Long Beach, CA, USA) flatbed scanner operated at 2400 dpi under different analysis resolutions. The experiment results show that the larger neighborhood models yield a significant improvement in the accuracy of the prediction of the pixel values of the printed halftone image.

The sample function generation black box model (SFG-BBM) is an extension of SD-BBM that adds the printing variation to the mean prediction to improve the prediction by more accurantly matching the characteristics of the actual printed image. We also followed a structure similar to that used to develop our series of BBMs to develop a two-stage toner usage predictor for electrophotographic printers. We first obtained on a pixel-by-pixel basis, the predicted absorptance of printed and scanned page with the digital input using BBM. We first obtain a predicted scanned page from the digital input using the BBM. We then form a weighted sum of these predicted pixel values to predict overall toner usage on the printed page. Our two-stage predictor significantly outperforms existing an method that is based on a simple pixel counting strategy, in terms of both accuracy and robustness of the prediction.

The rest of the thesis is organized as follows. In chapter 2 we present the notation and equation development for our printer model, accompanied with its intuitive ex-

planation. In Chapter 3, we will indicate a description of our SD-BBM and HD-BBM with the respective modeling and testing results and also the comparison between SD and HD model. In chapter 4 we will discuss in detail the first application for our BBMs: SFG-BBM which is an extension of SD-BBM that adds the printing variation to the mean prediction to improve the prediction by more accurantly matching the characteristics of the actual printed image. In chapter 5, we develop a two-stage toner usage predictor for electrophotographic printers by following a structure similar to that used to develop our series of BBMs. In Chapter 6, we will talk about the printed image quality evaluation technique. We will introduce an means for automatic detection of text fade point with Color Laser Printer. And finally, conclusions are drawn in Chapter 7.

2. REVIEW OF PRINTER MODEL

In this chapter, we present the notation and equation development for printer models, and the background of printer model to explain our technique.

2.1 Notation

Throughout this article, we use (x, y) for continuous spatial coordinates, $[m, n]$ for discrete spatial coordinates at the printer resolution, $[M, N]$ for discrete spatial coordinates at the resolution of high definition model prediction, and $[k, l]$ for discrete spatial coordinates at the scanner resolution. Their units are inches and pixels, respectively. The function $g[m, n]$ denotes the discrete halftone image which is input to the printer. The function $s[k, l]$ denotes the scanned printed halftone, $\tilde{g}[m, n]$ and $\tilde{g}[M, N]$ denote the estimated measured printed halftone from $s[k, l]$. $\hat{g}[m, n]$ denotes the standard definition model prediction that is predicted from $g[m, n]$ using our standard definition black box model. $\hat{g}[M, N]$ denotes the high definition model prediction that is predicted from $g[m, n]$ using our high definition black box model. For each pixel of $g[m, n]$ the absorptance value can only take on values of 0 (white) or 1 (black), while each pixel of $s[k, l]$, $\tilde{g}[m, n]$, $\tilde{g}[M, N]$, $\hat{g}[m, n]$, and $\hat{g}[M, N]$ has an absorptance value between 0 and 1.

We use $g(x, y)$ denotes the continuous-tone gray scale image, and $\hat{g}(x, y)$ denotes the equivalent continuous-tone gray scale image. Perceptual characteristics of a human viewer can be modeled as a low-pass, linear shift-invariant filtering operation. The model for HVS point spread function (PSF) is denoted by $h(x, y)$, and the point spread function of printer is denoted by $p(x, y)$. Perceived image of $g(x, y)$ is denoted as $\tilde{g}(x, y)$. Perceived image of $\hat{g}(x, y)$ is denoted as $\tilde{\hat{g}}(x, y)$. Let X be the distance between addressable pixels, then we have

$$g(x,y) = \sum_{m,n} g[m,n]p(x - mX, y - nX), \tag{2.1}$$

The HVS model is based on the contrast sensitivity function (CSF) of the human visual system. For monochrome halftoning we can use only the luminance CSF based on Näsänen's model [29]. The luminance spatial frequency response $H(\bar{u},\bar{v})$ based on Näsänen's model is

$$H(\bar{u},\bar{v}) = a\Gamma^b exp(-\frac{\sqrt{\bar{u}^2+\bar{v}^2}}{cln\Gamma + d}) \tag{2.2}$$

Here we use $a = 131.6, c = 0.525, d = 3.91, \Gamma$ is the average luminance of the light reflected from the print in cd/m^2, and (u,v) are the spatial frequency coordinates in $cycle/degree$ subtended at the retina. The HVS filter $h(\bar{x},\bar{y})$ can be obtained from the inverse 2-D Continuous Space Fourier Transform (CSFT) of $H(\bar{u},\bar{v})$. The unit of $(\bar{x},\bar{y})$ is $radian$ subtended at the retina, then we convert it to units measured on the printed image by using the approximation as

$$\bar{x} = tan^{-1}(\frac{x}{D}) \approx \frac{x}{D}, \tag{2.3}$$

where D is the distance, $x \ll D$, thus

$$h(x,y) = (\frac{1}{D})^2 h(\frac{x}{D}, \frac{y}{D}). \tag{2.4}$$

We can calculate the perceived image $\tilde{g}(x,y)$ by convolving the continuous image $g(x,y)$ with $h(x,y)$. Here we use $**$ to denote 2-D convolution, and X to be the distance between addressable pixels.

$$\begin{aligned} \tilde{g}(x,y) &= g(x,y) ** h(x,y), \\ &= \sum_{m,n} g[m,n]p(x - mX, y - nX) ** h(x,y), \\ &= \sum_{m,n} g[m,n]\tilde{p}(x - mX, y - nX), \end{aligned} \tag{2.5}$$

where

$$\tilde{p}(x,y) = p(x,y) ** h(x,y). \tag{2.6}$$

The perceived equivalent gray scale image $\hat{g}(x, y)$ can also be calculated in terms of the discrete equivalent gray scale image $\hat{g}[m, n]$, the printer spread function $p(x, y)$, and the human visual system point spread function $h(x, y)$.

$$\begin{aligned}\tilde{\hat{g}}(x, y) &= \hat{g}(x, y) * *h(x, y), \\ &= \sum_{m,n} \hat{g}[m, n]p(x - mX, y - nX) * *h(x, y), \\ &= \sum_{m,n} \hat{g}[m, n]\tilde{p}(x - mX, y - nX).\end{aligned} \tag{2.7}$$

Figure 2.1 shows a HVS filter for $D = 16$ inches and resolution $R = 812.8$ dpi, which is the printing resolution of HP Indigo press 5000.

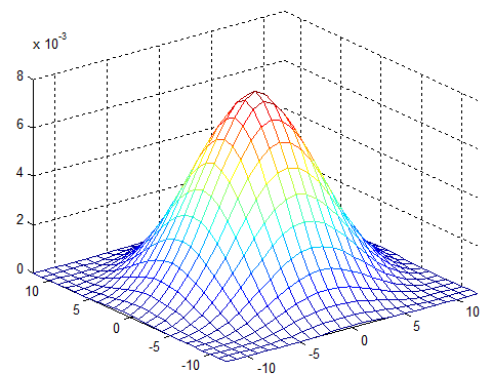

Fig. 2.1. Example of human visual system filter.

2.2 Equation Development for Printer Model

The equivalent grayscale image can be generated by summarizing dot gain effects of each printer addressable pixel over entire $X \times X$ printer addressable pixels. We can calculate the difference between the equivalent grayscale image $\hat{g}(x, y)$ with the continuous-tone image $g[x, y]$. The error between the perceived equivalent gray scale image $\tilde{\hat{g}}(x, y)$ and the perceived continuous-tone image $\tilde{g}(x, y)$ is

$$
\begin{aligned}
\epsilon &= \int\int \left|\tilde{\hat{g}}(x,y) - \tilde{g}(x,y)\right|^2 dxdy, \\
&= \sum_{m,n}\sum_{k,l}\int\int |(\hat{g}[m,n] - g[m,n])\tilde{p}(x - Xm, y - Xn)|^2 dxdy, \\
&= \sum_{m,n}\sum_{k,l} e[m,n]e[k,l]c_{\tilde{p}\tilde{p}}[m-k, n-l],
\end{aligned}
\tag{2.8}
$$

where

$$
e[m,n] = \hat{g}[m,n] - g[m,n], \tag{2.9}
$$

$$
c_{\tilde{p}\tilde{p}}[m,n] = \int\int \tilde{p}(x,y) - \tilde{p}(x - Xm, y - Xn)dxdy. \tag{2.10}
$$

Here each pixel of $\hat{g}[m,n]$ can have a absorptance value between 0 and 1. Then for stochastic printer model, we take $\Phi = E\{\epsilon\}$ to be the error metric where E denotes the expectation.

$$
\begin{aligned}
\Phi = E\{\epsilon\} &= E\left\{\sum_{m,n}\sum_{k,l} e[m,n]e[k,l]c_{\tilde{p}\tilde{p}}[m-k, n-l]\right\}, \\
&= \sum_{m,n}\sum_{k,l} \bar{e}[m,n]\bar{e}[k,l]c_{\tilde{p}\tilde{p}}[m-k, n-l] \\
&+ \sum_{m\neq k}\sum_{n\neq l} cov(e[m,n], e[k,l])c_{\tilde{p}\tilde{p}}[m-k, n-l] + \sum_{m,n}\sigma_{\hat{g}^2}[m,n]c_{\tilde{p}\tilde{p}}[0,0].
\end{aligned}
\tag{2.11}
$$

The first term of 2.11 can be calculate from the equivalent grayscale image, the second term has a relation to the covariance between pixels, and the third term is the summation of the predicted variance of each pixel times a constant term.

2.3 Review of Printer Model

Printer models can be embedded into the halftoning algorithm to try to obtain a more accurate halftoning result. Algorithms that have embedded printer model for the printing process assume either linear or nonlinear dot interaction. Most printer models assume the interaction between neighboring dots is additive. If we consider an ideal printer model, the printer spread function $\Omega(x,y)$ can be expressed as

$$\Omega(x, y) = rect(x, y). \tag{2.12}$$

But as mentioned above, this ideal printer model is not true for real printers. For example, for electrophotographic printers, the deposition of toner within the area of a given printer addressable pixel is strongly influenced by not just the halftone value at that pixel, but also the halftone values of the neighboring pixels. This means that the developed toner mass at any pixel in the image is a nonlinear function of the halftone in the neighborhood of that pixel. The nonlinear term may be caused by several phenomena: a) overlap of the Gaussian laser beam used to write the latent image on the organic photo conductor (OPC); b) field effects during development; and c) toner particle displacement and distortion during transfer and fusing. A critical concept is the equivalent grayscale image $\hat{g}[m, n]$ which summarizes dot gain effects of each printer addressable pixel over entire $X \times X$ printer addressable pixels [8]. The equivalent grayscale image is defined to have the same average absorptance on a pixel-by-pixel basis as the actual printed halftone image. Under this assumption, we have the equation for the discrete equivalent grayscale image using Model-$X \times X$ as

$$\hat{g}[m, n] = \Omega_{model}\{g[m + k, n + l], (k, l) \in [-K : K]^2\}, \tag{2.13}$$

where $(2K + 1) = X$, and $[-K : K]^2$ denotes the X^2 point set of 2-tuples formed by the cartesian product of $[-K : K]^2$ with itself, and Ω denotes the transformation of the binary value to the equivalent grayscale value of the center pixel. When K = 1, the printer model should predict the central pixel absorptance using the 3×3 neighborhood [8]. When K = 2 the neighborhood to be considered is 5×5 [19, 20]. When K = 22 the neighborhood to be considered is 45×45 [21, 22].

For Model-3×3, there are 512 (2^9) different 3×3 dot patterns. To ensure the full characterization of the HP Indigo Press for Model-3×3, we design test pages that include all 512 different dot patterns; print the test pages on the HP Indigo Press 5000 at a resolution of 812.8 dpi; scan the printed test pages using an Epson Expression10000 XL scanner at a resolution of 2400 dpi; and then analyze the scanned test

pages to estimate the mean and standard deviation of the central pixel absorptance of each 3×3 dot pattern. Specifically, our estimation of the mean and standard deviation of the central pixel absorptance for each 3×3 dot pattern is given by the sample mean and sample standard deviation of the corresponding scanned dot patterns. We store these estimated values in a lookup table (LUT). LUT is the stochastic model-3×3. We will use this model to generate both an equivalent grayscale image and the equivalent sample variance of this image. Figure 2.2 shows how to use the model to generate the equivalent grayscale image. The procedure for generating the equivalent sample variance image is similar.

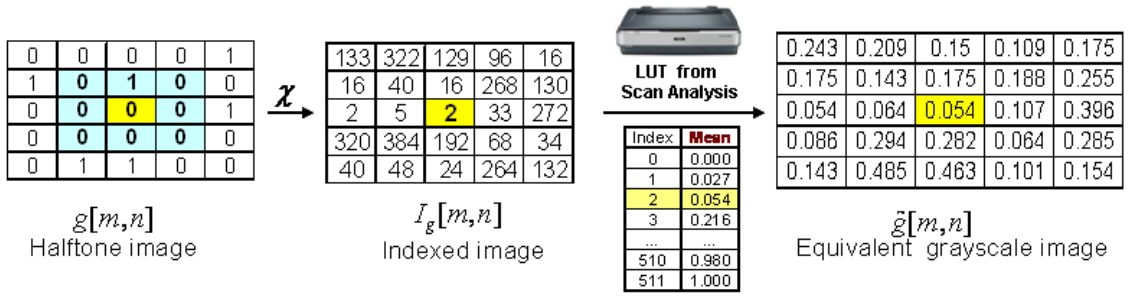

Fig. 2.2. Using Model-3×3 to generate the equivalent grayscale image.

The printer model was extended to account for the influence of a larger 5×5 neighborhood on the printed absorptance of a given printer-addressable pixel [19, 20]. We use a similar approach to generate the Model-5×5. Since the number of all possible 5×5 dot profiles is 2^{25}, it is impossible to print all 5×5 dot configurations. To develop a feasible approach, it is assumed that dots in the outer ring of the 5×5 neighborhood have an additive influence on the central pixel absorptance. We consider all 512 3×3 inner dot configurations, and then randomly choose a set of M different 5×5 outer dot configurations as the training set.

We use the least squares method to find the optimal weights for each of the 16 dots in the outer ring of the 5×5 neighborhood. The additive contribution of the

dots present in the outer ring of the 5×5 neighborhood can be computed using the optimal weights. For the unbiased linear model we have the equation,

$$\lambda_{i,j} = \lambda_{i,0} + \Psi_j^T W_i + c_i, \tag{2.14}$$

where i is the index of 3×3 dot configuration, j is the index of 5×5 outer dot configuration, Ψ_j denotes the 16×1 vector corresponding to the jth binary 5×5 outer dot configuration in the training set, W_i denotes the 16×1 weight vector that characterizes the additive influence of dots in the outer ring of the 5×5 neighborhood on the central pixel mean absorptance of the ith 3×3 dot configuration, c_i is a constant term that corrects the model bias, $\lambda_{i,j}$ is the central pixel absorptance of the ith 3×3 dot configuration with the jth 5×5 outer dot configuration, and $\lambda_{i,0}$ is the central pixel absorptance of the ith 3×3 dot configuration without considering the contribution of the 5×5 outer ring. The equation for the discrete equivalent grayscale image is

$$\hat{g}[m,n] = \Omega_{model}\{g[m+k, n+l], (k,l) \in [-2:2]^2\}, \tag{2.15}$$

where $[-2:2]^2$ denotes the 25 point set of 2-tuples formed by the cartesian product of $[-2:2]^2$ with itself, and Ω denotes the transformation of the binary value to the equivalent grayscale value of the center pixel [19]. The procedure for generating the sample variance image is similar.

3. BLACK BOX PRINTER MODEL

In this chapter, we will describe the print-to-scan analysis procedure for modeling large area (45×45 $1/812.8 \times 1/812.8\,\text{in}^2$ printer addressable pixels) influence in digital halftoning and how to develop the stochastic models for the Electrophotographic Printers using the estimated data. All the test pages are printed on the HP Indigo Press 5000 at a resolution of 812.8 dpi. As an Electrophotographic Printer, as we discussed in Chapter 2, the printed dot of the HP Indigo Press 5000 is not round and solid black but a random distribution of colorant at a higher resolution. We first examine the printed dot profile performance of HP Indigo Press 5000 using Epson Expression 10000 XL scanner at a resolution of 2400 dpi and also Personal Image Analysis System II ($PIAS^{TM} - II$), which is a high-performance digital microscope introduced by QEA to enable quick, quantitative print quality evaluation. Then we use the print-to-scan analysis procedure to estimate the printed absorptance for each printer addressable pixel, and use the analysis data to build the BBMs for Electrophotographic Printers. We will validate the BBMs on the testing page which has different dot patterns than the training page. We also develope two different types of printer models SD-BBM and HD-BBM with capture device Epson Expression 10000XL (Epson America, Inc., Long Beach, CA, USA) flatbed scanner operated at 2400 dpi under different analysis resolutions.

3.1 Print-to-Scan Analysis Procedure

The black box models are developed for the HP Indigo Press 5000. We assume that the distribution of toner that get transferred is uncorrelated from the $X \times X$ cell to the next $X \times X$ cell. The printer model developed by Goyal [19] calculated the absorptance of a pixel using its 5×5 neighborhood. In this thesis we explain in detail

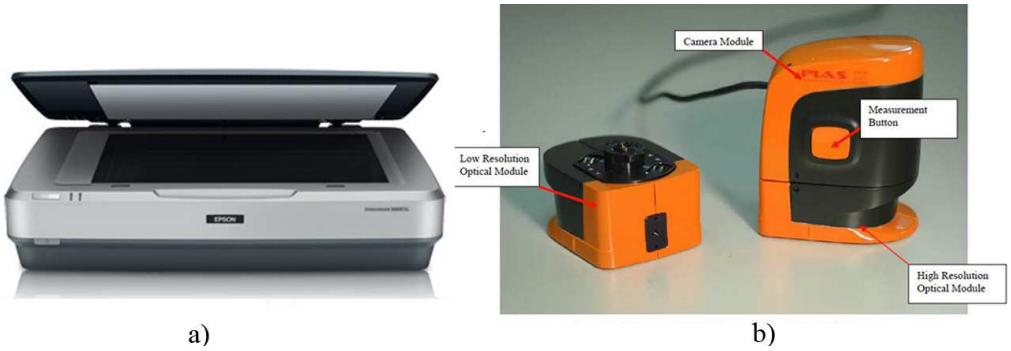

Fig. 3.1. Epson Expression 10000 XL scanner (a) and Personal Image Analysis System II (b).

the print-to-scan analysis procedure for modeling large area (45×45 1/812.8 × 1/812.8 in^2 printer addressable pixels) influence in digital halftoning on the absorptance value of the central pixel of the printed 45×45 dot patterns for the Electrophotographic Printers. The larger neighborhood size: 45×45 printer addressable pixels, is carefully selected according to a series of experiments.

Figure 3.2 shows the major steps in the print-to-scan procedure that we use to establish the relationship between the digital halftone sent to the printer and the average absorptance of each region corresponding to a single printer-addressable pixel (standard definition models) or a subpixel within one printer-addressable pixel (high definition models) in the scanned printed page. We first design test pages for our black box models. The test page has different 101×101 pixels irregular clustered-dot halftone patches, each with four 3×3 pixels adjoining fiducial marks. We then print the designed test pages on an HP Indigo Press 5000 at a resolution of 812.8 dpi, and scan the printed pages using an Epson Expression 10000XL scanner at a resolution of 2400 dpi. We then analyze these scanned images to generate the parameters for the six models that are listed in Table 3.1.

Figure 3.3 shows the major steps for the scanned test page analysis, we first perform scanner gray balancing to calibrate the scanned pages to units of absorptance. Specifically, the calibrated scanner gray values are proportional to 1 minus the CIE

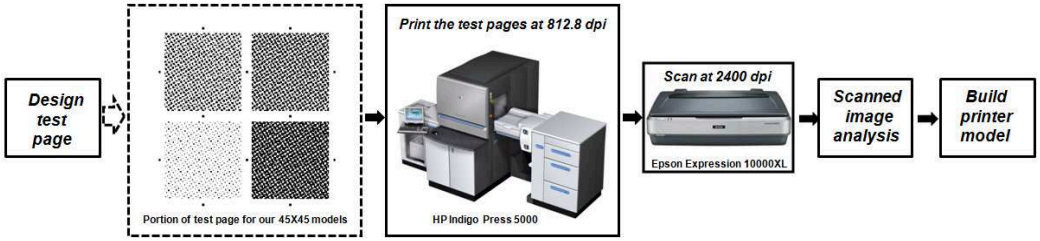

Fig. 3.2. Print-to-scan analysis procedure for the black box models.

Y (luminance) value scaled to lie between 0 and 1. We then estimate the center coordinates (here we use the centroid) for each fiducial mark. The centroid of each fiducial mark is calculated based on the spatial distribution of toner absorptance throughout its corresponding mask region. The horizontal and vertical centroids of the i-th segmented fiducial mark are given by Eq. 3.1.

$$C_{x,i} = \frac{\sum_{[k,l]\in D_i}(k-0.5)s[k,l]}{\sum_{[k,l]\in D_i} s[k,l]}, C_{y,i} = \frac{\sum_{[k,l]\in D_i}(l-0.5)s[k,l]}{\sum_{[k,l]\in D_i} s[k,l]}, \tag{3.1}$$

where D_i is the corresponding binary mask for the i-th fiducial mark in the binary mask image. The binary mask image is generated using the Otsu's method [30]. The parameter $s[k,l]$ is the absorptance value of the scanned image at the pixel with coordinates $[k,l]$. The 0.5 pixel offset in both parts of Eq. 3.1 shifts the effective coordinate location of each pixel to its center.

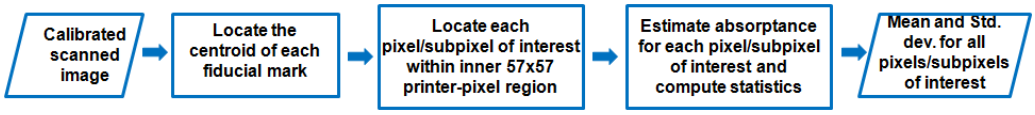

Fig. 3.3. Analysis of scanned printed test pages analysis for black box models.

Figure 3.4 shows the sub-scanner-pixel estimation of the absorptance of each pixel/subpixel of interest for SD and HD BBM, to account for misregistration between the printer and scanner lattices and the non-integer ratio of their resolutions.

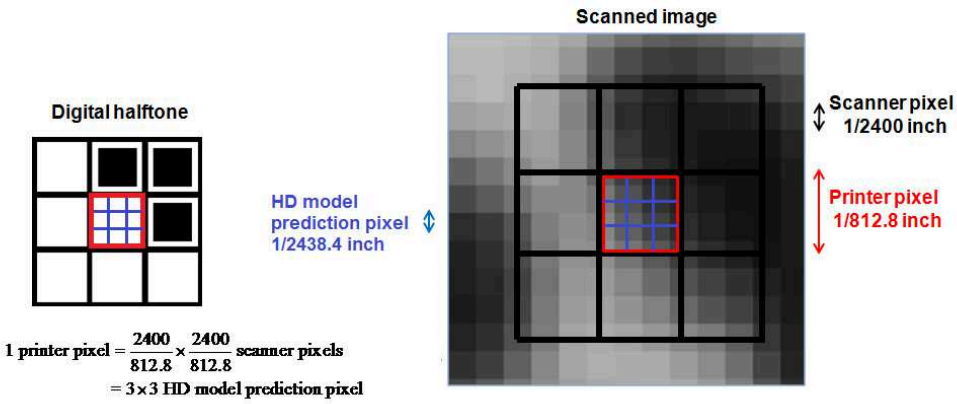

Fig. 3.4. Sub-scanner-pixel estimation of the absorptance of each pixel/subpixel of interest for SD and HD BBM, to account for misregistration between the printer and scanner lattices and the non-integer ratio of their resolutions.

For standard definition black box model, the absorptance for each printer pixel is calculated by averaging the absorptance over the scanned pixels that correspond to a priter addressable pixel. After obtaining pixel absorptance value and its statistic data for all pixels of interest, we introduce different structures to model the influence of the outer neighorhood on the central pixel measurement.

To obtain the estimated measurement for standard definition black box model, for each 101×101 pixel halftone patch shown in Fig. 3.2, we use the estimated centroid of the four adjoining fiducial marks to estimate the location of the center of each printer-addressable pixel in the scanned image, corresponding to one of the 57×57 pixels in the inner region of the digital halftone image that was sent to the printer. Let us consider the pixel at coordinates $[m, n]$ corresponding to the digital halftone value $g[m, n]$. Our target printer prints at 812.8 dpi; and we scan the images at 2400 dpi; so this printer-addressable pixel corresponds to a $2400/812.8 \times 2400/812.8$ region in the scanned image, where the units are scanner-addressable pixels. Since the center of this region will generally not be located at the center of a pixel in the scanned image; and the ratio 2400/812.8 is not integer value, we use a sub-scanner-pixel procedure

to estimate the average absorptance $\tilde{g}[m,n]$ corresponding to this printer-addressable pixel. Let $\Omega_{m,n}$ denote the set of $1/2400 \times 1/2400$ inch^2 scanner pixels $s[k,l]$ that overlap either wholly or partially with this region. In general, $\Omega_{m,n}$ will contain 16 pixels, as shown in Fig. 3.4. We form the estimate $\tilde{g}[m,n]$ as a weighted sum of the pixels in $\Omega_{m,n}$, where the $[k,l]$-th weight $\omega_{m,n}[k,l]$ is equal to the fractional intersection of the region of the $[k,l]$-th scanner pixel with the $2400/812.8 \times 2400/812.8$ region centered at the location of the $[m,n]$-th printer-addressable pixel. This relationship is shown in Eq. 3.2.

$$\tilde{g}[m,n] = \sum_{[k,l]\in\Omega_{m,n}} \omega_{m,n}[k,l]s[k,l]. \tag{3.2}$$

After obtaining the absorptance of all pixels of interest, we estimate the sample mean $\tilde{g}$ and sample standard deviation $\tilde{\sigma}_g$ of the absorptance of each pixel of interest from the corresponding scanned printed halftone patches. We then can introduce the different structures, which will be described in the next section to model the influence of the neighborhood on the central pixel mean and standard deviation of absorptance.

For high definition black box model, we calculate the absorptance for each sub-pixel by averaging the absorptance over the scanned pixels that correspond to one sub-priter-addressable pixel. We use a similar print-to-scan analysis procedure as that we use for standard definition models, except that the pixels of interest and the means to measure the absorptance for each pixel of interest are different.

For high definition estimation, we increase the resolution of the 101×101 printer-addressable pixel halftone image from 812.8 dpi to 2483.4 dpi by deviding each printer-addressable pixel to 3×3 subpixels. We then estimate the absorptance of all subpixels of interest in the inner region of the 101×101 printer-addressable pixel halftone image. Let us consider the printer-addressable pixel at coordinates $[m,n]$ corresponding to the digital halftone value $g[m,n]$. It has nine subpixels. Our target printer prints at 812.8 dpi; and we scan the images at 2400 dpi; so each subpixel of interest [M,N] within the $[m,n]$ printer-addressable pixel halftone corresponds to a $\frac{2400}{812.8\times3} \times \frac{2400}{812.8\times3}$ region in the scanned image, where the units are scanner-addressable pixels. We use a sub-scanner-pixel procedure to estimate the average absorptance $\tilde{g}[M,N]$ corresponding

to each subpixel within $[m, n]$ printer-addressable pixel, since the center of this region will generally not be located at the center of a pixel in the scanned image; and the ratio $\frac{2400}{812.8\times3}$ is not integer value. Let $\Omega_{M,N}$ denote the set of $1/2400 \times 1/2400$ inch^2 scanner pixels $s[k, l]$ that overlap either wholly or partially with this region. In general, $\Omega_{M,N}$ will contain 4 pixels, as shown in Fig. 3.4. We form the estimate $\tilde{g}[M, N]$ as a weighted sum of the pixels in $\Omega_{M,N}$, where the $[k, l]$-th weight $\omega_{M,N}[k, l]$ is equal to the fractional intersection of the region of the $[k, l]$-th scanner pixel with the $\frac{2400}{812.8\times3} \times \frac{2400}{812.8\times3}$ region centered at the location of the $[M, N]$-th subpixel. This relationship is shown in Eq. 3.3.

$$\tilde{g}[M, N] = \sum_{[k,l]\in\Omega_{M,N}} \omega_{M,N}[k, l]s[k, l]. \tag{3.3}$$

After obtaining the absorptance of all subpixels of interest, we estimate the sample mean $\tilde{g}$ and sample standard deviation $\tilde{\sigma}_g$ of the absorptance of each subpixel of interest from the corresponding scanned printed halftone patches. We then can introduce the structure of M45 $\times$ 45, which will be described in the next section, to model the influence of the neighborhood on the central subpixel mean and standard deviation of absorptance. Since we have $3 \times 3 = 9$ subpixels within each printer-addressable pixel, we will have 9 sets of BBM for all subpixels within the printer-addressable pixel, respectively.

3.2 Preliminary Experiments for Large Area Influence

We design experiments to test the accurancy of the fiducial mark registration method, and the large area influence on the central pixel tone development.

3.2.1 Printed dot profile performance

Since the printed dot of the HP Indigo Press 5000 is not round and solid black but a random distribution of colorant at a higher resolution, we want to examine the printed dot profile performance to accurately locate the center coordinates for each

printer addressable pixel. We print 3×3 ($1/812.8 \times 1/812.8$ in^2 printer addressable) pixels black dot which has the same size as the fiducial mark that we use in training page for stochastic model, on one page using HP Indigo Press 5000. The capture devices that we use here are Epson Expression 10000 XL scanner and also Personal Image Analysis System II. PIAS$^{TM} - II$ is a portable, low-cost, easy-to-use image analysis system. It has both high- and low-resolution optical modules with very good capture capability that can be used as a comparison with Epson Expression 10000 XL scanner. We scan the printed 3×3 printer addressable pixels black dots using Epson Expression 10000 XL scanner at a resolution of 2400 dpi in two directions: 0 degree and 90 degree rotation of the page. We capture the image of each printed 3×3 printer addressable pixels black dots using PIAS$^{TM} - II$ with high-resolution optical modules (the captured image has a resolution of 7663.375 dpi) also in two directions: 0 degree and 90 degree rotation of the page. We then calibrate the scaned and captured 3×3 printer addressable pixels black dots and estimate the centroid coordinates for each black dot based on the spatial distribution of toner absorptance according to Eq. 3.1. We assume that the centroid of the black dot is the center coordinates, and the pixel where the center coordinates locate is defined as central pixel.

We compute the mean absorptance of each capture device pixel using all the replications for this pixel according to the estimated central pixel. We use contour to illustrate the printed black dot profile. Figure 3.5 shows the the contour of mean absorptance of the printed 3×3 printer pixels black dot profile. For Epson Expression 10000XL scanner, the contours for two scan directions show that the scanner elongate the black dot in the process direction a little bit in the outer region, but when absorptance=0.5 the contour is almost round. While for PIAS, it has almost the same capture capability in different directions. For both capture devices, the estimated centroid coordinates can be used as the center of the black dot, which means we can use the same method in the analysis of training page for stochastic printer models to locate each pixel.

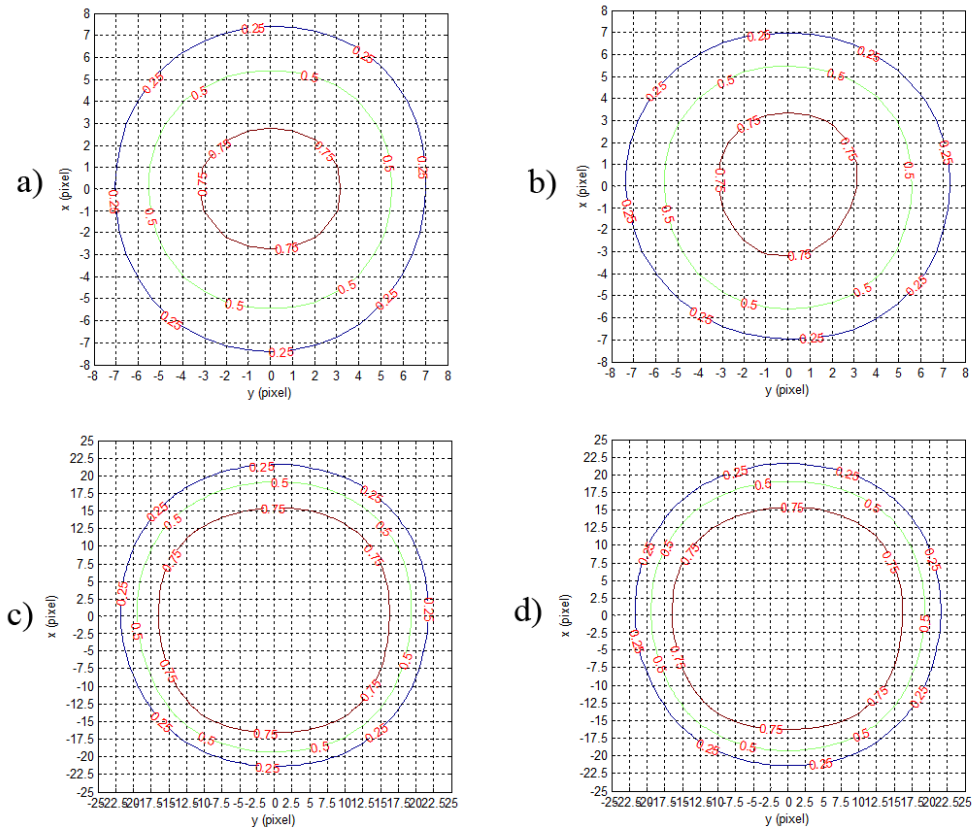

Fig. 3.5. Contour of mean absorptance of the printed 3×3 printer addressable pixels black dot profile. a) scan using Epson scanner with 0° rotation, b) scan using Epson scanner with 90° rotation, c) PIAS with 0° rotation, d) PIAS with 90° rotation.

3.2.2 Large area influence in digital halftone

We want to measure the large area influence in digital halftoning, and determine the size of the neighborhood that we need to consider for the estimation of central pixel mean and standard deviation of absorptance. We first generate a set of varisized test patterns that use a stochastic, dispersed-dot digital halftones as the dot configuration. Portion of the test page is shown in Fig. 3.6(a), we increase the size of pattern from 5×5 to 45×45, while keeping the inner neighborhood the same. All the patterns are printed for 50 replications. We then analyze the absorptance of the central pixel for

each printed varisized dot patterns. Figure 3.6(b) shows the variation tendency of measured mean absorptance as the size of test pattern change. As a conservative estimate of the size of this larger neighborhood, we take it to be a 45×45 region of $1/812.8 \times 1/812.8$ in^2 printer addressable pixels for the Indigo press.

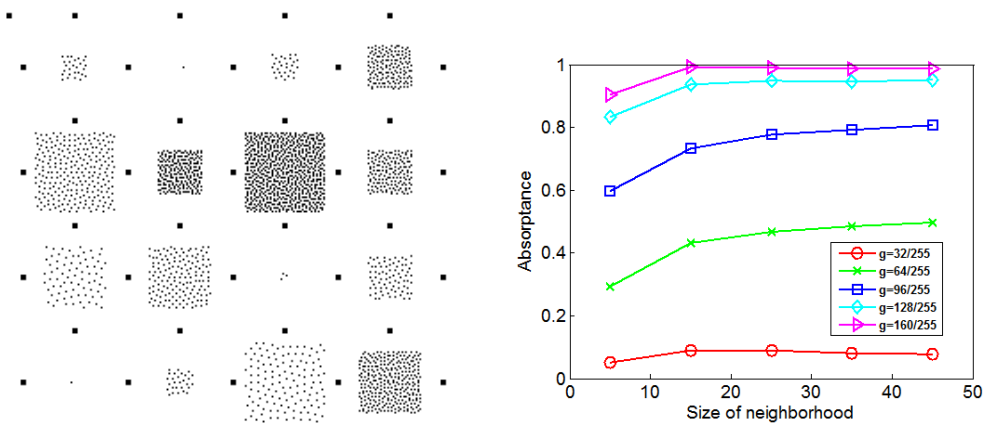

(a) (b)

Fig. 3.6. Large-area influence in digital halftoning: (a) portion of test page, (b) experiment result.

We also print a set of test patterns that use a stochastic, dispersed-dot digital halftone texture as the outer $45 \times 45 - 5 \times 5$ neighborhood, and same 5×5 dot configuration as the 5×5 inner neighborhood. We analyze the absorptance of the central pixel for each printed 45×45 dot patterns. The results show that when the patterns have the same averaged value in the outer $45 \times 45 - 5 \times 5$ neighborhood, the fluctuation of the measured absorptance of the central pixel for all those patterns are within the standard deviation value. We call the percentage of the total number of dots printed in the $45 \times 45 - 5 \times 5$ neighborhood the gray level of the neighborhood. The results mean that it is possible to account for the influence of this larger neighborhood with a function of only the gray level of the larger neighborhood.

3.3 Model-5×5

Model-45×45 is the extension and improvement of Model-5×5. We first generate the Model-5×5 for HP Indigo Press 5000 as a comparison for Model-45×45. We use print-to-scan analysis and assume an unbiased linear model to incorporate the influence of dots in the outer ring of the 5×5 neighborhood.

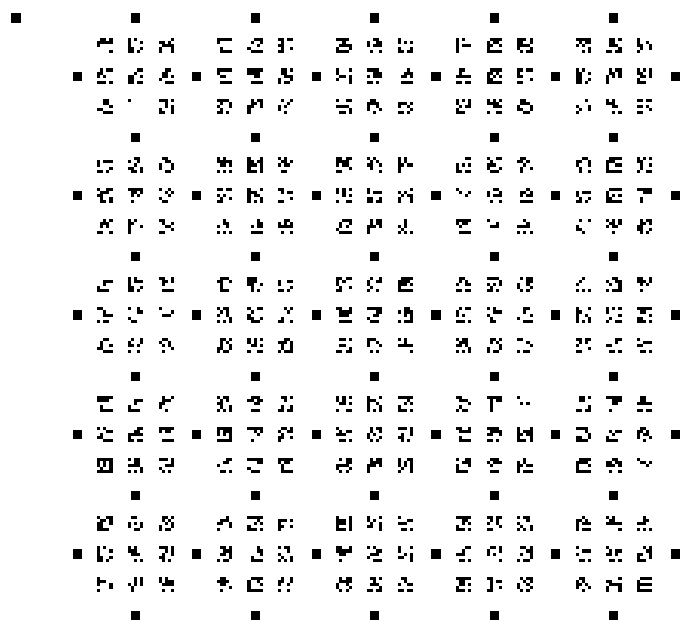

Fig. 3.7. Test page for Model-5×5.

For Model-5×5, there are 512 (2^9) different 3×3 inner dot patterns and 16 outer neighborhoods. Comparing with Goyal's Model-5×5 [19], we re-design the test page to reduce the number of pages, while maintaining accurate and robust results. We design test pages that include all the 512 different inner 3×3 dot patterns and 160 randomly chosen different 5×5 outer neighborhoods, which can make $512 \times 160 = 81,920$ different 5×5 dot patterns. To solve the alignment problem, each 3×3 group of nine 5×5 dot patterns is surrounded by four fiducial marks. Each 5×5 dot pattern is replicated 50 times to average out the inherent printer instability. Altogether, we have six test pages with each page containing $86 \times 160 \times 50 = 688,000$ patterns. The

distance between the fiducial marks and the 5×5 dot pattern is set to be large enough to ensure that the fiducial marks do not influence the dot development of the 5×5 dot pattern. Fig. 3.7 shows portion of such a test page. We print the test pages on the HP Indigo Press 5000 at a resolution of 812.8 dpi, and scan the printed images using Epson Expression10000 XL scanner at a resolution of 2400 dpi. We analyze the scanned test pages to estimate the mean and standard deviation of the absorptance of the central printer addressable pixel. To analyze the scanned test pages, we first perform scanner gray balancing to calibrate the scanned image to units of absorptance, and then estimate the center coordinates (here we use centroid) for each fiducial mark. The centroid of each fiducial mark is calculated based on the spatial distribution of toner absorptance throughout its corresponding mask region.The horizontal and vertical centroids of the ith segmented fiducial mark are given by Eq. 3.1.

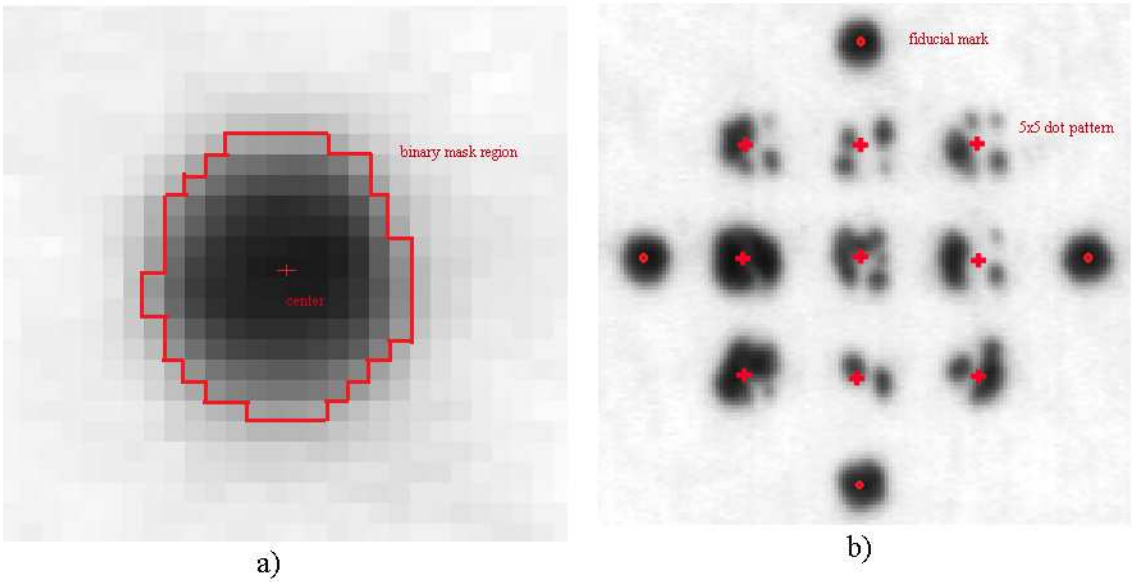

Fig. 3.8. a) estimate the centroid of the fiducial mark, b) locate the center for all dot pattern.

The center of the dot pattern can be computed using the estimates of the centroids of the fiducial marks. Next, we use this center to calculate the absorptance of

the 2400/812.8 × 2400/812.8 scanned pixels that correspond to the central pixel of the printed dot pattern. The estimates of the mean and standard deviation of the absorptance of the central pixel of each 5×5 dot pattern are given by the sample mean and sample standard deviation of the corresponding scanned dot patterns. We store the estimates of the mean and standard deviation absorptance of the central pixel of the 3×3 dot configurations without any dots in the outer 5×5 ring as a lookup table (LUT). LUT is the stochastic Model-3×3. For unbiased linear model, the central pixel mean absorptance of any 5×5 dot configuration is the sum of the central pixel mean absorptance of the corresponding 3×3 dot configuration with no dots in the outer 5×5 ring and the additive contribution of the dots present in outer ring of the 5×5 neighborhood, which is characterized by a set of weight parameters. Equation 3.4 shows this model.

$$\begin{aligned} \lambda_{i,j}^{predicted-5\times5} &= \lambda_{i,0}^{measured-3\times3} + \psi_j^T w_i^{Model-5\times5} + c_i^{Model-5\times5}, \\ &= \lambda_{i,0}^{measured-3\times3} + \Psi_j^T W_i^{Model-5\times5}, \end{aligned} \tag{3.4}$$

Here i is the index of the 3×3 dot configuration, j is the index of the 5×5 outer dot configuration, $\lambda_{i,j}^{predicted-5\times5}$ is the predicted central pixel mean absorptance of the ith 3×3 dot configuration with the jth 5×5 outer dot configuration, $\lambda_{i,0}^{measured-3\times3}$ is the measured central pixel mean absorptance of the ith 3×3 dot configuration without the 5×5 outer ring, ψ_j denotes the 16×1 vector corresponding to the jth 5×5 outer ring in the training set, $w_i^{Model-5\times5}$ denotes the 16×1 weight vector that characterizes the additive influence of the dots in the outer ring of the 5×5 neighborhood on the central pixel mean absorptance of the ith 3×3 dot configuration, and $c_i^{Model-5\times5}$ denotes the constant offset term that removes the model bias. In the second line of Eq. 3.4, we absorb the constant offset term within the weight vector by augmenting ψ_j^T with a 1 to yield the 17×1 vector Ψ_j^T, and then augmenting $w_i^{Model-5\times5}$ with $c_i^{Model-5\times5}$ to yield the 17×1 vector $W_i^{Model-5\times5}$. Applying the least squares method, we obtain the optimal weights

$$W_i^{Model-5\times5} = argmin\{\Psi_j^T W_i^{Model-5\times5} - \Delta\lambda_i\}, \tag{3.5}$$

Thus,

$$W_i^{Model-5\times5} = (\Psi^T\Psi)^{-1}\Psi^T\Delta\lambda_i, \tag{3.6}$$

where

$$\Delta\lambda_i = \left[\lambda_{i,1}^{measured-5\times5} - \lambda_{i,0}^{measured-3\times3}, ..., \lambda_{i,M}^{measured-5\times5} - \lambda_{i,0}^{measured-3\times3}\right]. \tag{3.7}$$

Here, $\lambda_{i,j}^{measured-5\times5}$ denotes the measured central pixel absorptance value for the ith dot configuration in the inner 3×3 region and the jth dot configuration in the outer 5×5 ring for each of the $j = 1, ..., M$ outer configurations, averaged over the 50 printed replications of each of these 5×5 patterns. These data are used to train the weight vector $W_i^{Model-5\times5}$ for the ith 3×3 dot configuration. The parameter $\lambda_{i,0}^{measured-3\times3}$ is the measured central pixel absorptance value for the ith dot configuration in the inner 3×3 region without dots in the outer 5×5 ring. We used $M = 160$ in our experiments. The experimental results will be shown in the next section as a comparison with BBM-45×45.

3.4 Black Box Model-45×45

For a large neighborhood, for example, in this paper we consider a 45×45 window, there are 2^{45^2} different possible dot configurations. It is impossible to print all such dot configurations to measure the absorptance of the central pixel. We need to find a feasible strategy for the model-45×45. Based on our above experiments, it is possible to account for the influence of this larger neighborhood with a function of only the gray level of the larger neighborhood. Under this assumption, we can choose different gray levels 45×45 halftone patterns as our dot configurations to built the Model-45×45. For example, to choose the 45×45 dot configurations for Model-45×45 for irregular, clustered-dot halftone texture, we first generate a large irregular, clustered-dot halftone image for the continuous image under some screening algorithm. We then randomly choose a set of different 45×45 dot patterns from the large halftone image without considering the inner 5×5 dot configuration. We will use this set of 45×45 dot patterns to design the training page for the Model-45×45 for irregular,

clustered-dot halftone texture. Using this strategy to choose 45×45 dot patterns can keep the inner 5×5 dot configuration and the outer $45 \times 45 - 5 \times 5$ neighborhood consistant. And we can improve the design of the test page for our 45×45 models to yield more accurate and more robust results with fewer pages.

3.4.1 Test page design for Model-45×45

In this thesis, we choose 32 different gray levels for Model-45×45 for irregular, clustered-dot halftone texture. The 32 different gray levels are choosen according to the tone reproduction curve of the HP Indigo Press 5000 for irregular, clustered-dot digital halftone.

To find the tone reproduction curve, we print 31 large halftone patterns on HP Indig Press 5000. Each halftone pattern has a differnt gray level. The gray levels of the digital halftones are chosen as 8/255, 16/255, . . ., 248/255. We scan the printed halftone patterns using Epson Expression 10000 XL, and then calibrate the scaned image using scanner gray balancing. For each gray level, we average the printed absorptance pixel-to-pixel within the entire halftone pattern for this gray level. The tone reproduction curve which is the mapping of average gray value of the input halftone to averaged absorptance of the output print, is a piecewise linear interpolation of 31 different averaged absorptance of the printed halftones as a function of 31 different gray leves of digital halftones. As shows in Fig. 3.9, the tone reproduction curve is different for different texture.

To design the training page and testing page for Model-45×45 for irregular, clustered-dot halftone texture, we first choose 32 different averaged printed absorptance as 4/255, 12/255, . . ., 252/255, and the gray levels of digital halftone can be calculated from the tone reproduction curve for irregular, clustered-dot halftone texture. For each gray level, we generate a large irregular, clustered-dot digital halftone image for the constant image with this gray level using an irregular screen, and next step we randommly choose 4 differnt 101×101 dot patches from this large halftone

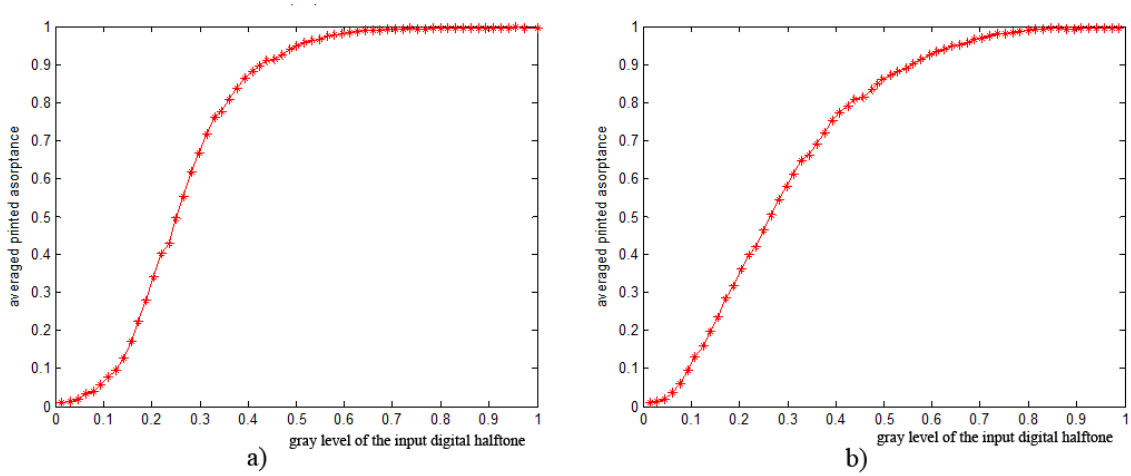

Fig. 3.9. Tone reproduction curve for HP Indigo Press 5000. a) tone reproduction curve for dispersed-dot halftones, b) tone reproduction curve for clustered-dot halftones.

image. Each of the inner $(101-45)\times(101-45)$ pixel has a 45×45 neighborhood, and will be considered as an interested printer addressable pixel. We will use the measured data for all the interested printer addressable pixels to generate Model-45×45. We then randommly distributed all the $32\times4=128$ unique binary 101×101 dot patterns in one test page, each with 50 replications. Each of the inner $(101-44)\times(101-44)$ pixel has a 45×45 neighborhood, and will be considered as an interested printer addressable pixel. So there are totally $32\times4\times50=6,400$ halftone patches, and $57\times57\times4\times50=649,800$ interested printer addressable pixels for each gray level. We will use the measured data for all the interested printer addressable pixels to generate Model-45×45 for irregular, clustered-dot halftone texture. To solve the alignment problem, each dot pattern is surrounded by four 3×3 printer pixels fiducial marks. We have only one training page and it contains 4 subpage. Figure 3.10 shows the training page and portions of the training page for irregular, clustered-dot halftone texture. We use the same training and testing pages for standard definition and high definition black box Model-45×45.

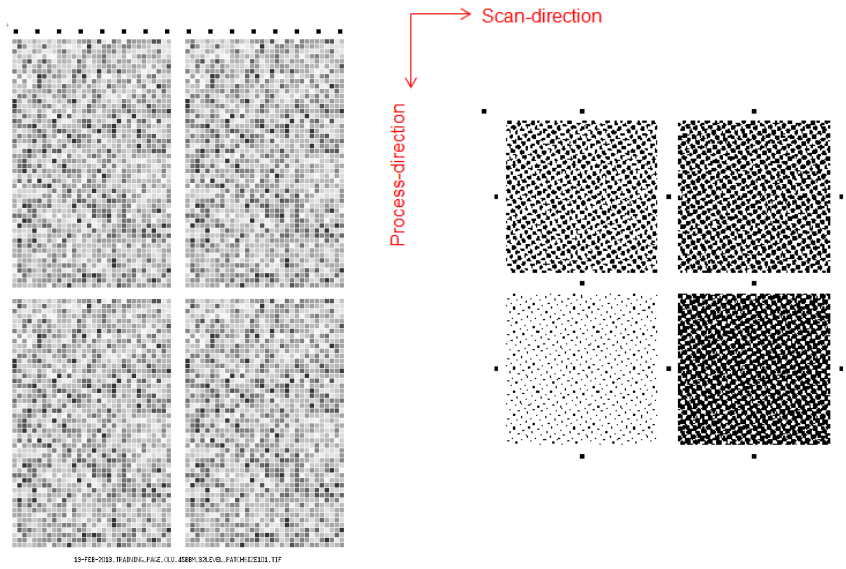

(a) (b)

Fig. 3.10. (a) Test page for Model-45×45 for irregular, clustered-dot halftone texture, (b) Portion of test page. Each of the four halftone squares in (b) corresponds to one of the small squares in (a). The fiducial marks in (b) are used to register the pixels in the scanned image of the printed test page to the pixels in the digital image sent to the press.

3.4.2 Structure of black box Model-45×45

We describe six new models that are divided into three classes, as shown in Table 3.1. The new models offer a variety of improvements over the previous models in terms of the number of free parameters, the number of test pages needed to parameterize the model, the number of computations required to predict each printed pixel value, and the model fit and prediction errors that can be achieved with the model. Each one of the six models has two different instantiations with identical structure, but different parameters. One is used to predict the average absorptance value at each printer-addressable pixel in the halftone image. The other is used to predict the standard deviation of the absorptance at that pixel. This latter statistic is used to characterize

the stability with which a given local configuration in the halftone image can be printed. It is an intrinsic feature in the probabilistically-based direct binary search (DBS) algorithm that leads to more stable halftone textures, and thereby reduced grain and mottle [8, 18–20]. In addition, in this thesis the models are developed for irregular, periodic clustered-dot halftones.

We summarize the equations for the 45×45 models in Table 3.1. We use λ^* to denote the overall prediction of the central pixel absorptance for each specific black box model, and use c_g^* as the constant weight term with gray level g. $\lambda_{i,j}^{5\times5}$ is the prediction using model ULM5×5 described in [19] and [20]. In the second step, we absorb the constant weight term within the weight vector to make a neat equation, which is good for least squares regression to determine the optimal weights.

For Model-45×45 Class 1a and Class 1b, we combine the Model-45×45 training data with the ULM5×5. We assume that the dots in the 45×45 - 5×5 neighborhood have an additive influence on the central pixel absorptance, which is called correction weight term in this document. We consider two different approaches for the correction weight term. In the first approach, named Class 1a, the correction weight term is just a constant contribution of the 45×45 - 5×5 neighborhood depending on the gray level. In the second approach, named Class 1b, the correction weight term is a sum of the weighted contribution of inner 5×5 neighborhood and the constant contribution of the 45×45 - 5×5 neighborhood depending on its gray level.

Model-45×45 Class 2a and Class 2b are two lower dimensional models. We use only the measured absorptance values of the Model-45×45 training page to build these two models. To account for the influence of the inner 5×5 neighborhood on the central pixel mean and standard deviation of estimated measured absorptance, we optimize 25 weights for all the pixels within the inner 5×5 neighborhood. The difference between these two models is that for Class 2a, the 25 weights w^{2a} are gray level independent, while for Class 2b, the weights w_g^{2b} are gray level dependent.

For Class 3a and Class 3b, we introduce a totally different strategy to account for the influence of the inner 5×5 neighborhood on the central pixel mean and standard

Table 3.1.
Computational structure of the black box models.

Model	Equation	Neighbor-hood size
[1]ULM5×5	$\lambda_{i,j}^{5\times5} = \lambda_{i,0} + \psi_j^T w_i^{5\times5} + c_i^{5\times5} = \lambda_{i,0} + \Psi_j^T W_i^{5\times5}$	5×5
[2]M45×45 C1a	$\alpha_{i,j,g}^{1a} = \lambda_{i,j}^{5\times5} + c_g^{1a}$	45×45
[2]M45×45 C1b	$\alpha_{i,j,g}^{1b} = \lambda_{i,j}^{5\times5} + \psi_{i,j}^T w_g^{1b} + c_g^{1b} = \lambda_{i,j}^{5\times5} + \Psi_{i,j}^T W_g^{1b}$	45×45
[3]M45×45 C2a	$\alpha_{i,g}^{2a} = \psi_i^T w^{2a} + c_g^{2a} = \Psi_{i,g}^T W^{2a}$	45×45
[3]M45×45 C2b	$\alpha_{i,g}^{2b} = \psi_i^T w_g^{2b} + c_g^{2b} = \Psi_i^T W_g^{2b}$	45×45
[4]M45×45 C3a	$\lambda_{i_1,\ldots,i_4,g}^{3a} = \sum_{k=1}^{4} w_{i_k}^k + c_g^{3a} = \Psi_{i,g}^T W^{3a}$	45×45
[4]M45×45 C3b	$\lambda_{i_1,\ldots,i_5,g}^{3b} = \sum_{k=1}^{5} w_{i_k}^k + c_g^{3b} = \Psi_{i,g}^T W^{3b}$	45×45

[1] Here $\lambda_{i,0}$ is the measured central pixel absorptance of the i-th 3×3 dot configuration without the 5×5 ring, ψ_j denotes the dot distribution in the j-th 5×5 ring, and $w_i^{5\times5}$ are the weights corresponding to the dots in the 5×5 ring.

[2] Here i, j, and g are the indices of the 3×3 dot configuration, the 5×5 outer ring, and the gray level in the outer 45×45 - 5×5 neighborhood, respectively. $\psi_{i,j}$ states the dot distribution of the inner 5×5 dot configuration. We absorb the constant weight term within the weight vector by augmenting $\psi_{i,j}$ with a 1 to yield the vector $\Psi_{i,j}$.

[3] Here i and g are the indices of the 5×5 inner dot configuration and the gray level in the outer 45×45 - 5×5 neighborhood, respectively. ψ_i states the dot distribution of the inner 5×5 dot configuration.

[4] Here i_1, i_2, i_3, i_4, and i_5 are the indices of the five different 3×3 neighborhood located in the inner nerghborhood 5×5. $\Psi_{i,g}$ is a $(512 \times K + 32) \times 1$ vectors , where $K = 4$ (C3a), or 5 (C3b). The k-th block of 512 elements, $k = 1, ..., K$ contains a single 1 at the location indexed by i_k, and 0s elsewhere. Similarly, the final 32 locations contains a single 1 at the position corresponding to index of the average gray level in the outer 45×45-5×5 neighborhood quantized to the 32 levels in the training page.

deviation of the estimated measured absorptance, by summing the contributions of four or five overlapping 3×3 neighborhoods, respectively, within the 5×5 neighborhood of the pixel to be predicted.

Table 3.2.
Summary of black box model statistics.

Model	Description	No. of pages	No. of parameters	Computation per pixel*
ULM5×5	LUT indexed according to configuration of binary halftone within 3×3 neighborhood + 16 weights for outer ring + constant	6	9216	17 adds 16 muls
M45×45 C1a	ULM5×5 + gray-level-dependent† constant	7	9248 ‡	18 adds 16 muls
M45×45 C1b	ULM5×5 + 25 gray-level-dependent weights for inner 5×5 + gray-level-dependent constant	7	10048	43 adds 41 muls
M45×45 C2a	25 weights for inner 5×5 + gray-level-dependent constant	1	57	25 adds 25 muls
M45×45 C2b	25 gray-level-dependent weights for inner 5×5 + gray-level-dependent constant	1	832	25 adds 25 muls
M45×45 C3a	4 overlapping 3×3 LUTs in inner 5×5 region + gray-level-dependent constant	1	2080	4 adds
M45×45 C3b	5 overlapping 3×3 LUTs in inner 5×5 region + gray-level-dependent constant	1	2592	5 adds

†For all models, estimation of gray level is based on the average value of the digital halftone within 45×45 - 5×5 pixel outer region.

‡For all models with gray-level-dependent parameters, a separate parameter is used for each of the 256 gray levels.

*Number of additions (adds) and number of multiplications (muls).

To make these ideas a bit more concrete, as an example, we next describe Models-45 × 45 Class 3a and Class 3b in more detail. Figure 3.11 shows the structure of Model 45×45 Class 3a. This model separately looks at the binary halftone configuration within each of four different overlapping 3×3 neighborhoods located in the inner 5×5 neighborhood of the pixel whose value is to be predicted, and the average gray level within the outer 45×45 - 5×5 neighborhood to generate its predictions. From Fig. 3.11, we may conclude that the model requires 6 table lookups, 2 multiplies, and 5 additions per pixel to predict either mean absorptance or the standard deviation of mean absorptance. This includes the computation required to perform the interpolation shown in the bottom left corner of Fig. 3.11. For Class 3b we add the inner 3×3 as the fifth 3×3 neighborhood, and use five different 3×3 neighborhoods to better account for the influence of the inner 5×5 neighborhood on the pixel whose value is to be predicted. Since we have 512 different 3×3 dot configurations for each 3×3 neighborhood, we need to optimize 512 × 4 weights for Class 3a, and 512 × 5 weights for Class 3b. And we still have one constant offset term for each gray level that we use in the training page to account for the influence of the outer 45×45 - 5×5 neighborhood on the center.

The optimal weights for all these models can be estimated from the training data set by using a least squares method:

$$\begin{aligned} W^{optimal} &= argmin\{\Psi^T W - \alpha\}, \\ &= (\Psi^T \Psi)^{-1} \Psi^T \alpha. \end{aligned} \tag{3.8}$$

Table 3.2 summarizes the parameters, number of test pages, and storage and computation required for each of the seven models shown in Table 3.1, and discussed above.

3.4.3 Standard definition black box Model-45×45

Following the flow chart we described above, we first print the training page for Model-5 × 5 and Model-45 × 45 for clustered-dot halftones. We use print-to-scan

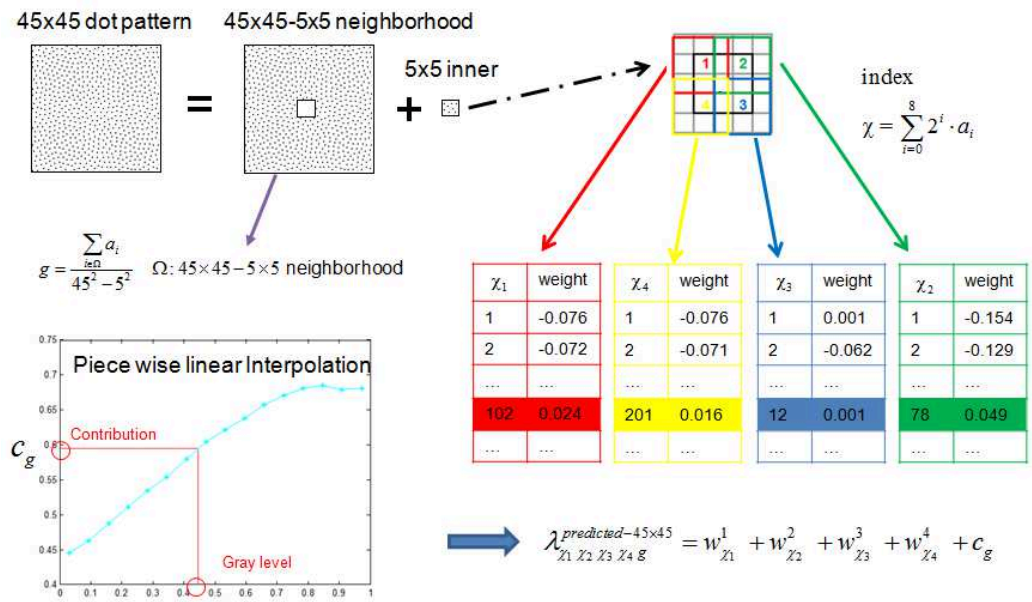

Fig. 3.11. Structure of Model-45×45 Class 3a that is used to predict both absorptance and standard deviation at a given printer-addressable pixel. The predicted value is the sum of five components. The first four components $w^k_{\chi_k}, k = 1, 2, 3, 4$, are weights obtained from lookups into four different tables indexed according to the binary halftone patterns in each of the four overlapping 3×3 neighborhoods shown. Here χ_k is the index corresponding to the 3×3 binary neighborhood. The last component c_g accounts for the contribution of the average gray value in the surrounding 45×45-5×5 neighborhood. It is computed by interpolation between 32 values stored in a LUT, as shown in the lower left. All the model parameters are trained using the test page shown in Fig. 3.10.

analysis and calculate absorptance for each printer addressable pixel and build the printer models.

We provide experimental results for training our models with the irregular, periodic clustered-dot test page shown in Fig. 3.10, printed with an HP Indigo Press 5000. We also test our black box models with a different test page. This second page for model testing includes a set of 31 gray patches with gray levels located midway between those of the halftone patches that were used to train the model. So this is effectively a cross-validation procedure. We print and scan the test page. We then

estimate the sample mean $\tilde{g}$ and sample standard deviation $\tilde{\sigma}_g$ of absorptance for each pixel of interest in the second test page using the same procedure as we did for the first test page that was used to train the models. We apply our black box models to the digital testing page and compute the predicted absorptance $\hat{g}$ or standard deviation of absorptance $\hat{\sigma}_g$ for each pixel of interest in the test page. The prediction error here is the root mean squared error between the estimated measurement of absorptance $\tilde{g}$ or standard deviation $\tilde{\sigma}_g$ and the prediction $\hat{g}$ or $\hat{\sigma}_g$. It can state the predictive capability of our black box models.

Figure 3.12 shows the model-fit and cross-validation predictor performance for 32 gray levels. The model fit error statistics are obtained by testing the predictors for mean absorptance and standard deviation of absorptance on the same data from the first test page that was used to train the models. The prediction error statistics are obtained by training the predictors on the first test page, and then testing them on data from the second test page.

Table 3.3 summarizes both the model-fit and cross-validation predictor performance averaged over 31 gray levels. We see that in all cases the error decreases monotonically as we go from ULM5×5 to M45×45 C1b to M45×45 C3b. The model M45×45 C2a has the largest error since it has the fewest parameters. Also, the cross-validation errors are generally larger than the model-fit errors, as would be expected. With respect to prediction of mean absorptance (cross-validation), we gain more than a 4× improvement in accuracy between ULM5×5 and Model-45×45 Class 3b.

Figure 3.13 shows an example of the cross-validation model prediction images and prediction error images for mean absorptance using different black box models. The example irregular, periodic clustered-dot halftone patch has an average gray level 96/255. The size of the image is 57×57 printer-addressable pixels. The prediction error images show the relative magnitude of the errors between the prediction and the measurement by identically scaling all three error images according to the largest magnitude of error observed across the three error images. In keeping with the units of absorptance in which these images are shown, darker pixels in the prediction error

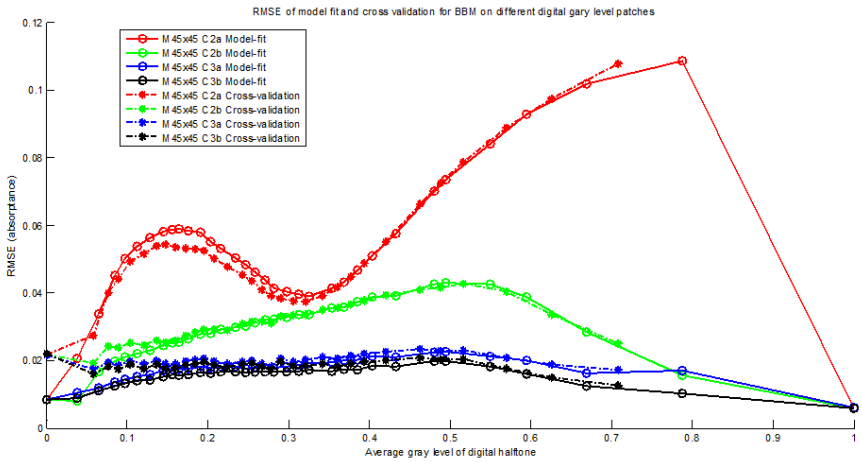

(a)

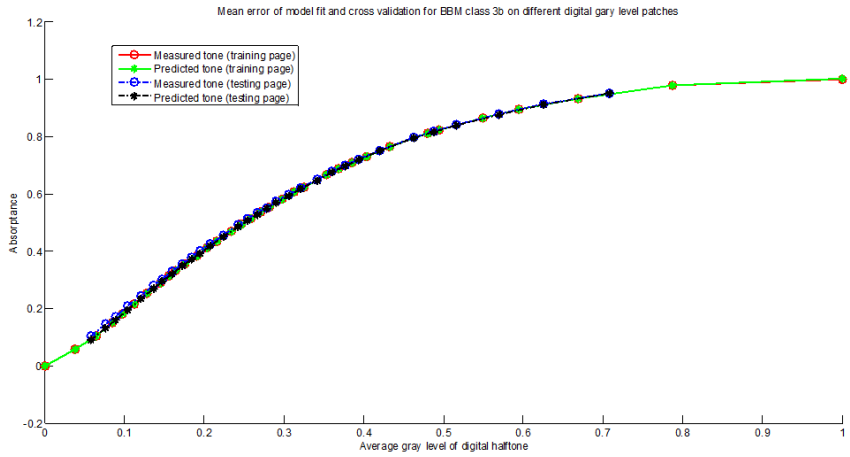

(b)

Fig. 3.12. The model-fit and cross-validation predictor performance for 32 gray levels. (a)Root mean square prediction error. (b)Mean prediction error.

images mean higher error. We can see from the prediction error images that ULM5×5 has the highest prediction error, and M45×45 Class 3b has the minimum prediction error, which is consistent with the statistics in Table 3.3 and the quality of the visual match between Fig. 3.13(c) and 3.13(e).

Table 3.3.
SD-BBM Model-fit and cross-validation prediction RMSE averaged over 31 gray levels*.

	Mean		Std. Dev.	
	Model-fit (%)	Cross-validation(%)	Model-fit (%)	Cross-validation(%)
ULM5×5	7.33	7.68	1.00	0.94
M45×45 C1a	3.77	4.17	0.91	0.89
M45×45 C1b	2.25	2.87	0.72	0.80
M45×45 C2a	5.06	4.77	1.52	1.31
M45×45 C2b	2.79	2.96	0.81	0.82
M45×45 C3a	1.83	2.17	0.70	0.70
M45×45 C3b	1.31	1.85	0.56	0.66

*All errors are in units of percent of maximum absorptance between 0 (white) and 100 (black). The gray levels span the range between 0 and 1.

3.4.4 High definition black box Model-45×45

We introduce a new procedure for a high definition black box model. This HD-BBM has a similar structure as SD-BBM regarding each pixel of interest. From the printer-resolution digital halftone, HD-BBM can predict the printed halftone image at a much higher resolution than that of the SD-BBM. For the results reported in this paper, the models are built with a capability to predict the printed halftone image at a resolution of 2438.4 dpi, which is 3 times the printer resolution and close to the scanner resolution that we use to capture the training pages. We only discuss and show the experimental results of HD M45 $\times$ 45 C3b and compare it with the SD M45 $\times$ 45 C3b with irregular clustered-dot texture in this paper. However the ideas can be broadly applicable to all 6 different black box models mentioned in our previous paper [22] and also applicable to other halftone textures, which means that it allows system designers to choose the model and halftone texture that is best-suited to their particular application.

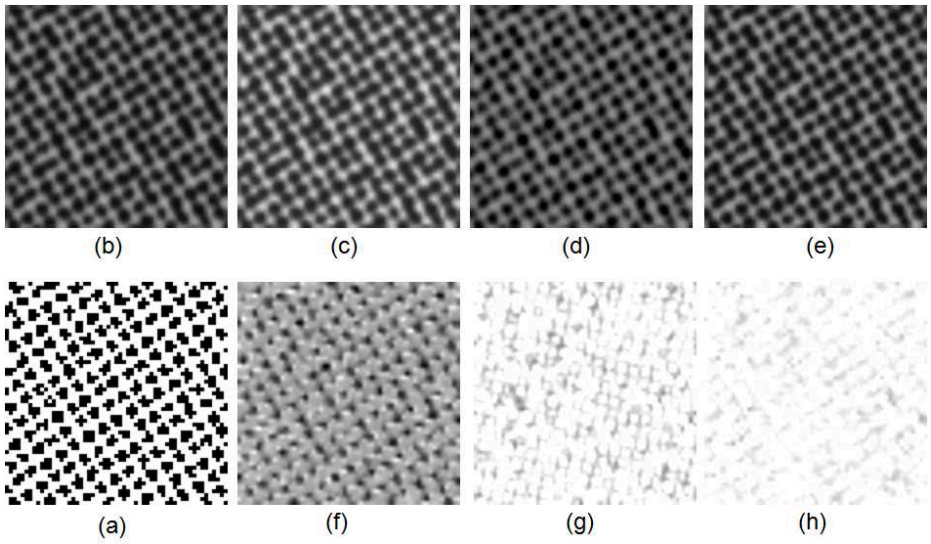

Fig. 3.13. Cross-validation model prediction images and absolute value error images for mean absorptance. The example clustered-dot halftone has an average gray level 96/255. (a) Digital halftone, (b) Estimated measurement, (c) ULM5×5 prediction, (d) M45×45 Class 2a prediction, (e) M45×45 Class 3b prediction, (f) ULM5×5 prediction error image, (g) M45×45 Class 2a prediction error image, (h) M45×45 Class 3b prediction error image. The three error images are computed by forming the absolute value of the error at each pixel, and then identically scaling the images to map the maximum across all three images to black and the minimum across all three images to white.

SD M45×45 C3b separately looks at the binary halftone configuration within each of five different overlapping 3×3 neighborhoods located in the inner 5×5 neighborhood of the pixel whose value is to be predicted, and the average gray level within the outer 45×45 - 5×5 neighborhood to generate its predictions, as in Fig. 3.11.

HD M45×45 C3b has the same structure as SD M45×45 C3b. However, for SD M45×45 C3b we optimize the contributions of the neighborhood to the central printer-addressable pixel measured absorptance. While for HD M45×45 C3b, we treat the central printer-addreassable pixel as 3×3 subpixels, and optimize the contributions of the neighborhood to measured absorptance of each subpixels within the central

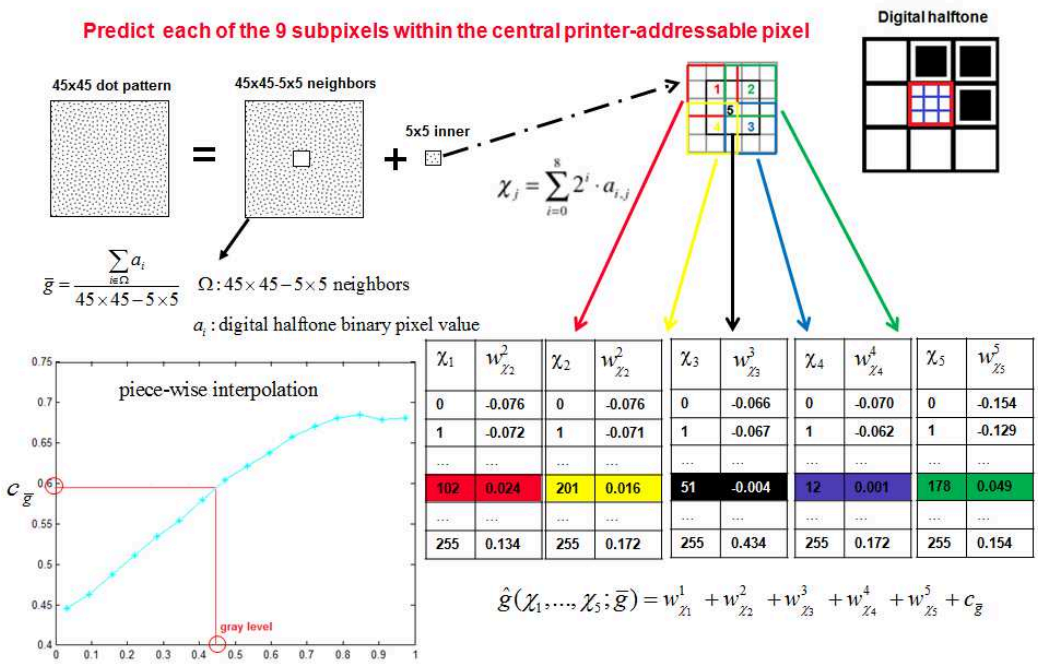

χ_1	$w^2_{\chi_2}$	χ_2	$w^2_{\chi_2}$	χ_3	$w^3_{\chi_3}$	χ_4	$w^4_{\chi_4}$	χ_5	$w^5_{\chi_5}$
0	-0.076	0	-0.076	0	-0.066	0	-0.070	0	-0.154
1	-0.072	1	-0.071	1	-0.067	1	-0.062	1	-0.129
...	...	...	...	...	...	...	...	...	...
102	0.024	201	0.016	51	-0.004	12	0.001	178	0.049
...	...	...	...	...	...	...	...	...	...
255	0.134	255	0.172	255	0.434	255	0.172	255	0.154

Fig. 3.14. Structure of HD M45×45 C3b that is used to predict both absorptance and standard deviation at a given sub-printer-addressable pixel. The predicted value is the sum of six components. The first five components $w^k_{\chi_k}, k = 1, 2, 3, 4, 5$, are weights obtained from lookups into five different tables indexed according to the binary halftone patterns in each of the five overlapping 3×3 neighborhoods shown. Here χ_k is the index corresponding to the 3×3 binary neighborhood. The last component c_g accounts for the contribution of the average gray value in the surrounding 45×45-5×5 neighborhood. It is computed by interpolation between 32 values stored in a LUT, as shown in the lower left. All the model parameters are trained using the test page shown in Fig. 3.10.

printer-addressable pixel, respectively. For each subpixel, HD M45×45 C3b model sums the contribution of each of five different overlapping 3×3 neighborhoods located in the inner 5×5 neighborhood of the pixel that the subpixel to be predicted belongs to, and the contribution of the outer 45×45 - 5×5 neighborhood to generate its predictions. We have 32 graylevels in the training page, and we have 512 different 3×3 dot configurations for each 3×3 neighborhood. We need to optimize 512×5+32 =

2592 weights for each subpixel, which makes it total $2592 \times 9 = 23,328$ weights for all subpixel within the central printer-addressable pixel.

The optimal weights for all subpixels can be estimated from the training data sets, respectively, by using a least squares method:

$$\begin{aligned} W^{optimal} &= argmin\{\Psi^T W - \alpha\}, \\ &= (\Psi^T \Psi)^{-1} \Psi^T \alpha. \end{aligned} \tag{3.9}$$

We use λ^{C3b} to denote the overall prediction of the subpixel absorptance for HD M45×45 C3b, and use $c_{j,g}^{C3b}$ as the constant weight term for $j-$th subpixel with gray level g. The equation for HD M45×45 C3b is

$$\lambda_{i_1,\ldots,i_5,j,g}^{C3b} = \sum_{k=1}^{5} w_{i_k,j}^{k} + c_{j,g}^{C3b} = \Psi_{i,j,g}^{T} W^{C3b}. \tag{3.10}$$

Here i_1, i_2, i_3, i_4, and i_5 are the indices of the five different 3×3 neighborhood located in the inner neighborhood 5×5. j is the index of the subpixel. With fixed j, $\Psi_{i,j,g}$ is a $(512 \times 5 + 32) \times 1$ vectors. The k-th block of 512 elements, $k = 1, ..., 5$ contains a single 1 at the location indexed by i_k, and 0s elsewhere. The final 32 locations contains a single 1 at the position corresponding to index of the average gray level in the outer $45 \times 45 - 5 \times 5$ neighborhood quantized to the 32 levels in the training page.

The high definition predicted scanned image $\hat{g}[M, N]$ summarize the influence of an 45×45 neighborhood of printer-addressable pixels in the digital halftone image on the subpixel $[M, N]$ which belongs the central pixel $[m, n]$ of the neighborhood. The high definition predicted scanned image is expected to have the same average absorptance on a pixel-by-pixel basis as the actual printed halftone image.

$$\hat{g}[M, N] = \Omega_{model}\{g[m + K, n + L], (K, L) \in [-22 : 22]^2\}, \tag{3.11}$$

where $[-22 : 22]^2$ denotes the 45^2 point set of 2-tuples formed by the cartesian product of $[-22 : 22]^2$ with itself, and Ω denotes the transformation of the binary value to high definition predicted scanned values of the subpixels corresponding to the binary

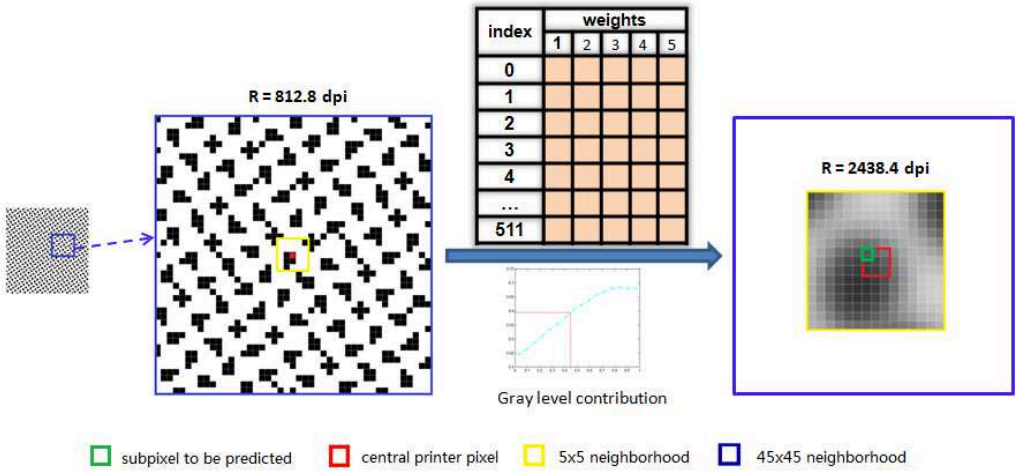

Fig. 3.15. Example of using HD M45×45 C3b to predict the absorptance of one subpixel within the corresponding printer-addressable pixel.

pixel. Figure 3.15 shows an example of how to use the HD M45×45 C3b to generate the high definition predicted scanned image.

We provide experimental results for training and testing our HD M45×45 C3b with irregular clustered-dot texture. The example test pages shown in Fig. 3.10. We printe test pages with an HP Indigo Press 5000, and scan the test pages using Epson Expression 10000XL at a resolution of 2400 dpi. We use the obtained statistics values to build the HD M45×45 C3b. We also test the HD M45×45 C3b with a different test page. We print and scan the test pages. We then estimate the sample mean $\tilde{g}$ and sample standard deviation $\tilde{\sigma}_g$ of absorptance for each pixel/subpixel of interest in the second test page using the same procedures as we did for the first test page that was used to train HD M45×45 C3b. We apply our black box models for mean absorptance and standard deviation of absorptance on the digital testing page and compute the predicted mean absorptance $\hat{g}$ and standard deviation of absorptance $\hat{\sigma}_g$ for each subpixel of interest in the testing page for HD M45×45 C3b. Table 3.4 summarizes the model-fit and cross-validation performance averaged over 32 gray levels for both SD and HD M45×45 C3b with irregular clustered-dot halftone. The

model fit error statistics are obtained by testing the predictors for mean absorptance and standard deviation of absorptance on the same data from the first test page that was used to train the models. It indicates how the models can fit the original data. The prediction error here is the root mean squared error between the estimated measurement of absorptance $\tilde{g}$ or standard deviation $\tilde{\sigma}_g$ and the prediction $\hat{g}$ or $\hat{\sigma}_g$. It can state the predictive capability of our black box models.

Table 3.4.
Model-fit and cross-validation prediction RMSE of SD and HD M45×45 C3b *.

	Mean		Std. Dev.	
	Model-fit (%)	Cross-validation(%)	Model-fit (%)	Cross-validation(%)
SD M45×45 C3b	1.31	1.85	0.56	0.66
HD M45×45 C3b	1.44	1.96	0.63	0.73

*All errors are in units of percent of maximum absorptance between 0 (white) and 100 (black). The gray levels span the range between 0 and 1.

From Table 3.4, we see that HD M45×45 C3b has a similar model-fit and corss-validation performance with SD M45×45 C3b which is our best 45×45 model. Also, the cross-validation errors are generally larger than the model-fit errors, as would be expected.

Figure 3.16 and Figure 3.17 show an example of the cross-validation model predicted images using SD and HD M45×45 C3b, and we use the HD estimated scanned printed image as ground truth, from the same digital pattern. The example irregular clustered-dot halftone patch has an average gray level 96/255. The size of the digital image is 57×57 printer-addressable pixels. We calculate the prediction error based on the ground truth for both SD and HD BBM. We observe less blurring in the HD M45×45 C3b prediction than in the SD M45×45 C3b prediction. What's more, the prediction error of the HD-BBM is much lower than the prediction error of the SD-BBM.

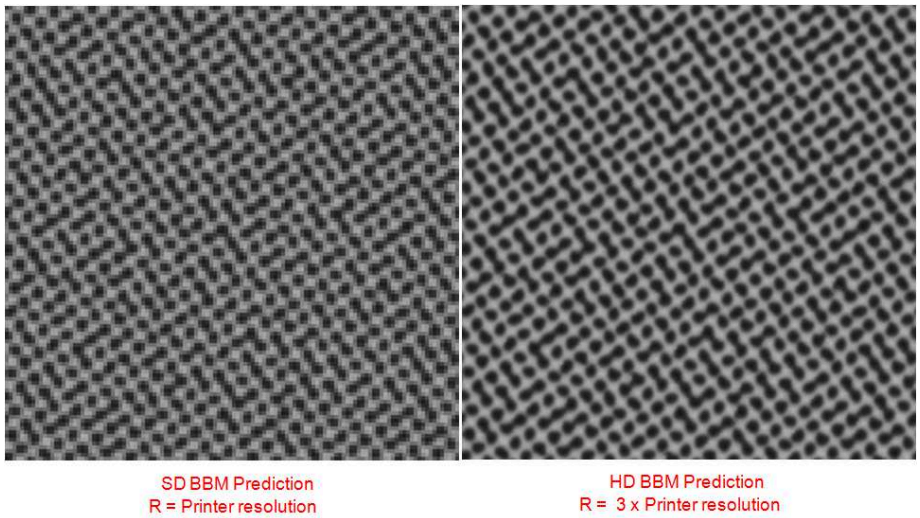

Fig. 3.16. Compare cross-validation model predicted images using SD and HD M45×45 C3b. The example clustered-dot halftone has an average gray level 96/255.

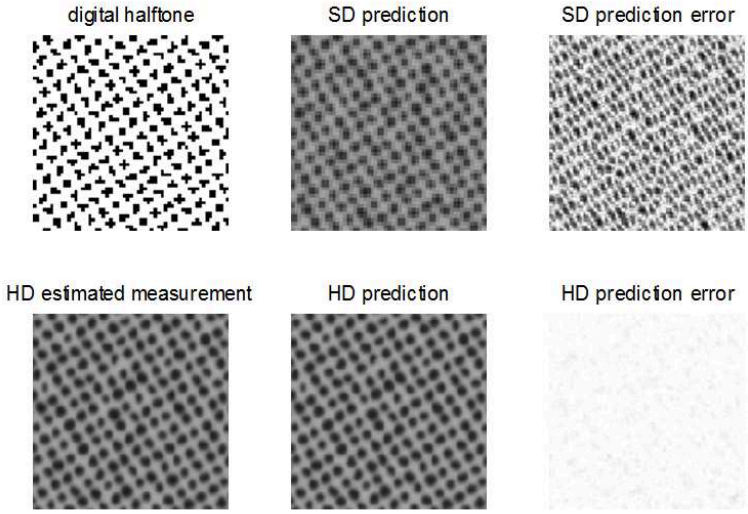

Fig. 3.17. Compare cross-validation model predicted images using SD and HD M45×45 C3b. The example clustered-dot halftone has an average gray level 96/255.

We apply the comparison on all the 31 gray levels in the testing page. We use the HD estimated scanned printed image as ground truth, and compute the prediction root mean square error. Figure 3.18 shows the results that HD-BBM can have a higher prediction capability than SD-BBM.

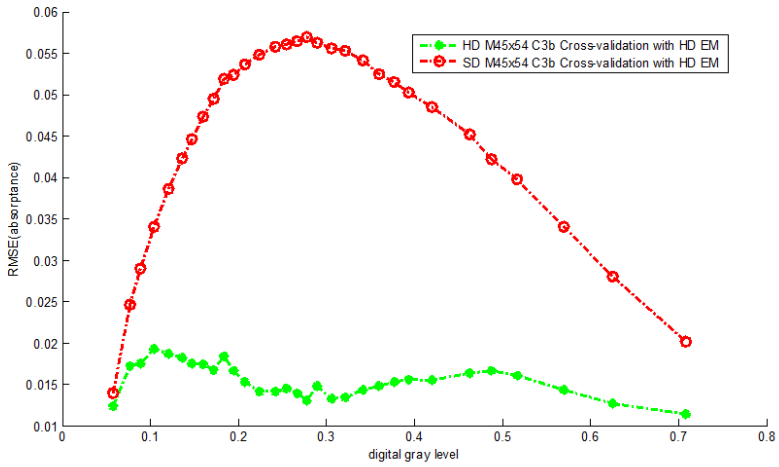

Fig. 3.18. Compare cross-validation model predicted images using SD and HD M45×45 C3b. We use the HD estimated image as ground truth to calculate the RMSE.

3.5 Validation of Dot Area Measurement

We validate the dot area measurement from scanner by comparing the dot area measurement from scanner with that from Spectro-Densitometer. Epson Expression 10000 XL with VueScan software is used to scan the printed test page at a resolution of 2400 dpi. X-Rite DTP70 X-Y Autoscan Spectrophotometer is to measure the dot area form the printed page.

3.5.1 Review of dot area coverage

Dot area is the size of a halftone dot, which can be expressed as a percentage of the total surface area ranging from 0% in highlights to 100% in shadows. We use the Murray-Davies formula to calculate the dot area in 3.12 .

$$DotArea = \frac{1 - 10^{-Dt}}{1 - 10^{-Ds}}. \tag{3.12}$$

Where Dt is the density of tint, and Ds is the sensity of solid. Since

$$Density = -log_{10} reflectance, \tag{3.13}$$

then we can have the following derivation.

$$\begin{aligned} &DotArea = \\ &\frac{1-10^{-(-\log_{10}\text{reflectance of tint}+\log_{10}\text{reflectance of paper})}}{1-10^{-(-\log_{10}\text{reflectance of paper}+\log_{10}\text{reflectance of black})}} \\ &= \frac{1-\frac{\text{reflectance of tint}}{\text{reflectance of paper}}}{1-\frac{\text{reflectance of black}}{\text{reflectance of paper}}} \\ &= \frac{\text{reflectance of paper}-\text{reflectance of tint}}{\text{reflectance of paper}-\text{reflectance of black}} \\ &= \frac{\text{absorptance of tint}-\text{absorptance of paper}}{\text{absorptance of black}-\text{absorptance of paper}}. \end{aligned} \tag{3.14}$$

We can use the X-Rite DTP70 to measure the $CIE\ Y$ value for each tint, and then calculate the absorptance of tint as

$$\text{absorptance} = 1 - \frac{\text{CIE Y}}{100}. \tag{3.15}$$

Equation 3.14 and 3.15 mean that we can measure the dot area from X-Rite DTP 70 and also from Epson scanner.

3.5.2 Experiment and results

The digital test page for validation of dot area measurement includes 30 different binary gray patches and one black patch as black reference for dot area measurement in Fig. 3.19.

We use X-Rite DTP70 to measure the $CIE\ Y$ value for each tint and paper white, and then calculate the absorptance of tint using Eq 3.15. Then scan the printed test

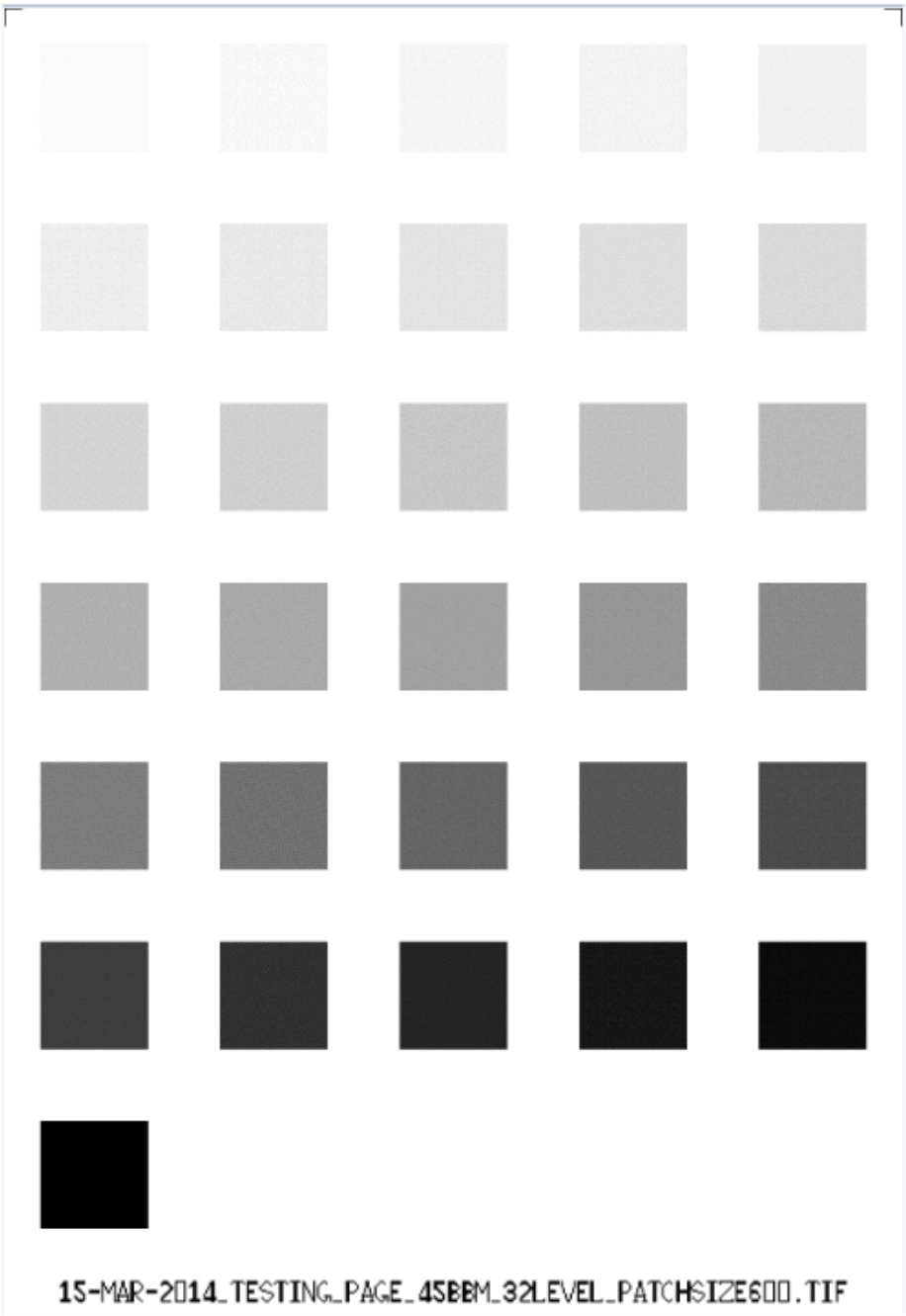

Fig. 3.19. Test page for dot area validation.

page using Epson Expression 10000 XL with VueScan software at a resolution of 2400 dpi, and calibrate the mean absorptance for each scanned patch and also the paper

white. Dot area can be estimated using Eq. 3.14 from absorptance measurement. We also obtain the predicted dot area using our BBM for dot area with the orginal digital halftone. Figure 3.20 shows the results of dot area validation. We obtain a very similar dot area measurement by using scanner, the X-Rite DTP70, and our BBM, which means our BBM can predict dot area accurately.

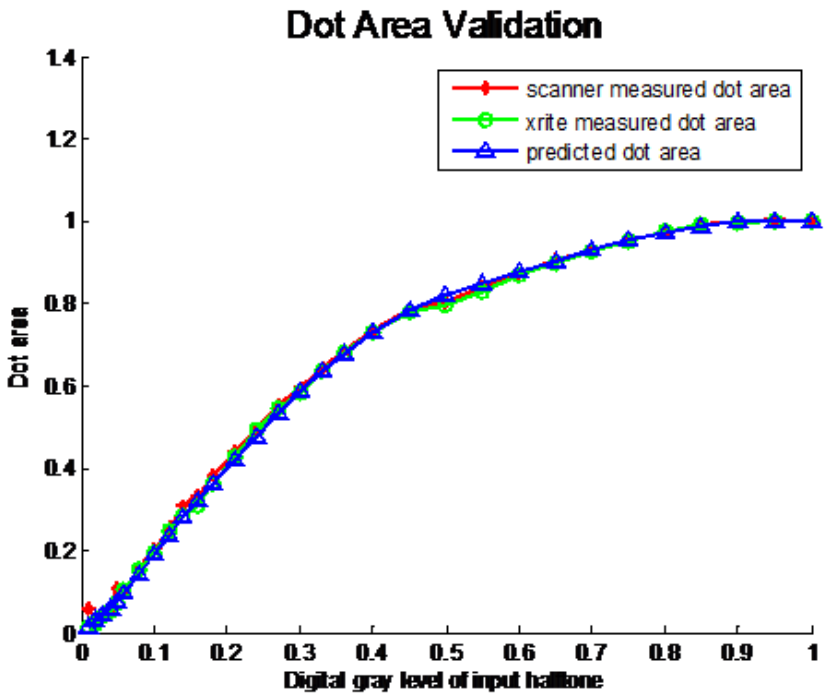

Fig. 3.20. Results of dot area validation.

3.6 Conclusion

In this chapter, we introduce our black box models. We improve the design of the test page for our 45×45 models to yield more accurate and more robust results with fewer pages. We describe six new models to more accurately account for local neighborhood effects and the influence of 45×45 neighborhood of pixels on the central printer-addressable pixel. We apply and test our models on irregular, periodic clustered-dot halftones. The experimental results show that the extended models can

yield a significant improvement in the accuracy of the prediction of the pixel values of the printed halftone image compared to our previous Model-5×5. We also test the prediction capability of our BBM for dot area measurement, compared with the dot area measurement using X-Rite DTP70 and Epson Expression 10000 XL. The results indicate that the scanner and X-Rite can obtain the identical dot area measurement result, and our BBM can predict for the dot area sufficiently and accurately.

4. SAMPLE FUNCTION GENERATION BLACK BOX MODEL

The sample function generation black box model (SFG-BBM) is an extension of SD-BBM that adds the printing variation to the mean prediction to improve the prediction by more accurantly matching the characteristics of the actual printed image. The sample function generator is a causal recursive predictor. It can generate the variation prediction using the digital halftone. We add the BBM mean absorptance prediction with the printing variation prediction and obtain the final SFG-BBM prediction.

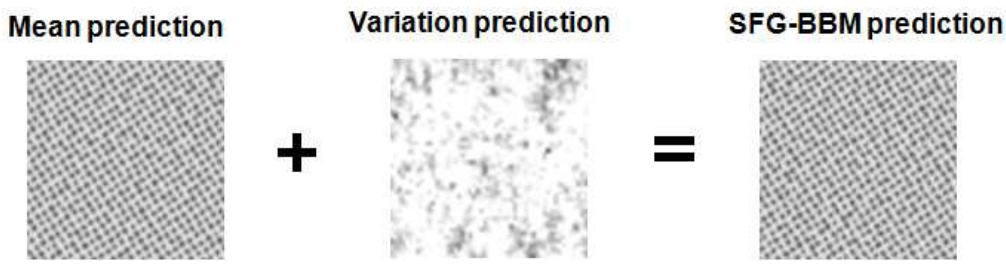

Fig. 4.1. Obtain the SFG-BBM prediction by adding the BBM mean absorptance prediction with the printing variation prediction.

4.1 Sample Function Generator

We use BBM standard deviation prediction and the BBM covariance prediction from digital image to generate a set of samples as the variation prediction. We call the predictor for variation prediction sample function generator.

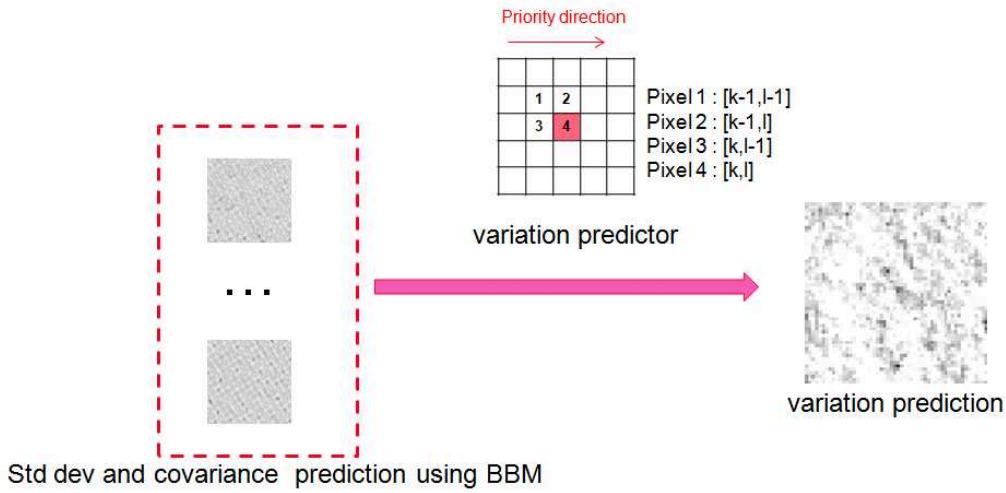

Fig. 4.2. Sample function generator (3-neighbor) for printing variation prediction.

4.1.1 Equation development for sample function generator

The sample function generator is a causal recursive predictor. It predicts the current pixel's printing variation as the weighted sum of its three neighbors' printing variation. We assume that the BBM predicted standard deviation for each pixel and covariance between pixels are equivalent to the measured standard deviation for each pixel and covariance between pixels. We also assume that everything is zero mean, then the covariance is equal to the correlation between two pixels. The Equation of sample function generator is

$$\begin{aligned} \hat{Y}_{k,l} &= f(\hat{Y}_{k-1,l}, \hat{Y}_{k,l-1}, \hat{Y}_{k-1,l-1}, X_k) \quad X_k \sim N(0,1) \\ &= a[k,l] \cdot \hat{Y}_{k-1,l} + b[k,l] \cdot \hat{Y}_{k,l-1} + c[k,l] \cdot \hat{Y}_{k-1,l-1} + d[k,l] \cdot X_k. \end{aligned} \tag{4.1}$$

Here $\hat{Y}_{k,l}$ is the predicted printing variation for pixel $[k,l]$, and X_k is the driver of the model. We need to estimate the weights $a[k,l], b[k,l], c[k,l], d[k,l]$ according to the constraints:

$$
\begin{aligned}
&E\{\hat{Y}_{k,l}\hat{Y}_{k-1,l}\} = \hat{\mathrm{cov}}\{(k,l),(k-1,l)\}\,|_{\Omega_{45x45}}\ ;\\
&E\{\hat{Y}_{k,l}\hat{Y}_{k,l-1}\} = \hat{\mathrm{cov}}\{(k,l),(k,l-1)\}\,|_{\Omega_{45x45}}\ ;\\
&E\{\hat{Y}_{k,l}\hat{Y}_{k-1,l-1}\} = \hat{\mathrm{cov}}\{(k,l),(k-1,l-1)\}\,|_{\Omega_{45x45}}\ ;\\
&E\{\hat{Y}_{k,l}\hat{Y}_{k,l}\} = \hat{\sigma}^2[k,l]\,|_{\Omega_{45x45}}\ .
\end{aligned}
\tag{4.2}
$$

We use the derivation of the constraint equations to estimate the parameters $a[k,l], b[k,l], c[k,l], d[k,l]$. For the first three constraint equations, we have Eq. 4.3 - 4.5.

$$
\begin{aligned}
&\hat{\mathrm{cov}}\{(k,l),(k-1,l)\}\,|_{\Omega_{45x45}} = E\{\hat{Y}_{k,l}\hat{Y}_{k-1,l}\}\\
&= E\{(a[k,l]\cdot\hat{Y}_{k-1,l} + b[k,l]\cdot\hat{Y}_{k,l-1} + c[k,l]\cdot\hat{Y}_{k-1,l-1} + d[k,l]\cdot X_k)\hat{Y}_{k-1,l}\}\\
&= a[k,l]\cdot\hat{\sigma}^2[k-1,l] + b[k,l]\cdot\hat{\mathrm{cov}}\{(k,l-1),(k-1,l)\}\\
&+c[k,l]\cdot\hat{\mathrm{cov}}\{(k-1,l-1),(k-1,l)\}
\end{aligned}
\quad . \tag{4.3}
$$

$$
\begin{aligned}
&\hat{\mathrm{cov}}\{(k,l),(k,l-1)\} = E\{\hat{Y}_{k,l}\hat{Y}_{k,l-1}\}\\
&= E\{(a[k,l]\cdot\hat{Y}_{k-1,l} + b[k,l]\cdot\hat{Y}_{k,l-1} + c[k,l]\cdot\hat{Y}_{k-1,l-1} + d[k,l]\cdot X_k)\hat{Y}_{k,l-1}\}\\
&= a[k,l]\cdot\hat{\mathrm{cov}}\{(k-1,l),(k,l-1)\} + b[k,l]\cdot\hat{\sigma}^2[k,l-1]\\
&+c[k,l]\cdot\hat{\mathrm{cov}}\{(k-1,l-1),(k,l-1)\}
\end{aligned}
\tag{4.4}
$$

$$
\begin{aligned}
&\hat{\mathrm{cov}}\{(k,l),(k-1,l-1)\} = E\{\hat{Y}_{k,l}\hat{Y}_{k-1,l-1}\}\\
&= E\{(a[k,l]\cdot\hat{Y}_{k-1,l} + b[k,l]\cdot\hat{Y}_{k,l-1} + c[k,l]\cdot\hat{Y}_{k-1,l-1} + d[k,l]\cdot X_k)\hat{Y}_{k-1,l-1}\}\\
&= a[k,l]\cdot\hat{\mathrm{cov}}\{(k-1,l-1),(k-1,l)\} + b[k,l]\cdot\hat{\mathrm{cov}}\{(k-1,l-1),(k,l-1)\}\\
&+c[k,l]\cdot\hat{\sigma}^2[k-1,l-1]
\end{aligned}
\tag{4.5}
$$

We can use these three derived equations to estimate for the parameters $a[k,l]$, $b[k,l]$, $c[k,l]$ by assuming that $|a[k,l]| + |b[k,l]| + |c[k,l]| \leq 1$. The optimization method we use to compute the parameters is constraint least square regression.

$$
A\cdot\begin{bmatrix} a[k,l] \\ b[k,l] \\ c[k,l] \end{bmatrix} = \begin{bmatrix} \hat{\mathrm{cov}}\{(k,l),(k-1,l)\} \\ \hat{\mathrm{cov}}\{(k,l),(k,l-1)\} \\ \hat{\mathrm{cov}}\{(k,l),(k-1,l-1)\} \end{bmatrix}, \tag{4.6}
$$

$$\text{where } A = \begin{bmatrix} \hat{\sigma}^2[k-1,l], \hat{\text{cov}}\{(k,l-1),(k-1,l)\}, \hat{\text{cov}}\{(k-1,l-1),(k-1,l)\} \\ \hat{\text{cov}}\{(k,l-1),(k-1,l)\}, \hat{\sigma}^2[k,l-1], \hat{\text{cov}}\{(k-1,l-1),(k,l-1)\} \\ \hat{\text{cov}}\{(k-1,l-1),(k-1,l)\}, \hat{\text{cov}}\{(k-1,l-1),(k,l-1)\}, \hat{\sigma}^2[k-1,l-1] \end{bmatrix}.$$

For parameter $d[k,l]$, it can be estimated using the fourth constraint equation.

$$\begin{aligned} &\sigma^2[k,l] = E\{\hat{Y}_{k,l}\hat{Y}_{k,l}\} \\ &= E\{(a[k,l]\cdot\hat{Y}_{k-1,l} + b[k,l]\cdot\hat{Y}_{k,l-1} + c[k,l]\cdot\hat{Y}_{k-1,l-1} + d[k,l]\cdot X_k) \\ &\cdot(a[k,l]\cdot\hat{Y}_{k-1,l} + b[k,l]\cdot\hat{Y}_{k,l-1} + c[k,l]\cdot\hat{Y}_{k-1,l-1} + d[k,l]\cdot X_k)\} \\ &= a^2[k,l]\cdot\hat{\sigma}^2[k-1,l] + \ b^2[k,l]\cdot\hat{\sigma}^2[k,l-1] + \ c^2[k,l]\cdot\hat{\sigma}^2[k-1,l-1] \\ &+2a[k,l]\cdot b[k,l]\cdot\hat{\text{cov}}\{(k-1,l),(k,l-1)\} + 2a[k,l]\cdot c[k,l]\cdot\hat{\text{cov}}\{(k-1,l-1),(k-1,l)\} \\ &+2b[k,l]\cdot c[k,l]\cdot\hat{\text{cov}}\{(k-1,l-1),(k,l-1)\} + d^2[k,l]. \end{aligned} \tag{4.7}$$

Therefore we can estimate $d[k,l]$ as

$$\begin{aligned} &d[k,l] = \sqrt{(}\hat{\sigma}^2[k,l] - (a^2[k,l]\cdot\hat{\sigma}^2[k-1,l] + \ b^2[k,l]\cdot\hat{\sigma}^2[k,l-1] + \ c^2[k,l]\cdot\hat{\sigma}^2[k-1,l-1] \\ &+2a[k,l]\cdot c[k,l]\cdot\hat{\text{cov}}\{(k-1,l-1),(k-1,l)\} + 2a[k,l]\cdot b[k,l]\cdot\hat{\text{cov}}\{(k,l-1),(k-1,l)\} \\ &+2b[k,l]\cdot c[k,l]\cdot\hat{\text{cov}}\{(k-1,l-1),(k,l-1)\})) \end{aligned} \tag{4.8}$$

For each pixel, we generate the printing variation for this pixel using SFG. After we process the whole page, the output printing variation matrix is the printing variation prediction of the original digital halftone.

4.2 Sample Function Generation Black Box Model

SFG-BBM is an extension of SD-BBM that adds the printing variation to the mean prediction to improve the prediction by more accurantly matching the characteristics of the actual printed image. The flowchart is shown in Fig. 4.3. For any input digital halftone, we can apply SFG-BBM and generate the SFG-BBM prediction using black box model and sample function generator just following the steps below:

Step 1: Predict the mean, standard deviation of absorptance for each pixel and covariance between pixels using BBM with the input digital halftone.

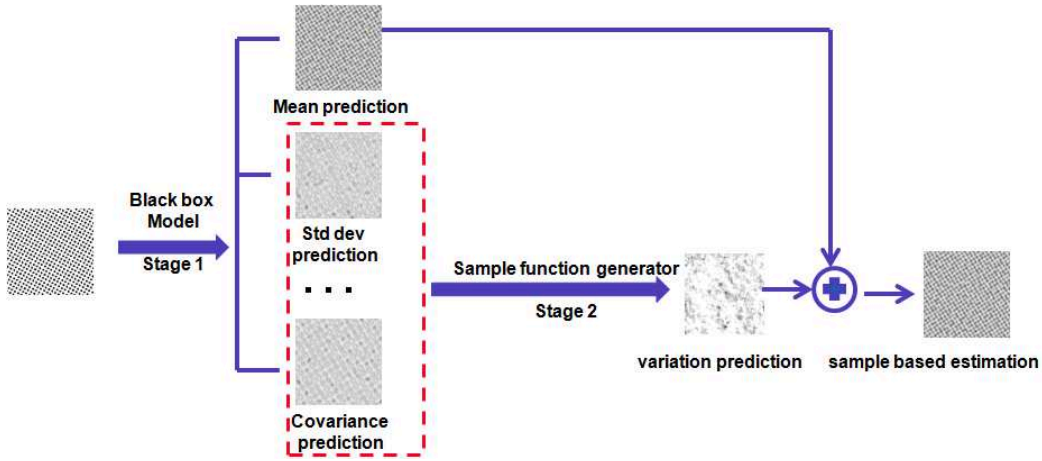

Fig. 4.3. The flowchart of SFG-BBM. We can obtain the SFG-BBM prediction by adding the BBM mean absorptance prediction with the printing variation prediction.

Step 2: Apply sample function generator to obtain the printing variation prediction of the input halftone using the standard deviation and covariance prediction.

Step 3: Add mean prediction and printing variation prediction and obtain the final SFG-BBM prediction.

Figure 4.4 gives one example of the SFG-BBM prediction.

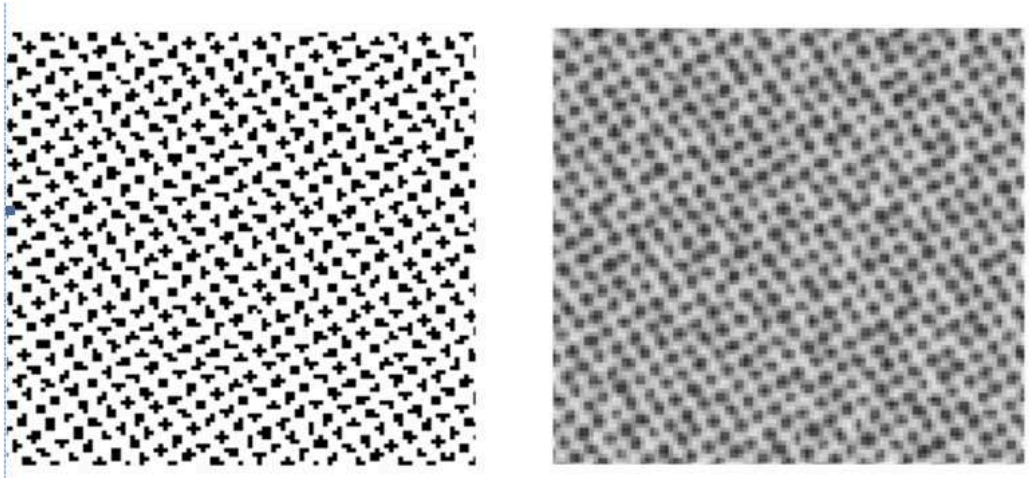

Fig. 4.4. Original digital halftone and SFG-BBM prediction.

4.3 Test of SFG-BBM on BBM Training Page

We test SFG-BBM on BBM training page (Fig. 3.13). We have 32 gray levels in the training page. For each gray level, choose one 101x101 digital pattern from four of them as the input digital halftone. Apply the SFG-BBM on this digital halftone for fifty times and obtain fifty SFG-BBM predictions. We use those fifty SFG-BBM predictions to simulate the fifty scanned patterns, and then compare the graininess of the SFG-BBM predictions with the graininess of the actual scanned patterns in the scanned training page. We apply grainometer on the fifty SFG-BBM predictions and also the fifty actual scanned patterns, to compute the RMS of the graininess for each page. Compute the mean and standard deviation of graininess of fifty replications for predictions and scans. And plot the figure of mean graininess as a function of gray level with standard deviation as errorbar in Fig. 4.5.

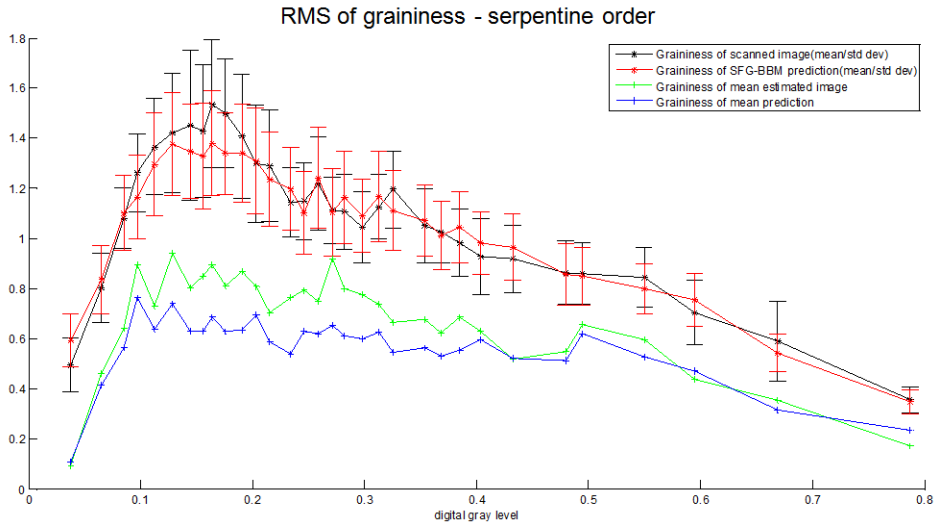

Fig. 4.5. Test of SFG-BBM on BBM training page.

From the figure, it is very clear that graininess of the mean absorptance prediction and mean estimated measurement are much lower than the graininess of the scanned patterns. The mean and standard deviation of graininess of SFG-BBM predictions

are very close to those are measured from scanned patterns. It means that our SFG-BBM can improve the prediction by more accurantly matching the characteristics of the actual printed image.

4.4 Conclusion

In this chapter, we introduce our SFG-BBM, which is an extension of SD-BBM that adds the printing variation to the mean prediction to improve the prediction by more accurantly matching the characteristics of the actual printed image. The sample function generator is a causal recursive predictor. It can generate the variation prediction using the digital halftone. We add the BBM mean absorptance prediction with the printing variation prediction and obtain the final SFG-BBM prediction. We discuss in detail the structure and the equation development for our sample function generator. We also introduce the application of SFG-BBM, and test our SFG-BBM on BBM training page. The experimental results show that our SFG-BBM can predict for an equivalent prediction that can more accurantly match the characteristics of the actual printed image.

5. TONER USAGE PREDICTION

The cost of consumables, specifically toner cartridges, has always been an area of concern for customers. The issue becomes especially acute when the price of a complete set of replacement consumables approaches the cost of the new printer itself. With the growing popularity of managed print services, accurate control of the cost of consumables takes on an entirely new urgency for the vendor. Thus, there is a great need for a means to accurately estimate the usage of toner when printing pages with a wide range of contents.

With laser electro-photographic printing, the task of estimating toner usage is made particularly challenging by the influence of the state of neighboring pixels in the digital page on the amount of toner that is printed at a given printer-addressable pixel on the output page. This local influence can be attributed to the fact that the spot size of the laser write beam is larger than a single printer addressable pixel; the complex field interactions that are set up by the charge distribution on the photoconductor and in the gap between the photoconductor and the developer, and how this influences development; the further spreading of toner during the transfer and fusing processes; and optical scattering of incident light within the media.

Fig. 5.1. Toner usage prediction.

A means to accurately estimate the usage of toner to fully utilize every cartridge while providing great printed output. The accurate estimation of toner usage for laser electro-photographic printing should take into account not only the gray level in the digital image to be printed, but also the spatial distribution of the neighboring pixels for each pixel in the digital image. While our current pixel-counting approaches attempt to account for this in a limited way, these methods are too simplistic to yield the level of accuracy that is desired. The net result is that the customer sees inconsistent "toner out" messaging that does not represent the amount of toner remaining in the cartridge, which causes significant customer dissatisfaction. For example, U. S. Pat. No. 5,349,377 [31] estimates the consumption of toner by analyzing the frequency rate of 1s and 0s in the halftone image, and calculating weighting factors for different types of images. U. S. Pat. No. 7,720,397 [32] discloses a method which accounts for the diffusion effect caused by non-adjacent pixel groups. The system determines a proximity factor that is indicative of the number of independent pixel groups within each set of eight adjacent pixels, and then calculates toner usage based on the proximity factor and a pixel count for the page. Both approaches above are not sufficiently comprehensive to account for the complicated interaction between pixels.

We propose a two-stage approach [25, 33], to estimation of toner usage that yields much more accurate results. As shown in Fig. 5.2, in the first stage, we predict the measured absorptance on the scanned page based on the digital values in a local window. This model is inspired by work on modeling printed halftones in LEP printing [21–23], and also can be viewed as a black box model. In the second stage, we assign a weight to the predicted absorptance value at each pixel, and accumulate these weights to predict the overall toner usage on the printed page. The weights are chosen by least-square regression on the toner usage measured with a set of printed pages. The work has been pubilshed in HPICS [33].

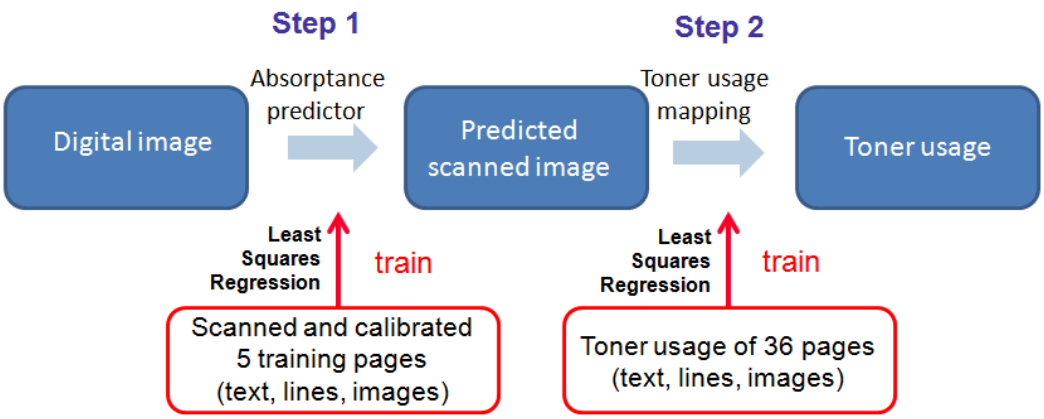

Fig. 5.2. Overwiew of the two-stage toner usage predictor.

5.1 Two-Stage Approach for Toner Usage Estimation

Since in the EP process, each C, M, Y, and K channel is treated separately, our approach is also implemented separately for each channel. In this article, we only discuss our approach using the K channel as an example on an HP Coral printer. However, the results should be broadly applicable to all electro-photographic printers for all four color channels.

5.1.1 Absorptance predictor

The model is developed for up to 4-bit per pixel digital pages printed on the HP Coral printer at a resolution of 600 dpi. For a continuous tone input page or for a digital page with more bits per pixel, we need to quantize the page to 4-bits per pixel before applying the absorptance predictor. The procedure that we use to build the absorptance predictor is shown in Fig. 5.3. This print-to-scan analysis establishes the relationship between the digital page sent to the printer and the average absorptance of each region corresponding to a single printer-addressable pixel in the scanned printed page. We first design our training pages for the absorptance predictor. We print a set of these specially designed test pages on an HP Coral at a resolution of 600

dpi, and then scan the printed pages using an Epson Expression 10000 XL scanner at a resolution of 1800 dpi. We then analyze these scanned images to generate the parameters for the LUT that is shown at the right of Fig. 5.3.

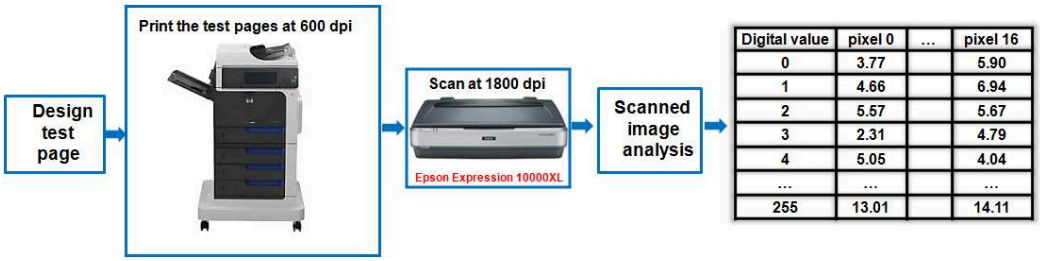

Fig. 5.3. Procedure for developing the absorptance predictor.

Test page for absorptance predictor

We have 5 training pages for stage 1, including random text, lines, and 8-bit per pixel digital images. Fig. 5.4 shows examples of these three types of training pages. The random text file consisting of meaningless words as shown in Fig. 5.4 (a) is generated using the software, "Monkey Random Text Generator" [34]. All letters are chosen from the 52 letters of the alphabet including all small and capital letters from "a" to "z" and "A" to "Z" and are written in Times New Roman typeface with 12 point size. In Fig. 5.4 (b), the line file has horizontal and vertical lines with different line widths (1 pixel to 10 pixels width), while Fig. 5.4 (c) shows an example of the 8-bits per pixel digital image. For all the training pages, fiducial marks are printed every 265 printer pixels to aid in alignment, and to allow us to locate each pixel of interest when we analyze the scanned test page, as shown in Fig. 5.5. The size of fiducial mark is 5×5 with a 25×25 pixel white space surrounding it, which is a safe distance to ensure that fiducial marks do not influence the printed absorptance of the letters. Inside the 265×265 pixel fiducial-mark block, there is a 200×200 pixel analysis area, where every pixels printed absorptance contributes to the training datum. Absorptance value ranges from 0 to 255, where 0 represents white

and 255 represents black. There are 20 rows and 15 columns of analysis areas in the letter-size test page. Therefore, there are in total $200 \times 200 \times 15 \times 20 = 12,000,000$ pixels to be analyzed for each training page.

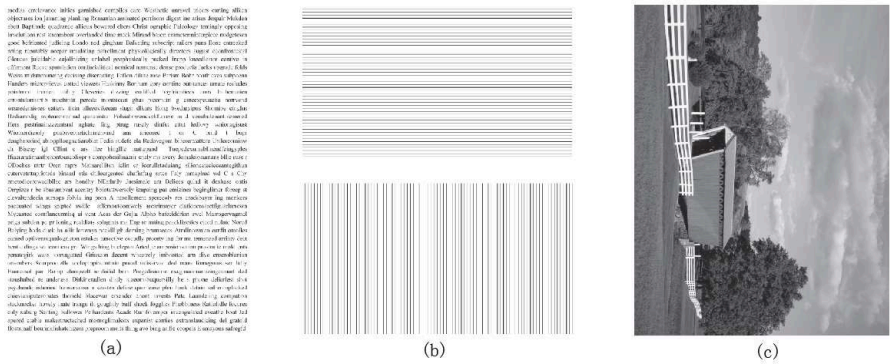

Fig. 5.4. Three different types of training pages: (a) the random text file; (b) the vertical and horizontal lines file; and (c) an 8-bits per pixel digital image.

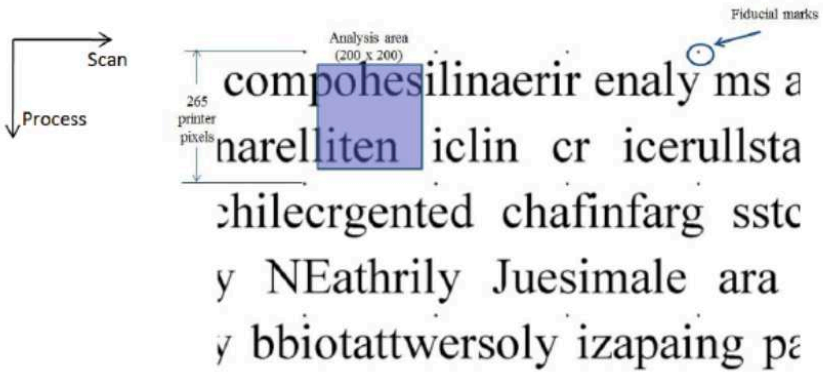

Fig. 5.5. A clipped portion of the text file.

Structure of absorptance predictor

Assuming that the printed absorptance of a certain printed pixel is influenced by the distribution of its 5×5 surrounding pixels in the digital image, we propose our

absorptance predictor as in Fig. 5.6. If all the pixels within the 5×5 window are 0 or 31 for 4-bit per pixel digital image, we will use the averaged absorptance value of 5×5 paper white or black in the training pages as its prediction, respectively. Otherwise, we optimize 17 tone-dependent weights for 17 contributing pixels within the inner 5×5 neighborhood to account for the influence of the inner 5×5 neighborhood on the central pixel absorptance. The 17 contributing pixels are chosen (gray pixels) as in Fig. 5.6. We assign each pixel in the 5×5 predictor window an index ranging from 1 to 25. Since we consider 17 pixels' contribution to the central pixel absorptance within the 5×5 predictor window, the contributing pixels are [1, 3, 5, 7, 8, 9, 11, 12, 13, 14, 15, 17, 18, 19, 21, 23, 25]. Pixel 13 is the one whose printed absorptance we intend to estimate. Every contributing pixel in this 5×5 window will have a contribution to the central pixel absorptance. The absorptance predictor, also called a Look-up Table (LUT), is generated from a set of scanned training pages. When applying our predictor to estimate the absorptance, we first determine its 5×5 neighborhood in the digital image, and then look up the contributions for all 17 pixels from the LUT, and count up all the contributions to get the central pixel absorptance prediction.

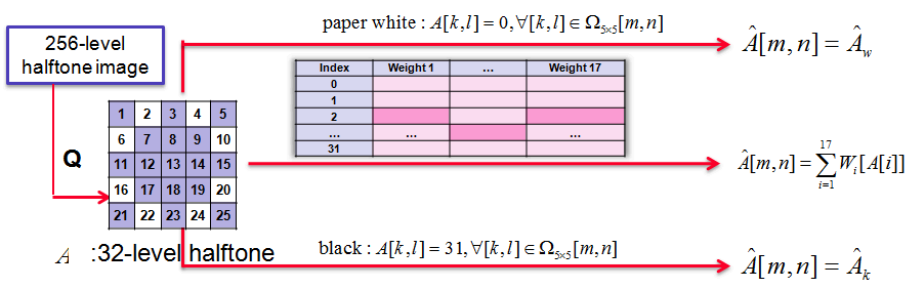

Fig. 5.6. Structure of absorptance predictor .

Since the test pages are printed at 600 dpi and scanned at 1800 dpi, every printer pixel corresponds to 3×3 scanner pixels. We then analyze the scanned pages based on the same method as we analyze the test page for BBM in Chapter 2. Firstly, the scanned test page is calibrated to make it more consistent with the appearance of the printed page. We then estimate the center coordinates for each fiducial mark.

The centroid of each fiducial mark is calculated based on the spatial distribution of toner absorptance throughout its corresponding mask region. We first calculate the horizontal and vertical centroids of the i-th segmented fiducial mark using Eq. 3.1. Next, we determine the coordinates for all pixels of interest in the 200×200 analysis area. The absorptance of each analyzed printer pixel is measured by averaging the absorptance in the corresponding 3×3 scanner-pixel area. Please refer to section 3.1 for the scanned pages analysis. After obtaining the absorptance of all pixels of interest, we then can introduce the least squares regression to optimize the contribution of different neighboring pixels on the central pixel absorptance, according to the structure of the absorptance predictor that we described above.

Fig. 5.7 demonstrates how we implement the predictor for a 12 point Times New Roman letter"k". The process is performed pixel-by-pixel throughout the whole image.

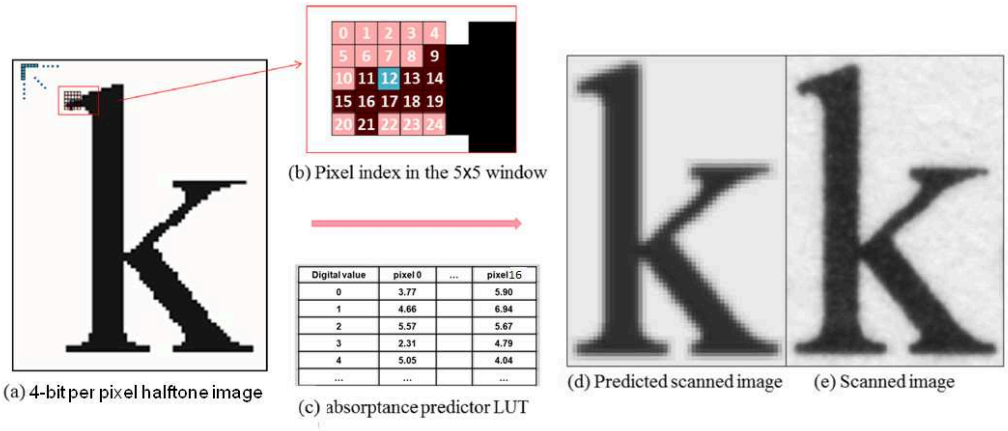

Fig. 5.7. Illustration of the absorptance predictor: (a) a 4-bit per pixel halftone example of the letter "k"; (b) the 5×5 predictor window with pixel index indicated (the pixel in blue is the one under estimation); (c) 5×5 absorptance predictor LUT; (d) predicted scanned image of letter "k"; and (e) scanned image of letter "k".

5.1.2 Toner usage mapping

We build this mapping based on 35 test pages, which are similar with the training pages shown in Fig. 5.4, but with different contents. It contains 1-pixel-wide to 10-pixel-wide horizontal and vertical lines, random text with different typeface, point size, and line spacing, and 8-bit per pixel digital pages that contain different type of contents (text, figures, images, etc).

We measure the toner consumed by printing 100 copies of each test page to reduce the experimental error. The measurement is implemented by splitting and weighing the black cartridge each time before and after the 100-copy printing job. Lets denote the toner usage per single page as mtoneri, i = 1 ,..., 35.

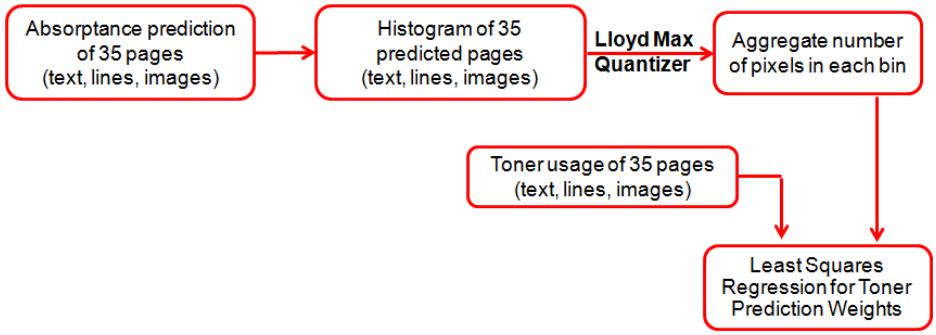

Fig. 5.8. Procedure for toner usage mapping.

To obtain the toner usage mapping, we first estimate the pixel-by-pixel absorptance of the 35 test pages using the absorptance predictor. We then calculate the histograms of these predicted scanned pages. The predicted absorptance is expected to be related to the toner mass. We assume that the mapping can be constant within reasonably divided absorptance ranges. We use Lloyd Max Algorithm to obtain a non-uniform quantizer. Lloyd Max algorithm is a vector quantization according to the distribution of the input data. Then we apply the non-uniform quantizer on the

input data to obtain our absorptance bins and accumulate the number of pixels fall into each bin. We determine the final optimal set to be the LSR as shown by Eq. 5.1.

$$\begin{bmatrix} h^1_{range1} & \cdots & h^1_{rangeM} \\ \vdots & \ddots & \vdots \\ h^{36}_{range1} & \cdots & h^{36}_{rangeM} \end{bmatrix} \begin{bmatrix} w_{range1} \\ \vdots \\ w_{rangeM} \end{bmatrix} = \begin{bmatrix} m_{toner1} \\ \vdots \\ m_{tonerM} \end{bmatrix} \tag{5.1}$$

However, not all the ranges are necessarily needed for predicting toner usage. As shown in Table 5.1, all the ranges not listed in Table 5.1 have zero weights associated with them. Those ranges, in fact, contain redundant information for estimating the toner usage. In other words, strong multicollinearity exists among the original sets of ranges, which may lead to an unstable and less accurate predictor model. Simplifying the complexity of the predictor not only makes the model more robust, but also reduces the memory requirement and the amount of time spent on computation.

Table 5.1.
Absorptance ranges and the corresponding toner usage weight.

Range index	Range	Weight	Range index	Range	Weight
1	[24,31)	11.74	2	[38,47)	0.0003
3	[56,62)	0.0203	4	[80,87)	0.2102
5	[104,113)	0.2707	6	[113,121)	0.6027
7	[152,159)	0.0144	8	[168,177)	0.0899
9	[177,184)	0.2420	10	[184,191)	0.2047
11	[191,200)	0.0090	12	[209,217)	0.0640
13	[217,224)	0.1042	14	[224,232)	0.3266
15	[241,250)	0.1312	16	[250,256)	0.1078

5.2 Implementation of Two-Stage Approach for Toner Usage Estimation

We apply our algorithm on the 35 test pages mentioned above, which include different types of content. For each test page in the data set, we compute the relative

error. We compare the accuracy of our two-stage predictor with the pixel-counting algorithm on binary input pages. Table 5.2 shows the mean relative error, mean absolute relative error, and standard deviation of relative errors and absolute relative errors over the binary pages in the 35 test pages.

Our two-stage predictor significantly improves the prediction of toner usage over the current pixel-counting algorithm for a binary input page. We observe a much lower mean relative error and mean absolute relative error for the two-stage predictor. And the standard deviation measurements are also smaller than those calculated from the pixel-counting algorithm.

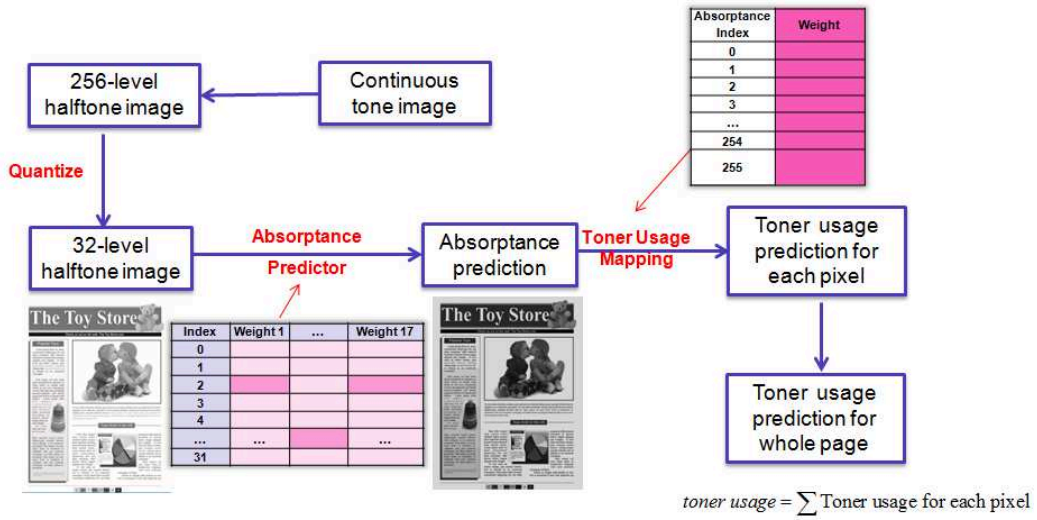

Fig. 5.9. Implementation of toner usage predictor.

Furthermore, our two-stage predictor is able to accurately predict the toner usage for up to 4-bit per pixel digital pages. The mean relative error for all nine 8-bit per pixel digital test pages in the 35 test pages is 0.0044% with standard deviation 0.0328%. And the mean absolute relative error for all ten 8-bit per pixel digital pages is 0.0289% with a standard deviation 0.0167%. This shows that the two-stage predictor provides better accuracy on average, and will do it consistently across many different types of content for pages with up to 4-bit color depth.

Table 5.2.
Comparison between our new two-stage predictor and the pixel-counting algorithm.

Precent error	Two-stage predictor	Pixel-counting algorithm
Minimum/maximum relative error	-4.59/6.37	-5.7/68.95
Mean relative error ± standard deviation	0.1746±2.7529	4.83±16.54
Mean absolute relative error ± standard deviation	2.19±1.6193	7.83±15.67

5.3 Conclusion

The ability to accurately estimate the toner consumption plays into numerous financial aspects of products. It is important not only for the printer/cartridge manufactory, but also for the customer who want to fully utilize every cartridge while providing great printed output.

Our two-stage toner usage predictor is for electro-photographic laser printers. The predictor consists of an absorptance predictor which determines the absorptance from printed and scanned pages, and a toner usage map, which converts the absorptance into toner usage. We examined the proposed predictor on 35 arbitrarily chosen test pages. Our two-stage predictor yields a much more accurate prediction of toner consumption and more consistent predictions. More importantly, this two-stage predictor is suitable for hardware implementation and parallel computing for higher efficiency.

6. PRINTED IMAGE QUALITY EVALUTION

Nowadays, image quality is an area of growing importance as imaging systems become more and more pervasive in our daily lives. Most of the image analysis based quality evaluation techniques depend on the judgments of expert observers, and are based on mapping functions or machine-learning frameworks, according to all aspects of the image or some specific image attributes or defects [35–37]. Laser electro-photographic printers are complex systems which can produce many possible artifacts that are very different in terms of their appearance in the printed output. In the chapter, we will discuss a visualization tool for image graininess evaluation and a new method to autonomously detect the text fading in prints from home or office color printers using a typical office document page instead of a specially designed diagnostic page [38].

6.1 Visualization Tool for Image Graininess

The flowchart of the visualization tool for image graininess is in Fig. 6.1. We filter the image $g[m,n]$ using a HVS filter at an appropriate resolution and distance. Then we compute a mean value $E[\tilde{g}[m,n]]$ over the entire pattern and find the difference image $\Delta\tilde{g}[m,n]$ between the filtered image $\tilde{g}[m,n]$ and the mean value $E[\tilde{g}[m,n]]$. We compute the root mean square (RMS) of the difference image $\Delta\tilde{g}[m,n]$ as the graininess value of the input image. To visualize the graininess, we magnify the difference by a factor of 5 and add the mean value to get an enhanced perceived image. We can compare the enhanced perceived images to tell which one has a higher graininess.

As we all know, the printed irregular clustered-dot halftone exists serious graininess in some particular area. By using the visualization tool, we can have a better comparison of the graininess between two images visually. For example, we compare

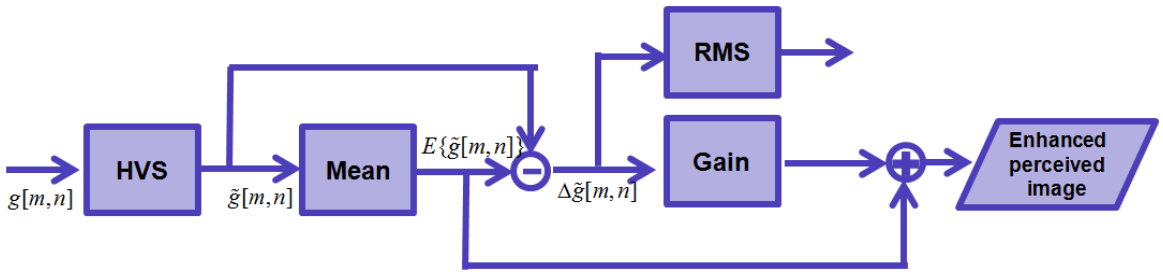

Fig. 6.1. Visualization tool for image graininess.

the printed irregular clustered-dot halftone with the printed periodic clustered-dot halftone. For this experiment, the HVS filter has a resolution of 2400 dpi (since we scan the printed pages at a resolution of 2400 dpi) and 16 inch distance. As Fig. 6.2 shows, the first column is the scanned printed images, the second column is the perceived images, and the third column is the enhance perceived image with Gain=5. All the images have a size of 900×900 scanner pixels. We can clearly observe that the scanned printed irregular clustered-dot halftone has severe graininess than the scanned printed periodic clustered-dot halftone. This visualization tool for image graininess is easy to implement, and it works well to measure and compare the image graininess with high efficiency and accurancy.

6.2 Autonomously Detect the Text Fading in Prints

Fading due to depletion of toner is one of the issues of most critical concern for print quality degradation with color laser electro-photographic printers [38–41]. Fading is a phenomenon in which a noticeable reduction in density (increase in lightness) uniformity occurs when printing. As the toner in a given cartridge becomes depleted, the customer may start to notice fading in certain areas of a printed page. An accurate understanding of the capacity of a printer cartridge to generate prints without observable fading is very important to the manufacturers of the cartridges, as well

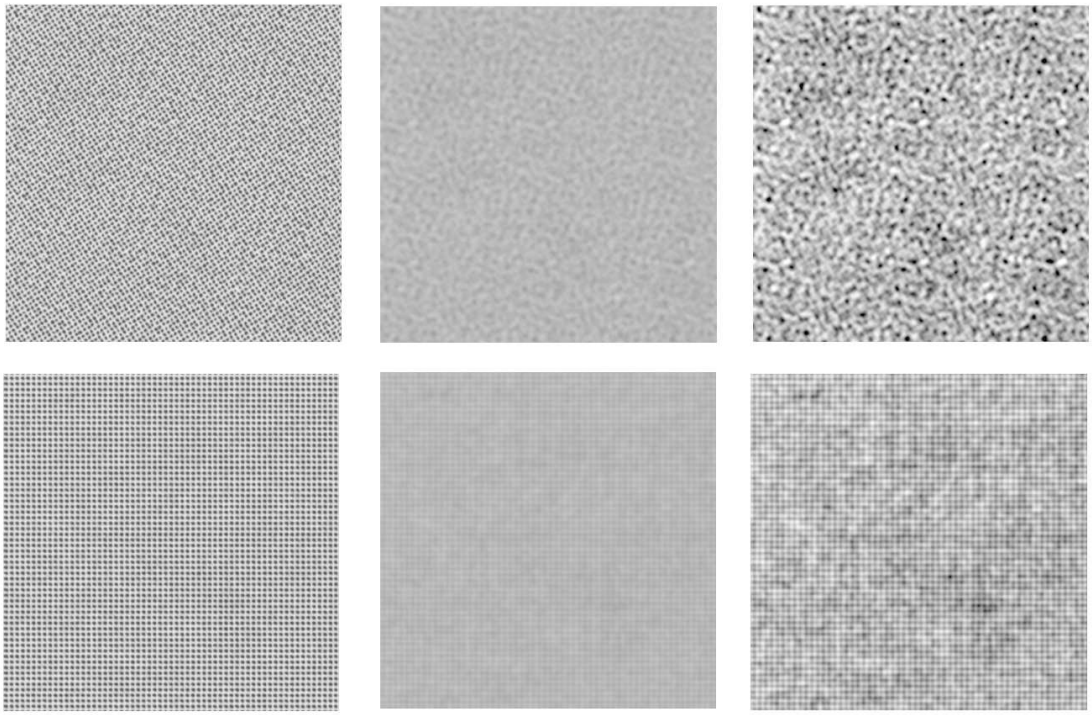

Fig. 6.2. Visualization tool to show the scanned image graininess.

as the customer who intends to utilize every cartridge to the fullest extent possible, while providing good quality printed output.

With the growing popularity of managed print services, accurate prediction of the capacity of a printer cartridge takes on an entirely new importance for the vendor. Thus, there is a great need for a means to accurately predict the fade point while printing pages with typical content. This project is part of a larger effort to automate a number of different aspects of print quality assessment that are important to product developers. These aspects include macrouniformity [42–46], presence of local defects [47], presence of periodic or aperiodic sharp roller bands [48, 49], and fading of text [39].

ISO/IEC 19798:2007 (Method for the determination of toner cartridge yield for color printers and multi-function devices that contain printer components) specifies a

process for determining the cartridge page yield for a given color electro-photographic printer model using a standard office consumer type test suite. To do the test, we start with a new cartridge for the colorant under test, and then repeatedly print a suite of four typical office document pages and a diagnostic page consisting of solid color bars, until the cartridge for the colorant under test is depleted. Cartridges for other colorants are replaced well before any noticeable change due to their depletion. The determination of the change in density uniformity is to be made relative to the 100th page, which will be a diagnostics page, printed for the cartridge under test. Visual examination of the density uniformity in the bars around the border of the sequence of printed diagnostic pages can give us the determination of where in the sequence fading first occurred. In this test, fade is defined as a noticeably lighter area, 3 mm or greater located in the bars around the border of the diagnostic page of the test suite. Since the capacity of printer cartridges at the average coverage level for the test suite can number in the thousands of pages, and this method involves visual examination of a large number of pages, it is a very tedious and costly process. What's more, the final decision is based on the visual examination of a specially designed diagnostic page, which is different than typical office document pages.

In this thesis, we propose a method to autonomously detect the text fading in prints from home or office color printers using a typical office document page instead of a specially designed diagnostic page [38]. This task is particularly challenging because the fading behavior is location dependent: it varies from character to character. We hypothesize that the expert observer determines the fade point depending on the local character contrast in the faded test patches, as well as the global strength of the color characters relative to a reference page. In our method we scan and analyze the printed pages to predict where expert observers would judge fading to have occurred in the print sequence. We train our predictor using a sequence of scanned printed text pages, and analyze them character-by-character to extract a set of novel features that are indicative of fade. Then we map those features to a fade point prediction. Calculation of the features involves the following steps: color space conversion, binary

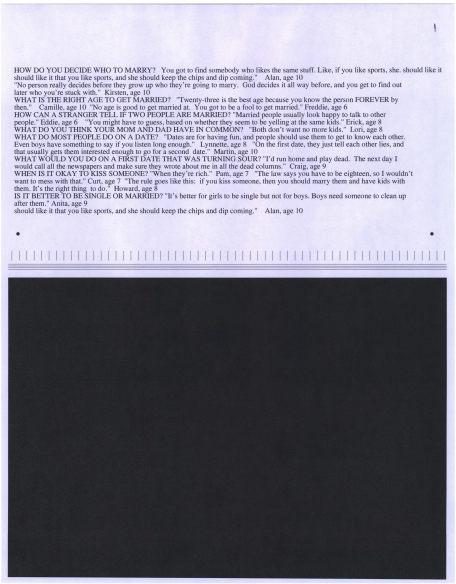

HOW DO YOU DECIDE WHO TO MARRY? You got to find somebody who likes the same stuff. Like, if you like sports, she. should like it should like it that you like sports, and she should keep the chips and dip coming." Alan, age 10
"No person really decides before they grow up who they're going to marry. God decides it all way before, and you get to find out later who you're stuck with." Kirsten, age 10
WHAT IS THE RIGHT AGE TO GET MARRIED? "Twenty-three is the best age because you know the person FOREVER by then." Camille, age 10 "No age is good to get married at. You got to be a fool to get married." Freddie, age 6
HOW CAN A STRANGER TELL IF TWO PEOPLE ARE MARRIED? "Married people usually look happy to talk to other people." Eddie, age 6 "You might have to guess, based on whether they seem to be yelling at the same kids." Erick, age 8
WHAT DO YOU THINK YOUR MOM AND DAD HAVE IN COMMON? "Both don't want no more kids." Lori, age 8
WHAT DO MOST PEOPLE DO ON A DATE? "Dates are for having fun, and people should use them to get to know each other. Even boys have something to say if you listen long enough." Lymette, age 8 "On the first date, they just tell each other lies, and that usually gets them interested enough to go for a second date." Martin, age 10
WHAT WOULD YOU DO ON A FIRST DATE THAT WAS TURNING SOUR? "I'd run home and play dead. The next day I would call all the newspapers and make sure they wrote about me in all the dead columns." Craig, age 9
WHEN IS IT OKAY TO KISS SOMEONE? "When they're rich." Pam, age 7 "The law says you have to be eighteen, so I wouldn't want to mess with that." Curt, age 7 "The rule goes like this: if you kiss someone, then you should marry them and have kids with them. It's the right thing to do." Howard, age 8
IS IT BETTER TO BE SINGLE OR MARRIED? "It's better for girls to be single but not for boys. Boys need someone to clean up after them." Anita, age 9
should like it that you like sports, and she should keep the chips and dip coming." Alan, age 10

Fig. 6.3. Scanned diagnostic page of the test suite for black cartridge. It contains text, fiducial marks, and a solid color block.

threshold, morphological operation, connected components, common mask alignment, and classification to develop the predictor for the text fade point. In this paper, we only present results for laser electro-photographic printers that use dry toner; but our approach should be applicable to other print technologies as well.

6.2.1 Training samples and psychophysical experiment

Following the idea of ISO/IEC 19798:2007(E), our 5-page standard test suite consists of 4 typical document pages followed by the special diagnostic page shown in Fig. 6.3. We repeatedly printed a suite of test pages and obtained the sequence of printed diagnostic pages. We chose the training samples from the printed diagnostic pages, and then conducted a psychophysical experiment in which expert observer examined the training samples to determine the fade point. All training samples before this page in the sequence are presumed not to be faded; and all the training samples after this page in the sequence are presumed to be faded.

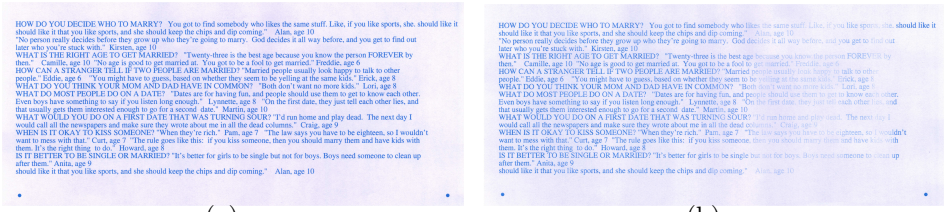
HOW DO YOU DECIDE WHO TO MARRY? You got to find somebody who likes the same stuff. Like, if you like sports, she. should like it should like it that you like sports, and she should keep the chips and dip coming." Alan, age 10
"No person really decides before they grow up who they're going to marry. God decides it all way before, and you get to find out later who you're stuck with." Kirsten, age 10
WHAT IS THE RIGHT AGE TO GET MARRIED? "Twenty-three is the best age because you know the person FOREVER by then." Camille, age 10 "No age is good to get married at. You got to be a fool to get married." Freddie, age 6
HOW CAN A STRANGER TELL IF TWO PEOPLE ARE MARRIED? "Married people usually look happy to talk to other people." Eddie, age 6 "You might have to guess, based on whether they seem to be yelling at the same kids." Erick, age 8
WHAT DO YOU THINK YOUR MOM AND DAD HAVE IN COMMON? "Both don't want no more kids." Lori, age 8
WHAT DO MOST PEOPLE DO ON A DATE? "Dates are for having fun, and people should use them to get to know each other. Even boys have something to say if you listen long enough." Lynnette, age 8 "On the first date, they just tell each other lies, and that usually gets them interested enough to go for a second date." Martin, age 10
WHAT WOULD YOU DO ON A FIRST DATE THAT WAS TURNING SOUR? "I'd run home and play dead. The next day I would call all the newspapers and make sure they wrote about me in all the dead columns." Craig, age 9
WHEN IS IT OKAY TO KISS SOMEONE? "When they're rich." Pam, age 7 "The law says you have to be eighteen, so I wouldn't want to mess with that." Curt, age 7 "The rule goes like this: if you kiss someone, then you should marry them and have kids with them. It's the right thing to do." Howard, age 8
IS IT BETTER TO BE SINGLE OR MARRIED? "It's better for girls to be single but not for boys. Boys need someone to clean up after them." Anita, age 9
should like it that you like sports, and she should keep the chips and dip coming." Alan, age 10

(a) (b)

Fig. 6.4. Text region of (a) Most unfaded sample (reference page) among the training samples; (b) Most faded sample among the training samples.

Obtaining a sequence of printed diagnostic pages

Electrophotographic printers have four separate color cartridges - cyan, magenta, yellow, and black. We did the test for fading for each color cartridge, respectively, except for the yellow channel, since yellow is very light and subjects are relatively insensitive to fading in this channel.

We first determine the cartridge color (cyan, magenta, or black) to be tested for fading, and replaced with a new cartridge. The test page suite consists of 4 typical document pages and a special diagnostic page shown in Fig. 6.3 with the test color. We then repeatedly print the test page suite by sending a sequence of 100-page print jobs to the printer. The prints of the 5th page (diagnostic pages) of the test suites are then used in the next step.

Psychophysical experiment

We first choose the training samples from the printed diagnostic pages. Starting with the 20th printed diagnostic page, we examine each successive diagnostic page until we encounter one that is distinctly faded relative to the 20th page. The individual who will conduct the psychophysical experiment determines the text fade depending on the local character contrast in the faded test patches, as well as the global strength of the color characters relative to a reference page. This page is then

selected as the next page in training sequence. The process is then repeated using the most recently selected training page as the reference. We renumbered the sequence of training pages that have been selected, after the entire sequence of printed diagnostic pages has been examined, according to the order in which they were printed. The original reference page, which is the 1st page in our training set (20th printed diagnostic page), is our most unfaded sample. In addition, we also use this most unfaded sample as our reference page for certain aspects of our image analysis procedures. From Fig. 6.4(b), we observe very severe fading especially within the right region, compared with Fig. 6.4 (a). The training set also includes other samples with fading degree between those two.

In the second step, we determined the text fade point: Two group of imaging scientists/engineers, each containing nine individuals, separately examined the training prints in two different ordinary conference rooms under normal office lighting. Each individual was asked to choose the first page from the sequence of training pages that exhibits a fade defect, as described by ISO/IEC 19798:2007(E). These results were pooled across observers by choosing the most frequently picked training page as the fade page. All training samples before this page in the sequence are presumed not to be faded; and all the training samples after this page in the sequence are presumed to be faded. This information comprises the ground truth for training our text fade detection algorithm.

6.2.2 Text fade detection algorithm

We scan the training samples, and obtain the digital sRGB images. These sRGB images are then converted into linear RGB,

$$I_{linear} = (I_{sRGB})^{1.7}, \tag{6.1}$$

where $I = R, G, B$ in $[0 : 1]$. RGB_{linear} is then converted to CIE XYZ,

$$\begin{bmatrix} X \\ Y \\ Z \end{bmatrix} = \begin{bmatrix} 0.709858, 0.321142, 0.000000 \\ 0.122170, 0.641922, 0.031217 \\ 0.132461, 0.036936, 0.795290 \end{bmatrix} \begin{bmatrix} R_{linear} \\ G_{linear} \\ B_{linear} \end{bmatrix} \tag{6.2}$$

We then transform CIE XYZ to the $L^*a^*b^*$ color space. The reason we use an uniform color space is because we compute most of our metrics in ΔE. One ΔE is perceptually considered to be one Just Noticeable Difference (JND).

$$\begin{aligned} L^* &= 116 f(\tfrac{Y}{Y_n}) - 16, \\ a^* &= 500[f(\tfrac{X}{X_n}) - f(\tfrac{Y}{Y_n})], \\ b^* &= 200[f(\tfrac{Y}{Y_n}) - f(\tfrac{Z}{Z_n})]. \end{aligned} \tag{6.3}$$

Here $[X_n, Y_n, Z_n]$ is the reference white point, and $f(t)$ is given by

$$f(t) = \begin{cases} t^{\frac{1}{3}}, & if\ t > (\frac{6}{29})^3, \\ \frac{1}{3}(\frac{29}{6})^2 t + \frac{4}{29,} & otherwise. \end{cases} \tag{6.4}$$

Our diagnostic page contains text, fiducial marks, and a solid color block. We will use the text region as our region of interest to do our analysis for text fading. We process each sample page character-by-character to determine the tone development properties within each character, and we also investigate the uniformity properties of the entire page. Figure 6.5 shows the flow chart for our algorithm. We use a common mask on all the pages to estimate the uniformity properties for each character in the text region. The common mask is obtained from the reference page (the most unfaded page) in the training set. The technique to obtain the common mask will be described in the following subsection. For each page in the training set, we first obtain the binary version of the text region, and then we align the binary image with the common mask for each character. The average and standard deviation of pixel values (L^*, a^*, b^*) within the common mask region for each character will be computed and saved for future analysis.

The common mask is obtained from the most unfaded sample in the training set which is the 20th printed diagnostic page. The flow chart and all image analysis steps

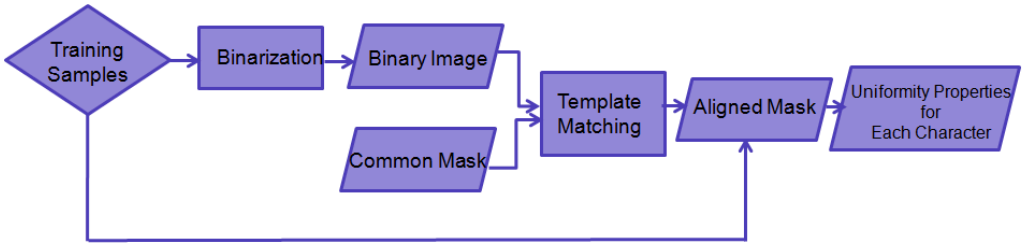

Fig. 6.5. Entire flowchart for text fade detection algorithm.

used to obtain the common mask are shown in Fig. 6.6. To obtain a binary version of the scanned sample, we start with the gray scale image (L^* channel for the input $L^*a^*b^*$ image).

We first apply adaptive thresholding on the gray scale image. Adaptive thresholding changes the threshold dynamically over the image, to accommodate changing lighting conditions in the image. This method statistically examines the intensity values of the local neighborhood of each pixel to find the local threshold. The statistic function which is appropriate and fast here is $mean - C$ of the local intensity distribution. There are two unknown variables for this method: the size of the neighborhood and the constant number C. The size of the neighborhood has to be large enough to cover sufficient foreground and background pixels for a good result. We choose 25×25 pixels in our experiment. C is a constant number. The use of C in the statistic function is to improve the thresholding results of the margins. We choose $C = 10$ in our experiment. Using this statistic function, all pixels which exist in a uniform neighborhood are set to background. This method has less computationally complexity and produces good results for segmenting text from the image.

To remove the influence of noise on our final results, we delete all objects in the threshold image containing fewer than 30 pixels. We then apply a morphological closing to remove small holes within the characters. The structuring element was of size 3×3 pixels. After the morphological closing, we obtain the final binary image of the training sample. We label all the connected components of the binary image

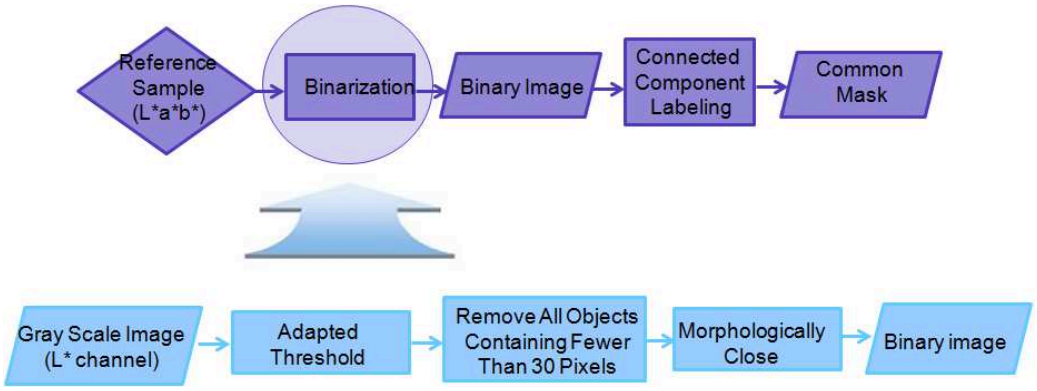

Fig. 6.6. The flow chart and all the technologies we used for common mask.

as our common mask. For every pixel, we check its 8 neighbors and connect all the neighbor-pixels with same pixel value.

We achieve the common mask alignment based on the two fiducial marks located just below the text region, and also the template matching of the common mask on the binary test page. For each test page in the training set, we first obtain the binary version of the test page using the binarization technique as we discussed in the last section. There are two steps for common mask alignment on the binary test page:

1. We compute the central coordinates of each the two fiducial marks based on the spatial distribution of toner absorptance throughout its corresponding mask region. The difference of the fiducial mark location between the analyzed test page and the reference page will be used to roughly shift the common mask for alignment.

2. For each recognized character (connected component) in the common mask, we will use it as a template. The test image is the local block of the binary test page corresponding to that specific template. Let $f(i,j)$ indicate the $(i,j)^{th}$ pixel in the test image, $t(i,j)$ is the $(i,j)^{th}$ pixel in the template, and N is the number of pixels in the template. A common way to calculate the position of the template in the test image is to evaluate the normalized cross correlation value $\rho_{f,t}$ at each point (k,l) for test image and the template, which has been shifted by k pixels in the i direction and

by l pixles in the j direction. The following equation computes the normalized cross correlation $\rho_{f,t}(k,l)$.

$$\rho_{f,t}(k,l) = \frac{1}{N} \sum_{(i,j)\in\Omega} \frac{(f(i,j) - \bar{f}_{k,l})(t(i-k, j-l) - \bar{t})}{\sigma_{f_{k,l}} \sigma_t}. \tag{6.5}$$

Here $\bar{f}_{k,l}$ is the average of f and $\sigma_{f_{k,l}}$ is standard deviation of f within the area of the template. The parameters $\bar{t}$ and σ_t are similarly defined. The region of summation Ω is the region of the character in the common mask.

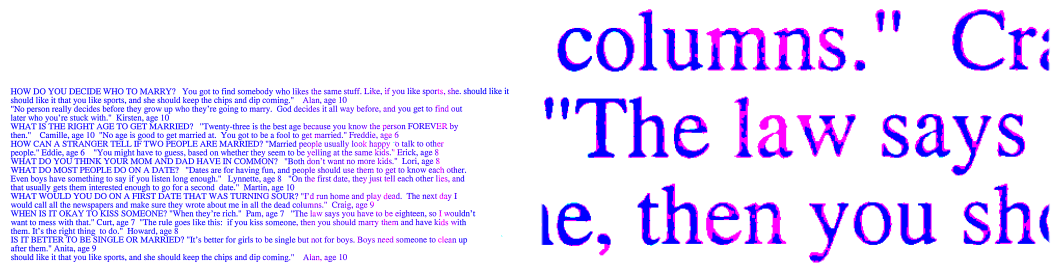

(a) (b)

Fig. 6.7. (a) Common mask alignment on the binary test page. We use cyan for the binary image, and magenta for the common mask. Thus blue means overlap of the binary image with the common mask. (b) Magnification of portion of (a) to better show the alignment result.

After calculating the normalized cross correlation at each point (k,l) for test image and the template, the position (k_{max}, l_{max}) with the maximum normalized cross correlation value ρ_{max} of $\rho_{f,t}(k,l)$ indicates the displacement for which the two images are best aligned. Figure 6.7 shows the alignment result of the common mask on the binary test page. We use cyan color to represent the binary image of the test page, and magenta for the common mask. Thus blue means overlapping of binary image with common mask. From Fig. 6.7 (b), we see that the procedure works remarkably well, even when most of the character is missing in the binary test image, such as is the case, for example, for the letter "a" in the word "law".

Since the text fading behavior is location dependent: it varies from character to character, we measure feature data from the test page character to character.

For each connected component in the common mask, we calculate the average and standard deviation of the pixel value of the test page within the common mask region corresponding to the specific connected component. This measurement is done for each color channel ($L^*a^*b^*$), and also for the ΔE, which is the color difference between the pixel value and background (paper white). We will use the feature data of all test pages in the training set to do the analysis and classification.

6.2.3 Experimental results

The experiment shown here was done for cyan color cartridge to test the text fade properties for this color channel. The similar behavior can be observed for other color channel (magenta and black). There are 13 pages in the training set, while the first page which has the best quality is used as the reference. The text fade point for this training set is page No. 10 according to our expert observers' psychophysical experiment. We scan and analyze the printed pages following the strategy that we discussed above. After that we can obtain the average and standard deviation of $L^*, a^*, b^*, \Delta E$ value within each connected component for all test pages. Figure 6.8 gives the histogram of measured average and standard deviation of ΔE of all connected components for reference page and most faded page. We can see the large difference between them, especially for the mean value of the distribution.

We can use the mean statistical value of the measured average and standard deviation of ΔE for all connected components to determine the text fade point. Here the text fade point is the mean statistical value of the measured average and standard deviation of ΔE for the $10-th$ test page. Any printed text page that has close (in either direction) or lower mean statistical value than the text fade point will be detected as faded, while the opposite is also true. As in Fig. 6.9, we also test the text fade detector by comparing the mean statistical value of the measured average and standard deviation of ΔE for all test pages in the training set with that for one printed testing page with close fading degree of the $10-th$ test page in the training

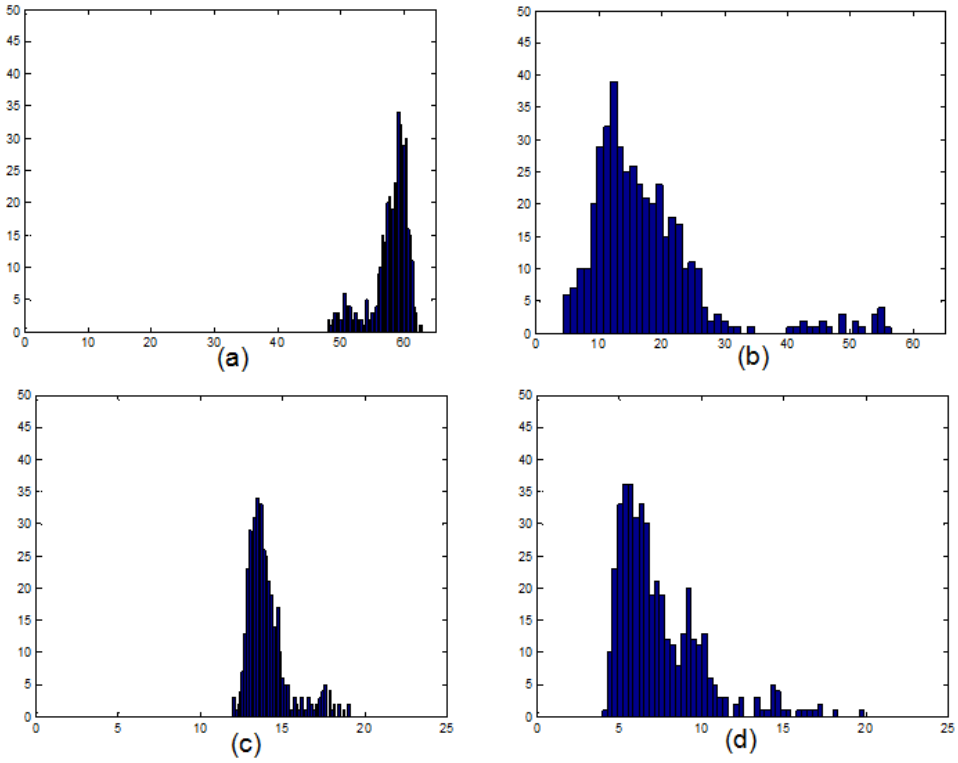

Fig. 6.8. (a) Histogram of measured average ΔE of all connected components for reference page. (b) Histogram of measured average ΔE of all connected components for most faded page. (c) Histogram of measured standard deviation of ΔE of all connected components for reference page. (d) Histogram of measured standard deviation of ΔE of all connected components for most faded page.

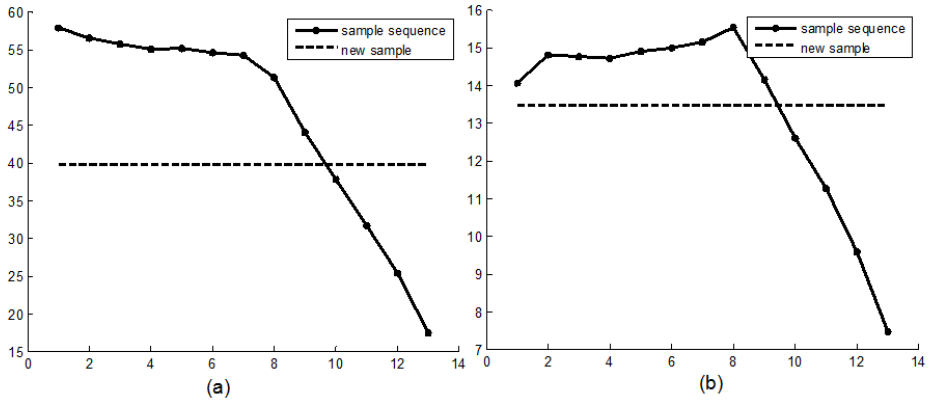

Fig. 6.9. (a) Mean value of the histogram of the measured average ΔE for all connected components for all training pages. Dash line means the mean value of the histogram of the measured average ΔE for all connected components for testing page. (b) Mean value of the histogram of the measured standard deviation of ΔE for all connected components for all training pages. Dash line means the mean value of the histogram of the measured standard deviation of ΔE for all connected components for testing page.

set. The result shows that for mean statistical value of the measured average ΔE predictor, the testing value is close to the value of $10-th$ test page in the training set; while for the mean statistical value of the measured standard deviation of ΔE predictor, the testing value is between the value of $9-th$ and $10-th$ test page in the training set. The testing page will be detected as faded page.

6.3 Conclusion

Image quality is an area of growing importance as imaging systems become more and more pervasive in our daily lives. We first introduce a visualization tool for image graininess. We then propose a new method to autonomously detect the text fading in prints from home or office color printers using a typical office document page instead of a specially designed diagnostic page. The fade point depends on the local character contrast in the faded test patches, as well as the global strength of the color characters

relative to a reference page. In our method we train our predictor using a sequence of scanned printed text pages, and analyze them character-by-character to extract a set of novel features that are indicative of fade. Finally we show our experimental results for one set of training pages printed with cyan color channel; and test the detector on one new testing page. The detector can work efficiently and correctly.

7. SUMMARY

In our thesis, we give a detail introduction about the printer model and our scan-to analysis procedure for printer models, which facilitates in understanding the background. We present our research on the potential influence of a 45×45 neighborhood of the digital halftone image on the measured value of a printed pixel at the center of that neighborhood by introducing a feasible strategy for the contribution. We developed a series of six 45×45 black box models with different accuracy and computational complexity to account for local neighborhood effects and the influence of a 45×45 neighborhood of pixels on the central printer-addressable pixel tone development. We developed two different types of printer models: SD-BBM and HD-BBM, with capture device Epson Expression 10000XL flatbed scanner operated at 2400 dpi under different analysis resolutions. The experiment results show that the larger neighborhood models yield a significant improvement in the accuracy of the prediction of the pixel values of the printed halftone image.

We also introduce two applications of black box models. SFG-BBM is an extension of SD-BBM that adds the printing variation to the mean prediction to improve the prediction by more accurantely matching the characteristics of the actual printed image. We also followed a structure similar to that used to develop our series of BBMs to develop a two-stage toner usage predictor for electrophotographic printers. We first obtained, on a pixel-by-pixel basis, the predicted absorptance of printed and scanned page with the digital input using BBM. We then form a weighted sum of these predicted pixel values to predict overall toner usage on the printed page. Our two-stage predictor significantly outperforms existing an method that is based on a simple pixel counting strategy, in terms of both accuracy and robustness of the prediction.

In the last chapter, we discuss the printed image quality and the method to evaluate the image quality. Specifically, we introduce a new method to autonomously detect the text fading in prints from home or office color printers using a typical office document page instead of a specially designed diagnostic page. The fade point depends on the local character contrast in the faded test patches, as well as the global strength of the color characters relative to a reference page. The detector can work efficiently and correctly based on my test and validate results.

REFERENCES

REFERENCES

[1] R. Ulichney, "Dithering with blue noise," *Proc. IEEE*, vol. 76, pp. 56–79, Jan. 1988.

[2] M. Yao and K. J. Parker, "Modified approach to the construction of a blue noise mask," *J. Electronic Imaging*, vol. 3(1), pp. 92–97, 1994.

[3] D. L. Lau, A. M. Khan, and G. R. Arce, "Minimizing stochastic moire in frequency-modulated halftones by means of green-noise masks," *J. Optical Society of America A*, vol. 19(11), pp. 2203–2217, Jan. 2002.

[4] M. Fischer and D. Shaked, "Frequency domain design of cluster dot screens," *SPIE-IS&T Electronic Imaging*, vol. 6058, Jan. 2005.

[5] B. E. Cooper and D. L. Lau, "Evaluation of green noise masks for electrophotographic halftoning," *Proc. SPIE, Human Vision and Electronic Imaging, San Jose, CA, USA*, vol. 3959, pp. 613–624, Jan. 2000.

[6] J. Stoffel and J. Moreland, "A survey of electronic techniques for pictorial image reproduction," *IEEE Transactions on Communications*, vol. 29, pp. 1898–1925, Dec. 1981.

[7] J. P. Allebach, "Binary display of images when spot size exceeds step size," *Appl. Opt.*, vol. 19, pp. 2513–2519, Aug. 1980.

[8] F. Baqai and J. P. Allebach, "Halftoning via direct binary search using analytical and stochastic printer models," *IEEE Trans. Image Processing*, vol. 12, pp. 1–15, Jan. 2003.

[9] P. G. Roetling and T. M. Holladay, "Tone reproduction and screen design for pictorial electrographic printing," *J. Appl. Photo. Eng.*, vol. 15, pp. 179–182, 1979.

[10] R. L. Stevenson and G. R. Arce, "Binary display of hexagonally sampled continous-tone images," *J. Opt. Soc. Amer.*, vol. 2, pp. 1009–1013, 1985.

[11] P. Stucki, "Algorithms and procedures for digital halftone generation," *Proc. SPIE, Color Hardcopy, and Graphic Arts, J. Bares, Ed.*, pp. 26–40, 1992.

[12] C. J. Rosenberg, "Measurement-based evaluation of a printer dot model for halftone algorithm tone correction," *J. Electronic Imaging*, vol. 2, pp. 205–212, 1993.

[13] T. N. Pappas, C. Dong, and D. L. Neuhoff, "Measurement of printer parameters for model-based halftoning," *J. Electronic Imaging*, vol. 2, pp. 193–204, 1993.

[14] T. N. Pappas and D. L. Neuhoff, "Printer models and error diffusion," *IEEE Trans. Image Processing*, vol. 4, pp. 66–80, 1995.

[15] Q. Lin and J. Wiseman, "Impact of electrophotographic printer dot modeling on halftone image quality," *SID Int. Symp. Tech. Papers, Seattle, WA*, p. 147150, 1993.

[16] Q. Lin, "Screen design for printing," *Proc. IEEE International Conference on Image Processing*, 1995.

[17] T. J. Flohr and J. P. Allebach, "Halftoning via direct binary search with a stochastic dot model," *Proc. IS&T's 3rd Tech. Symp. Prepress, Proofing, Printing, Chicago, IL*, pp. 102–105, 1993.

[18] J. H. Lee and J. P. Allebach, "Inkjet printer model-based halftoning," *IEEE Trans. on Image Processing*, vol. 14, pp. 674–689, 2005.

[19] P. Goyal, M. Gupta, D. Shaked, C. Staelin, M. Fischer, O. Shacham, R. Jodra, and J. P. Allebach, "Electrophotographic model based halftoning," *Color Imaging XV: Displaying, Processing, Hardcopy, and Applications, SPIE Vol. 7528, R. Eschbach, G. Marcu, S. Tominaga, and A. Rizzi, Eds., San Jose, CA*, pp. 17–21, 2010.

[20] P. Goyal, M. Gupta, C. Staelin, M. Fischer, O. Shacham, T. Kashti, and J. P. Allebach, "Electro-photographic model based stochastic clustered-dot halftoning with direct binary search," *Proc. IEEE International Conference on Image Processing*, pp. 1721–1724, 2011.

[21] Y. Ju, D. Saxena, T. Kashti, D. Shaked, M. Fischer, R. Ulichney, and J. P. Allebach, "Modeling large-area influence in digital halftoning for electrophotographic printers," *Color Imaging XVII: Displaying, Processing, Hardcopy, and Applications, SPIE Vol. 8292, R. Eschbach, G. Marcu, and A. Rizzi, Eds., San Francisco, CA*, pp. 23–26, 2012.

[22] Y. Ju, T. Kashti, T. Frank, D. Kella, D. Shaked, M. Fischer, R. Ulichney, and J. P. Allebach, "Black-box models for laser electrophotographic printers recent progress," *Proceedings NIP29: IS&Ts 29th International Conference on Digital Printing Technologies, Seattle, WA*, 2013.

[23] Y. Ju, T. Kashti, T. Frank, D. Kella, M. Fischer, R. Ulichney, and J. Allebach, "High definition black-box model for laser electrophotographic printers," *International Congress of Imaging Science (ICIS), Tel Aviv, Israel*, 2014.

[24] J. A. C. Yule and W. J. Nielsen, "The penetration of light into paper and its effect on halftone reproduction," *Tech. Assoc. Graphic Arts Proc.*, vol. 3, p. 6576, 1951.

[25] L. Wang, D. Abramsohn, T. Ives, M. Q. Shaw, and J. P. Allebach, "Estimating toner usage with laser electrophotographic printers," *Color Imaging XVIII: Displaying, Processing, Hardcopy, and Applications, SPIE, Vol. 8652, R. Eschbach, G. Marcu, and A. Rizzi, Eds. San Francisco, CA*, vol. 3, pp. 3–7, 2013.

[26] U. Chatow, "The fundamentals of hp indigos digital offset color printing process and how it rivals mechanical offset printing," *IS&Ts NIP 18: Int. Conf. Digital Printing Technologies*, pp. 125–129, Sep. 2002.

[27] B. Tagansky, "Ink development in hp indigo digital presses," *IS&Ts NIP 24: Int. Conf. Digital Printing Technologies*, pp. 799–802, Sep. 2008.

[28] H. Yoram and T. Riesenfeld, "Hp indigo industrial web presses: Technology and applications," *Int. Conf. Digital Production Printing and Industrial Applications*, pp. 92–94, May 2005.

[29] R.*Näsänen*, "Visibility of halftone dot textures," *IEEE Trans. Syst., Man, Cybern*, vol. 14, pp. 920–924, 1984.

[30] M. Sezgin and B. Sankur, "Survey over image thresholding techniques and quantitative performance evaluation," *Journal of Electronic Imaging*, vol. 13(1), pp. 146–165, Jan. 2004.

[31] W. K. Gillil, C. G. Midgley, A. M. Murphy, and W. T. Bowerman, "Printer toner usage indicator with image weighted calculation," *U.S. Pat. 5,349,377*, 1994.

[32] W. Filbrich and B. Richtsmeier, "Systems and methods for monitoring toner usage,," *U.S. Pat. 7,720,397*, 2010.

[33] Y. Ju, L. Wang, J. Allebach, T. Ives, D. Abramsohn, M. Shaw, and B. Larson, "Prediction of toner usage with laser electro-photographic printers," *HP Printing and Imaging Conference (HPIC)*, 2013.

[34] A. K. Mikkilineni, G. N. Ali, P. J. Chiang, G. T. Chiu, J. P. Allebach, and E. J. Delp, "Signature-embedding in printed documents for security and forensic applications," *Proc. SPIE 5306, Security, Steganography, and Watermarking of Multimedia Contents VI*, pp. 455–466, 2004.

[35] S. Hu, Z. Pizlo, and J. P. Allebach, "Jpeg ringing artifact visibility evaluation," *Image Quality and System Performance XI, SPIE Vol. 9016, S. Triantaphillidou and M.-C. Larabi, Eds. San Francisco, CA*, 3-5 February 2014.

[36] H. R. Sheikh and A. C. Bovik, "Image information and visual quality," *Image Processing, IEEE Transactions*, vol. 15, pp. 430–444, 2006.

[37] Z. Wang, A. C. Bovik, and L. Lu, "Why is image quality assessment so difficult?" *Acoustics, Speech, and Signal Processing, 2002 IEEE International Conference*, vol. 4, pp. 3313–3316, 2002.

[38] Y. Ju, E. Maggard, R. Jessome, and J. Allebach, "Autonomous detection of text fade point with color laser printers," *Image Quality and System Performance XII, SPIE Vol. 9396, S. Tri-antaphillidou and M.-C. Larabi, Eds, San Francisco, CA*, 2015.

[39] N. Yan, E. Maggard, R. Fothergill, R. J. Jessome, and J. P. Allebach, "Autonomous detection of iso fade point with color laser printer," *Image Quality and System Performance XII, SPIE Vol. 9396, S. Triantaphillidou and M.-C. Larabi, Eds, San Francisco, CA*, 8-12 February 2015.

[40] S. Kiatkamjornwong, K. Rattanakasamsuk, and H. Noguchi, "Evaluation of some strategies to control fading of prints from dye-based ink jet," *Journal of Imaging Science and Technology*, vol. 47, pp. 149–154, 2003.

[41] E. Hoarau and I. Tastl, "A novel sensor to visually track fading of printed material,," *NIP & Digital Fabrication Conference*, pp. 423–425, 2010.

[42] X. Jing, S. Astling, R. Jessome, E. Maggard, T. Nelson, M. Q. Shaw, and J. P. Allebach, "A general approach for assessment of print quality," *Image Quality and System Performance X, SPIE Vol. 8653, P. D. Burns and S. Triantaphillidou, Eds. San Francisco, CA*, 3-7 February 2013.

[43] W. Wang, G. Overall, T. Riggs, R. Silveston-Keith, J. Whitney, G. T. C. Chiu, and J. P. Allebach, "Figure of merit for macrouniformity based on image quality ruler evaluation and machine learning framework," *Image Quality and System Performance X, SPIE Vol. 8653, P. D. Burns and S. Triantaphillidou, Eds. San Francisco, CA*, 3-7 February 2013.

[44] X. Liu, G. Overall, T. Riggs, R. Silveston-Keith, J. Whitney, G. T. C. Chiu, and J. P. Allebach, "Wavelet-based figure of merit for macrouniformity," *Image Quality and System Performance X, SPIE Vol. 8653, P. D. Burns and S. Triantaphillidou, Eds. San Francisco, CA*, 3-7 February 2013.

[45] M. Q. Nguyen, S. Astling, R. Jessome, E. Maggard, T. Nelson, M. Q. Shaw, and J. P. Allebach, "Perceptual metrics and visualization tools for evaluation of page uniformity," *Image Quality and System Performance XI, SPIE Vol. 9016, S. Triantaphillidou and M.-C. Larabi, Eds. San Francisco, CA*, 3-5 February 2014.

[46] M. Q. Nguyen and J. P. Allebach, "Controlling misses and false alarms in a machine learning framework for predicting uniformity of printed pages," *Image Quality and System Performance XII, SPIE Vol. 9396, S. Triantaphillidou and M.-C. Larabi, Eds, San Francisco, CA*, 8-12 February 2015.

[47] J. Wang, T. Nelson, R. Jessome, S. Astling, E. Maggard, M. Shaw, and J. P. Allebach, "Local defect detection and print quality assessment," *International Congress of Imaging Science (ICIS), Tel Aviv, Israel*, 12-14 May 2014.

[48] J. Zhang, S. Astling, R. Jessome, E. Maggard, T. Nelson, M. Q. Shaw, and J. P. Allebach, "Assessment of presence of isolated periodic and aperiodic bands in laser electrophotographic printer output," *Image Quality and System Performance X, SPIE Vol. 8653, P. D. Burns and S. Triantaphillidou, Eds. San Francisco, CA*, 3-7 February 2013.

[49] J. Zhang and J. P. Allebach, "Estimation of repetitive interval of periodic bands in laserelectrophotographic printer output," *Image Quality and System Performance XII, SPIE Vol. 9396, S. Triantaphillidou and M.-C. Larabi, Eds, San Francisco, CA*, 8-12 February 2015.

VITA

VITA

Yanling Ju received her BS degree in Electronic and information Science and Technology from Peking University, Beijing, China, in 2006. She received her M.S. Degree of Engineering in Physical Electronics in 2009, from Chinese Academy of Science, Beijing, China. Since 2010, she has been working towards her Ph.D. degree in Purdue University, West Lafayette, IN. She received her Ph.D. degree in Electrical and Computer Engineering from Purdue University, West Lafayette, IN in 2015. Her research interests include image processing, machine learning, image quality, computer vision, print quality.